INVESTIGATIONS OF PHASE CHANGE MATERIAL (PCM) BASED HEAT SINKS WITH DIFFERENT THERMAL ENHANCERS

Thesis

Submitted in partial fulfillment of the requirements for the degree of

DOCTOR OF PHILOSOPHY

by

MUTHAMIL SELVAN N

(Reg. No. 187037ME009)

DEPARTMENT OF MECHANICAL ENGINEERING

NATIONAL INSTITUTE OF TECHNOLOGY KARNATAKA

SURATHKAL, MANGALORE-575 025

December 2023

INVESTIGATIONS OF PHASE CHANGE MATERIAL (PCM) BASED HEAT SINKS WITH DIFFERENT THERMAL ENHANCERS

Thesis

Submitted in partial fulfillment of the requirements for the degree of

DOCTOR OF PHILOSOPHY

by

MUTHAMIL SELVAN N

(Reg. No. 187037ME009)

DEPARTMENT OF MECHANICAL ENGINEERING

NATIONAL INSTITUTE OF TECHNOLOGY KARNATAKA

SURATHKAL, MANGALORE-575 025

December 2023

DECLARATION

I hereby declare that the Research Thesis entitled "**INVESTIGATIONS OF PHASE CHANGE MATERIAL (PCM) BASED HEAT SINKS WITH DIFFERENT THERMAL ENHANCERS,**" which is being submitted to the **National Institute of Technology Karnataka, Surathkal,** in partial fulfillment of the requirements for the award of the Degree of **Doctor of Philosophy** in **Mechanical Engineering** is a *bonafide report of the research work carried out by me*. The material contained in this Research Thesis has not been submitted to any other Universities or Institutes for the award of any degree.

Register Number: **187037ME009**

Name of the Research Scholar: **MUTHAMIL SELVAN N**

Signature of the Research Scholar: 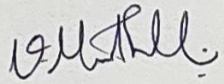

Department of Mechanical Engineering

Place: NITK, Surathkal

Date: 15.12.2023

CERTIFICATE

This is to certify that the Research Thesis entitled "**INVESTIGATIONS OF PHASE CHANGE MATERIAL (PCM) BASED HEAT SINKS WITH DIFFERENT THERMAL ENHANCERS**" submitted by Mr. **Muthamil Selvan N (Register Number: 187037ME009)** as the record of the research work carried out by him, *is accepted as the Research Thesis submission* in partial fulfillment of the requirements for the award of the degree of **Doctor of Philosophy**.

Research Guide

Dr. N. Gnanasekaran

Associate Professor

Department of Mechanical Engineering

NITK, Surathkal

Chairman-DRPC

Department of Mechanical Engineering

National Institute of Technology Karnataka,

Surathkal, Mangalore - 575025

Date: 15.12.2023

ACKNOWLEDGEMENT

I wish to convey my extensive sense of gratitude and gratefulness to my research guide **Dr. N. Gnanasekaran** for giving me this moment and being a pillar throughout my journey in research. His constant encouragement and guidance helped me overcome all the hurdles in the stages of my work and pushed me to bring this thesis to fulfillment.

I am very much obliged to my RPAC committee members, **Dr. P. Parthasarathy** and **Dr. T.K. Jagannathan,** for their valuable support and input in completing my research. I am highly thankful to **Dr. Ravikiran Kadoli**, Head of the department, for providing necessities during the research period. I want to express my sincere credit to my previous heads of the department **Dr. S. M. Kulkarni**, **Dr. Srikantha .S. Rao**, and **Dr. S. Narendranath,** for their invaluable support. I thank **Dr. Kumar G N** for providing the CFD laboratory facility to complete my numerical investigations. I express my heartfelt thanks to **Dr. D. Arumuga Perumal and Dr. Ajay Kumar Yadav** for providing me with their laboratory to conduct my experiments. I like to thank the industrial suppliers for cooperating in providing me with an experimental setup.

I am fortunate to have wonderful friends who supported me through my ups and downs. Especially, **Thirumoorthy, Krishna, Siva, Diva, Dinesh, Manikandan, Mani, Gokul Surya, Chella, Balaji, Deena, Arun, Kali, Nizam** and **Sundar,** who helped me in the stages of my carrier. **Dr. Arun Kumar**, my faculty in my undergraduate who, is the inspiration for me to travel through this research field, and I like to thank him from the bottom of my heart.

I am blessed to have talented colleagues **Dr. Prakash, Ram Prasad, Gopi, Trilok, Venky, Aditya, Diganjith, Pranav, Hemanth, Shyam, Neeraj, Ram Babu, Surya, Vamsi, Kishore, Jayasis, Raja, Arun, Susanth, Syam, Karthi, Jagadish, and Bakshi** who were always aiding me with their knowledge and care. I like to acknowledge the support from my seniors, **Dr. Narendran, Dr. Vishweshwara, Dr. Praveen, Dr. Vasista, and Dr. Ashok.**

My special thanks to the people who were with me during my life **Vikki anna, Parthi anna, Nilavan, Vimal, Amsa, Karthi, Ezhil, Kavin, Amar, Viswa, Ilam, Hari, and Akash**, who helped me in my completion of work by providing their support. I like to mention my chellakutties **Durga, Priya, Abhi and Sasi**.

Finally, I warmly thank my beloved family members for their love, sacrifice, patience, and understanding, which made me carry forward my purpose. Also, I feel happy to thank my cousin **Baji** who made a strong foundation in pursuing my goal.

DEDICATION

I dedicate my thesis to my beloved AMMA **Thirumalar,** who always aids me in whatever I do, and my late APPA, **Nedumaran,** who will be proud of my doctorate. Next, the persons who always stood by my side are my lovable brothers, **Senthamil Rajan** and **Karthikeyen**, my dearest sister **Anu**, and her husband, **Manimaran**. Next, I dedicate this work to my chithappa **Muthukumar** and chithi **Banu** for constantly supporting me in my research. I also like to specially mention my in-laws **Murugan, Muthulakshmi** and **Sobica** for their endless support in my decisions. I am really grateful to have such a wonderful family not to stop me from pursuing my goal.

Finally, and foremost, I devote my thesis to my adorable wife, **Jayasri**. She always stood by my side and motivated me to fulfill my wish, irrespective of staying away from her and my son. My entire effort in working was devoted to my son **Ilan Mughil**.

‘‘என்னை வாழ வைக்கும் தமிழுக்கு என் தேர்ந்தெடுத்த தொகுப்பை அர்ப்பிக்க விரும்புகிறேன்’’

"வாழ்க தமிழ், வெல்க தமிழ்"

ABSTRACT

Effective thermal management is crucial for ensuring the maximum performance and reliability of electronic devices. As the internal heat generation within a device increases, the risk of failure rises, leading to a decrease in its overall lifespan. A passive cooling method involving the use of Phase Change Materials (PCMs) proves to be a suitable technique for electronic cooling. However, due to the inherently poor thermal conductivity of PCMs, various enhancers, such as fins, metal foams, and nano-particles are employed to mitigate the thermal resistance they pose. Furthermore, the heat sink design must be optimized to establish an efficient storage and retrieval system under the charging and discharging cycles. The current thesis work aims to present both numerical and experimental investigations of PCM-filled heat sinks using different thermal enhancers Numerical simulations are conducted using ANSYS Fluent, employing the enthalpy-porosity formulation to model the melting/solidification of PCM. Subsequently, experiments are carried out to further explore the parametric aspects of the investigation.

In the first work, both the melting and solidification of n-eicosane filled heat sink are studied numerically. In order to enhance the thermal conductivity, fins and foams are used in this study. Here, a PCM-filled hybrid system of two cases is considered. In case 1, no fin case is compared with rectangular fins and tapered fins. In case 2, different filling heights, such as 10 mm, 15 mm, and 20 mm, with horizontal tapered fins are investigated. Results show that tapered fins are good for the distribution of temperature and uniform melting within the system. During solidification, the fin shape does not influence the process due to the poor natural convection effects. Regarding the foam filling height, during the melting process, filling heights have less significant effect. But it is observed that the solidification rate is faster by increasing the filling heights. For solidification cases, 20 mm filling height foam performs better than all other cases. Following this study, a multi-objective optimization is carried out using a reliable multi-criteria decision making approach for a hybrid heat sink with fins and foams. Different weightage is distributed to the objective functions in this method depending on the choice of the user. The pore size of 0.8-0.95 and pore density of 5-25 pores per inch vary for various filling heights, and 60

cases are considered for both the cycles. When the weightage is biased towards solidification or equally shared between melting and solidification, the 25 PPI, which possesses a more solid structure, has a better performance score. However, when the weightage is biased towards melting, the 0.95 porosity has a higher performance score due to the larger PCM volume. From the results, guidelines for selecting a preferable pore structure are provided based on the filling height and applied weightage.

In the next study, Phase change materials (PCM) RT-28HC, RT-35HC, and RT-44HC, with similar thermal properties, are considered, and a combination of PCM acts as an enhancer. The PCM is oriented in increasing order of melting temperature from the left to the right side of the heat sink. Additionally, the fins are attached to the heat sink longitudinally, and its orientation effects are studied. The effect of fins on the charging cycle is assessed by comparing a single and double PCM heat sink. Three initial conditions are investigated by altering the initial temperature to 300 K, 303 K, and 310 K. For high heat input, the negatively angled fins possess a higher melting rate. For different initial conditions, -60^{o} provides higher enhancement, and $+60^{o}$ possesses prolonged melting for almost all cases and applied weightage.

In the last study, a modified variable height fin heat sink is compared with the conventional constant height fin heat sink. Experiments are performed for constant loads and also different power surge conditions. The pulsed heat loads are applied for two scenarios: 1. Constant load 4 W - power surge and constant load 4 W - power surge - 1800 s no-load condition, and 2. Power surge (50 s, 100 s, and 150 s) - no-load conditions of 1800 s. During experiments, the proposed variable height fin heat sinks possess better thermal performance for all load scenarios. The variable height fin heat sink accelerates any load's melting rate. The time difference between the wall and the PCM is also less for the variable height fin heat sink. Similar to the melting, a faster discharging rate is noticed during solidification in the variable height fin heat sink.

Keywords**:** - PCM, Hybrid heat sink, Triple PCM design, Multi-Objective Optimization, TOPSIS methodology, Modified fins, Pulsed heat loads.

TABLE OF CONTENTS

LIST OF FIGURES

LIST OF TABLES

ABBREVIATIONS

ANN	artificial neural network
CFD	computational fluid dynamics
CHS	composite heat sink
COP	coefficient of performance
DSC	differential scanning calorimetry
FHP	flat heat pipe
FOM	figure of merit
FVM	finite volume method
GA	genetic algorithm
LHSU	latent heat storage unit
LMPCM	liquid metal phase change material
LSA	least square approach
LTE	local thermal equilibrium
LTNE	local thermal non-equilibrium
MCHS	mini-channel heat sinks
MWCNT	multi-wall carbon nanotubes
PCM	phase change materials
PPI	pores per inch
RSM	response surface method
SCD	simultaneous charging and discharging
SPT	set point temperature
TCE	thermal conductivity enhancers
TES	thermal energy storage
TOPSIS	technique for order performance by similarity to ideal solution
TSU	thermal storage unit
VOF	volume of fluid

NOMENCLATURE

A	mushy zone constant
a_{sf}	interfacial surface area (m^3/m^2)
b	width (mm)
b_f	fin thickness (mm)
b_s	substrate thickness (mm)
C	inertial resistance (1/m)
c_p	specific heat (kJ/kg K)
d_f	fiber diameter (m)
d_{pr}	pore diameter (m)
f	fin
$\vec{g}$	acceleration due to gravity (m/s^2)
H	enthalpy (J/kg)
h_f	fin height (mm)
h_{fill}	foam filling height (mm)
h_p	height of PCM (mm)
h_{ref}	reference enthalpy (J/kg)
h_s	height of sink (mm)
h_{se}	sensible enthalpy (J/kg)
h_{sf}	interstitial heat transfer coefficient (W/m^2K)
I_{it}	current input (A)
K	permeability (m^2)
k	thermal conductivity (W/mK)

L	latent heat of fusion (kJ/kg)
l	length (mm)
l_s	length of the sink (mm)
M_{max}	maximization of melting time
Mt	melting time (s)
P	pressure (N/m^2)
Pr	Prandtl number
P_{it}	power input (W)
P_i	performance score
p_f	fin positioning
q	heat flux (W/m^2)
Re	Reynolds number
S_{min}	minimization of solidification time
St	solidification time (s)
S^+	positive Euclidean distance
S^-	negative Euclidean distance
T	temperature (K)
T_l	liquidus temperature (K)
T_m	melting temperature of PCM
T_r	reference temperature (K)
T_s	solidus temperature (K)
T_w	wall temperature (K)
t	time (s)

U	overall heat transfer coefficient (W/m^2K)
u	velocity in x direction
V	weighted normalized values
V_{max}	maximum velocity (m/s)
V_{it}	voltage input (V)
V^+	ideal best value
V^-	ideal worst value
v	velocity in y direction
$\vec{v}$	velocity vector
W	weights
w_{st}	thickness of the substrate (mm)
w_f	thickness of the fin (mm)
x,y	spatial coordinates (m)

GREEK SYMBOLS

ε	porosity
ρ	density (kg/m^3)
μ	dynamic viscosity (kg/ms)
β_0	coefficient of thermal expansion (1/K)
Φ	liquid fraction
Θ	orientation angle
ω	uncertainty
λ	constant
φ	porosity of composite
ζ	effective thermal capacitance (kJ/Km^3)

Subscripts

e	enclosure
eff	effective
f	fluid
i	rows
ip	initial condition of PCM
l	liquid state
m	melting
mf	metal foam
n	total number of values

p	PCM
pl	a pitch from the long side of the enclosure
ps	a pitch from the short side of the enclosure
S_b	solidification for no-fin case
S_f	solidification for respective cases
s	solidification
sl	spacing from the long side of the enclosure
ss	spacing from the long side of the enclosure
sti	straight fin case for the initial condition
Θ_i	fin orientation of respective cases for the initial condition

Superscript

—	normalization

CHAPTER 1

INTRODUCTION

The pursuit of innovation necessitates a comprehensive approach to thermal management, ensuring not only optimal performance and reliability but also addressing the diverse needs of a technologically driven society. Thermal management plays a pivotal role in a myriad of applications across diverse industries, serving as a critical aspect of system design and operation. Originating from the fundamental principles of thermodynamics, it addresses the efficient control and dissipation of heat generated during the functioning of electronic devices, machinery, and industrial processes. The significance of thermal management lies in its ability to ensure optimal performance, reliability, and longevity of these systems.

In the automotive sector, it contributes to the performance and safety of vehicles by regulating engine temperatures. Additionally, industries like aerospace, energy, and manufacturing rely on advanced thermal management techniques to enhance energy efficiency and prevent system failures. As technological advancements continue, the importance of thermal management remains paramount in sustaining the functionality and durability of a wide array of applications.

1.1 ELECTRONIC COOLING

In the current era, with the increasing use of electronics, outstanding performance and diverse functions are expected with a compact and efficient design. Moreover, there is a demand from the customer end that the gadgets need to possess a longer lifetime. The electronic device can sometimes experience constant, periodic, and high peak loads. These loads determine the functionality and durability of the electronic components. There are several applications of electronics where periodic loads are induced: anti-lock brake controllers and power steering controllers, which possess periodic loading. The scenarios with peak loads are actuators in aircraft, ultracapacitor-powered electronics, and automated defibrillators. These peak load occurrences raise the temperature for a less period and may generate more heat than the periodic and constant loads. An electronic device’s reliability depends on how it performs a specified task based on the load applied. The causes of the

failure of electronic devices are given in Figure 1.1. If there is a rise in temperature due to high heat flux within the system, the device may not complete the assigned task. The operating temperature in electronic devices plays a major role in determining their lifetime. The device that runs for a longer time will generate more heat, leading to system failure. So, the heat generated from the device should be extracted or released to the surroundings for its increased performance. Hence, the reliability of any electronic device depends on the temperature rise within the system. Therefore, there is a necessity to provide efficient cooling of electronic devices. Miniaturization of devices further makes thermal management more difficult. So, the prime importance of a device is thermal management for its greater performance. The cooling methods are classified into active and passive cooling. In active cooling, heat is extracted by direct contact with extended surfaces called fins for natural convection. For forced convection, external devices, such as fans, blowers, pumps, etc., are added to the heat sink to dissipate the heat to the surroundings. This conventional cooling method has a disadvantage of noise, vibration, power consumption, and malfunctioning and maintenance of the fan. These limitations lead to passive cooling over active cooling for reliable and long-life operation of devices.

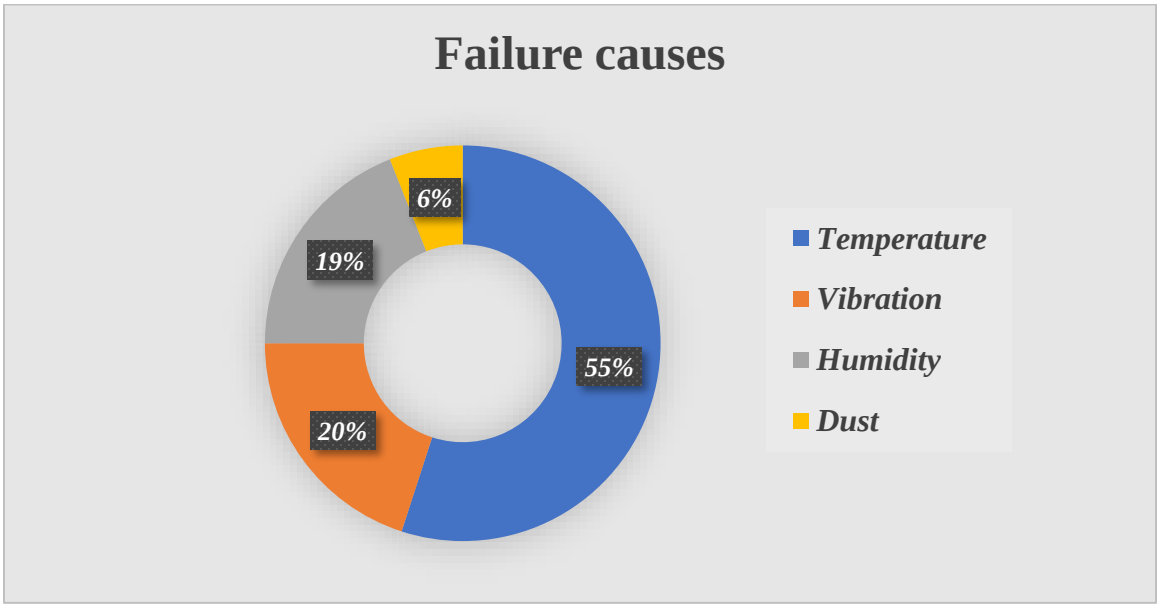

Figure 1.1 Electronic device failure causes Zhang et al. (2021).

The problem addressed in the previous studies pertains to electronic cooling applications within the medium-temperature range which encompass a specific temperature range relevant to electronic devices. In those researches, the medium temperature range is considered to be within the temperature range of 30°C to 80°C. This aims to provide a clear and bounded understanding of the thermal conditions under investigation, ensuring precision in the subsequent discussions and analyses related to electronic cooling within the specified temperature parameters.

1.2 THERMAL ENERGY SYSTEM (TES)

Thermal Energy System (TES) is a passive cooling technique and a better choice for providing an effective system. There are two methods to store energy in TES: chemical and the other is physical. In the chemical storage method, energy is stored and released by chemical reactions, and these chemical reactions are reversible processes. Thermochemical storage contains solid-gas, liquid-gas, or gas-phase systems. The physical method is the storage of energy at a molecular level. Physical methods are further classified into sensible heat storage and latent heat storage. Sensible heat storage is gained in temperature due to energy absorbed without any phase transition. It can be either a solid or liquid phase. It depends upon the specific heat capacity, mass, and temperature gradient of the material. Some examples of sensible energy storage are rock, gravel, metals-(solid), molten salts, and water-(liquid). Latent heat storage is an iso-thermal process where the material absorbs a certain amount of energy to undergo a phase transition from solid to liquid, liquid to gas, solid to gas, or vice versa. It mainly depends upon the mass and latent heat (fusion, vaporization) of the materials.

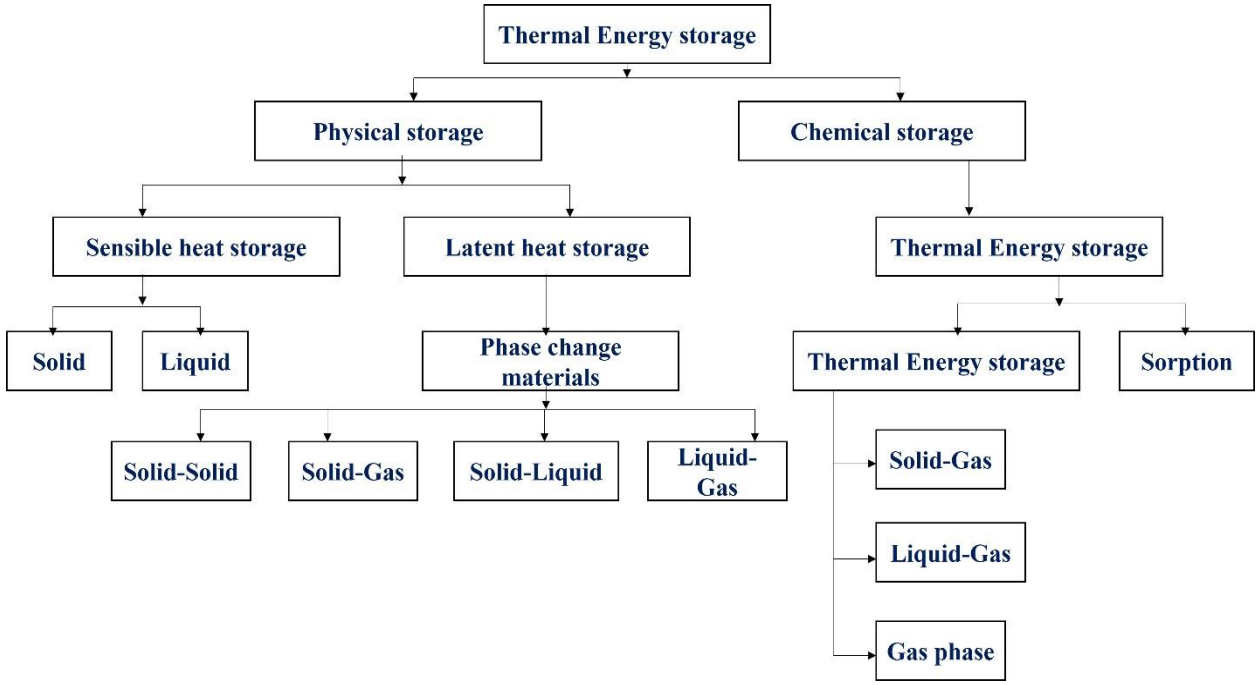

Figure 1.2 Classification of thermal energy storage materials Nazir et al. (2019).

Each of the three Thermal Energy Storage systems has its advantages. The sensible storage method has high durability but lowers energy storage density. The latent heat storage method has moderate durability and good energy storage density. The chemical storage method has the best energy storage density and poor durability. In terms of commercial availability, chemical storage materials are still in research, while sensible and latent materials are widely available. In light of all these factors, the Latent heat storage method is a better choice for a storage system due to its wide range of operating temperatures of materials available and better heat capacity. Figure 1.2 shows the broad classification of Thermal energy storage materials according to Nazir et al. (2019).

1.3 PHASE CHANGE MATERIALS (PCM)

Phase change materials are latent heat storage systems that comprise sensible and latent heats. The sensible heat process accumulates heat until it reaches the phase transition temperature. After reaching transition temperature, the heat accumulated is stored in the material by converting its phase with constant temperature, i.e., latent heat period. PCMs are subcategorized according to the state of the material into solid-solid, solid-liquid, solid-

gas, and liquid-gas. Solid-liquid is highly preferred among the above-categorized materials because of its low volumetric expansion, good chemical stability, and desired latent heat.

Figure 1.3 Classification of PCM.

Based on their chemical nature, the Phase change materials are classified into three types, as shown in Figure 1.3. Organic PCM has good chemical stability, non-toxic, inflammable, non-corrosive, and has low to medium operating temperatures. Inorganic PCMs are mainly hydrated salts, metals, and alloys with high latent heat, storage density, operating temperatures, and inflammability. Eutectic PCM is mainly composed of two or more materials mixed together for the betterment of operating parameters. The Phase change material is selected based on the following requirements:

1. Cost

2. Product Safety

3. Thermo-physical properties

4. Chemical properties

5. Number of cycles / Lifetime

6. Operating temperatures

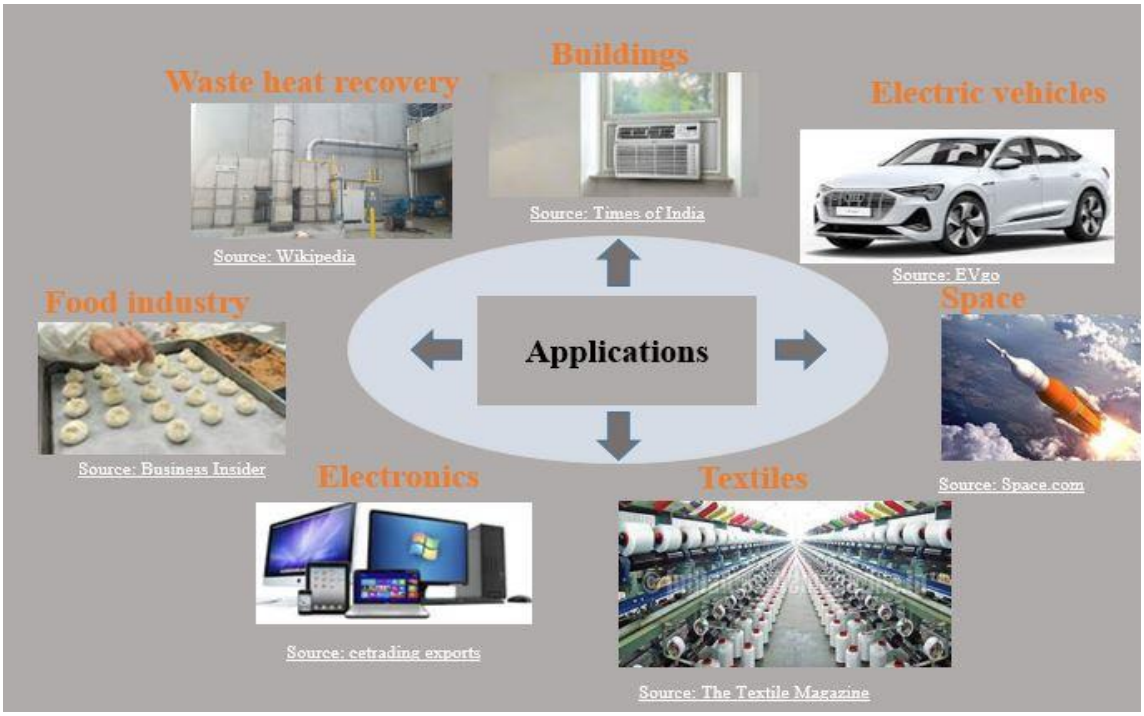

Figure 1.4 Applications of PCM.

PCM plays a vital role in many industries and is broadly used, as mentioned in Figure 1.4. In Solar plants, solar energy is abundant, but the availability of energy is periodical. So to overcome it, PCM can be a medium to store the available energy. Thermal management is crucial in electronic components and space because of its compactness, cost, and weight. Cooling strategies using active methods are costly and increase the system's weight. Hence, passive methods can be applied using PCM, which can provide the necessary cooling for the system. In buildings, the comfort of living standards is enhanced. So, Air conditioners and room heaters become essential in day-to-day life. Thus, the existing cooling system consumes a lot of energy and can be replaced with PCM. In the Food and textile industries, PCM can be used as an alternative source for their production. PCM can also be used in waste heat recovery systems to reduce heat loss from the system and improve the system's efficiency.

1.4 THERMAL CONDUCTIVITY ENHANCERS (TCE)

PCM has several advantages, as mentioned, but the main limitation in selecting PCM is its poor thermal conductivity. This poor thermal conductivity leads to increased thermal resistance within the system. Hence, PCM is not capable of transporting heat generated at a faster rate. Additionally, the temperature distribution within the material will also be disturbed. Even during the initial period, there will be a sudden rise in temperature due to its poor diffusivity. This sudden temperature rise may affect the wall surfaces of a heat sink by inducing hotspots. The hotspots in the heat sink will affect the heat transfer rate and reduce its response. In order to overcome this problem, some additional enhancers should be added. The additional enhancers which are incorporated should possess very high thermal conductivity. This high thermal conductivity material should increase the overall conductivity of the system so that there is an enhanced outcome. This enhancer can further provide a uniform temperature distribution within the PCM material. There are several types of techniques to enhance the overall conductivity, which are shown in Figure 1.5. Some are mixing nanoparticles into the material, adding a solid material like foams, and machining extended surfaces in the heat sinks.

Fins can provide a highly conductive pathway inside the PCM cavity. Fins can be introduced either within the enclosure, called internal fins, or outside the enclosure, called external fins. Fins can be of two types based on the fin shapes, straight fins and non-straight (modified structure) fins. For the straight fins, circular and longitudinal fins are preferred for shell and tube heat exchangers, and for heat sinks, pin, and plate fins are preferred. Based on the requirement, the non-straight fins can be modified to any kind of shape, namely, Y-type, T-type, snowflake shape, and tree-shaped fins.

Metal foams have a random internal structure, and their foam ligament distribution can reduce the thermal resistance offered by the PCM. The metal foams have a larger surface area for their specific volume, which can be suitable for heat transfer augmentation. Metal foam consists of two types, 1. Open-cell foams (void volume interconnected by fibers and 2. Closed cell foams (closed void volume). The heat transport within metal foams highly depends on the pore size and pore density.

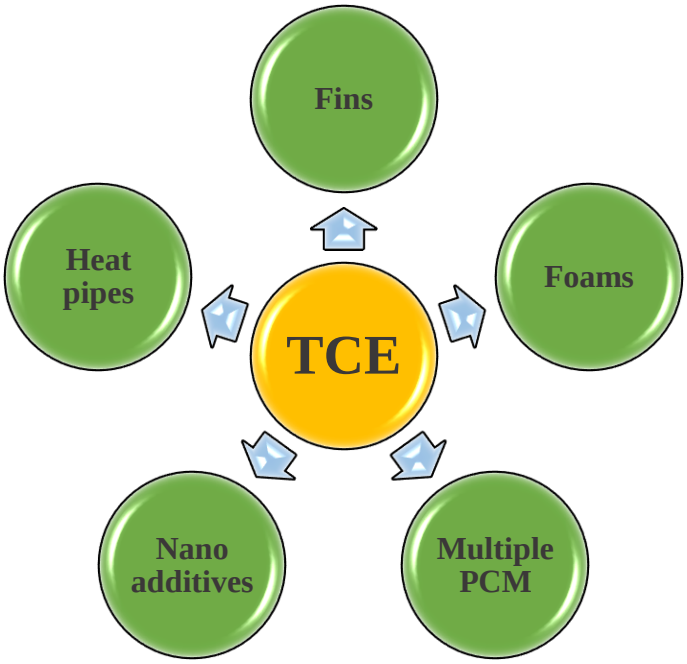

Figure 1.5 Different thermal conductivity enhancers.

Nano additives are external solid particles that are mixed with solid / liquid to enhance their physical properties. When the particles are suspended within the material, they should possess high thermal conductivity, better stability, and corrosion resistance. Nanoparticles are mainly based on ceramics, metals, and carbon-based. Depending on how well the nanoparticles dispersed within the material it can provide an effective enhancement in material properties. Moreover, for enhancement, the particles suspended in the working fluids (nano-fluids) are also used based on the applications or material incorporated in the heat sink.

A heat pipe is a type of heat exchanger, able to transport heat using the latent heat of working fluid inside the heat pipe. The heat exchange occurs using a minimal temperature as a driving force between the evaporator and condenser section. Two kinds of heat pipes are wicked heat pipes and wickless heat pipes (thermosiphon). Multiple PCM comprises different materials with the same/different physical properties together to form an effective system. These materials can be arranged in different sections or encapsulated and placed

within the enclosure. The energy storage capability can be influenced by how these materials are arranged and how any materials are comprised together.

1.5 OVERVIEW OF THE THESIS

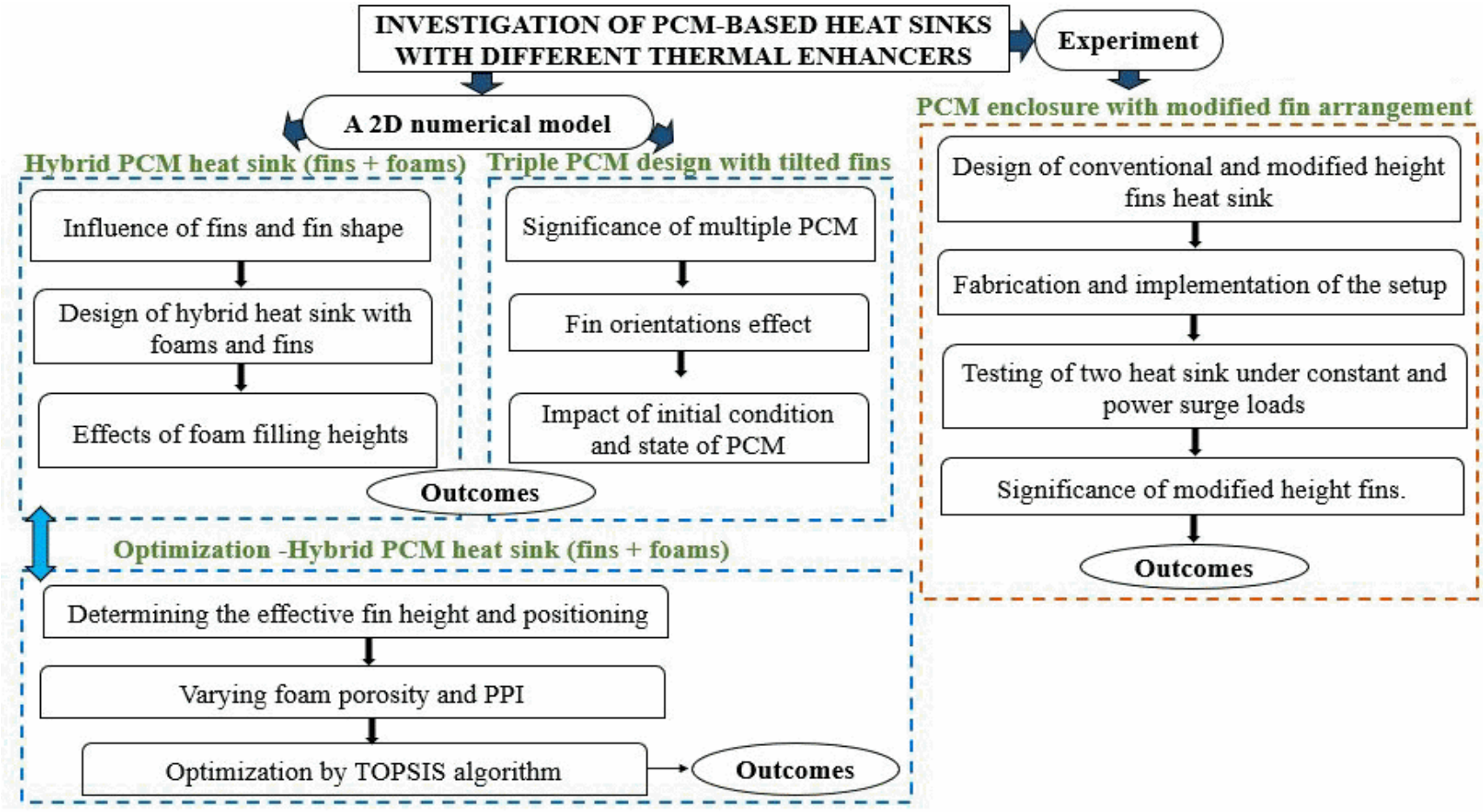

Figure 1.6 Overview of the thesis.

1.6 ORGANIZATION OF THE THESIS

Chapter 1 introduces the background, significance, and application of the PCM, its importance in electronic cooling, and the factors influencing the heat transfer performance when PCM is incorporated in a heat sink.

Chapter 2 contains the critical literature about the different investigations carried out using phase change materials. Additionally, the investigation relates the PCM-filled heat sink specifically for electronic cooling. The same chapter captures an extension of the optimization study from the recent literature. The outcomes of the literature and research gaps, along with the objective of the present research, are also reported.

Chapter 3 provides the 2D model of a PCM-based heat sink comprised of fins on the vertical wall surfaces. First, the fins are introduced on both horizontal and vertical wall surfaces, and the fin shape is modified by a generally rectangular shape and tapered shape. The impact of fin shape over the charging cycle is compared with a PCM-filled heat sink with no fins. Next, this chapter discusses the thermal performance effect of heat sinks with a combination of partially filled foams and horizontal fins placed on vertical wall surfaces. During discharging cycle, all cases of heat sinks with modified enhancers are compared based on their performance in the last section of the chapter.

Chapter 4 presents detailed investigations of the multiple PCM heat sinks. Three PCMs with similar and high-influencing properties are selected for these investigations. The significance of multiple PCM over single PCM and double PCM heat sinks is reported. The influence of fin orientation for a range of angles during the charging cycle is briefed. The conditions and state of the PCM vary, and its impact over the melting period is discussed based on the enhancement percentage.

Chapter 5 reports the extension of Chapter 3 work. This investigation initially discusses the optimization of effective fin size and shape for horizontal fins. Next, the partially filled foam with horizontal fins heat sink is selected, and the effect of filling height is captured. The porosities and the pore sizes of the foams are varied, and the simulations are carried out. Two objective functions, minimizing solidification time and maximizing melting time,

are found and reported in this chapter based on the technique for order of performance by similarity to ideal solution (TOPSIS) algorithm.

Chapter 6 provides a detailed analysis of the fin configuration of a PCM-filled heat sink. The conventional constant height fins and modified variable height fins are fabricated and compared experimentally in this chapter. The heat input applied to the heat sink is constant loads and power surge loads. The results are presented with temperature-time history curves for both melting and solidification processes at various heat input conditions.

Chapter 7 summarizes the major conclusion of the PCM incorporated in a heat sink with different enhancers and the specific contribution made in work. Also, the special mention of the scope of future work is highlighted.

CHAPTER 2

LITERATURE REVIEW

2.1 INTRODUCTION

In electronic devices, there is a demand for miniaturization and efficient performance. This led devices to high-end performance, and the possibility of high heat flux within the component rises. The heat generated by the devices raises the operating temperature, which affects the efficiency and reliability of those devices. Operating the devices within a temperature of 60-80^{o}C according to Ho et al. (2020) extends the service life of the components. An efficient thermal control is required to operate the device within a certain range. PCM has been incorporated in the recent past to accomplish an effective cooling technique and optimal heat sink. This PCM-filled heat sink can absorb a large amount of heat dissipated and provide the necessary cooling.

2.2 EXPERIMENTAL STUDIES BASED ON THE PCM INCLUSION

Avci and Yazici (2018) experimented with studying the effect of orientation in flat-type heat sinks. Melted n-eicosane (PCM) at 80^{o}C was poured and allowed to solidify inside the enclosure. The effect of orientation was significant in PCM-based heat sinks but had a negligible effect in heat sinks without PCM. Results show that the operation time of the heat sink was increased by increasing the inclination angle. Uniform mixing and uniform temperature distribution in melted PCM were observed by increasing the inclination angle.

For the passive cooling method, Ali et al. (2018a) investigated the thermal performance of a latent heat storage unit (LHSU). A storage unit was made of aluminum with a pin-fin of square cross-sectional area. N-eicosane was incorporated in a storage unit with three different volume fractions (0, 0.5, and 1). Steady-state and transient heating was conducted to quantify the performance of LHSU. Heat flux from the heater at the bottom of the heat sink varied from 1.2 kW/m^2 – 2.8 kW/m^2 at an interval of 0.4 kW/m^2. For steady-state heating, no significant effect was found at lower heat flux (1.2 kW/m^2). For transient heating, PCM was effective with increasing operation cycles.

In divergent mini-channel heat sinks (MCHS), Ho et al. (2020) experimentally studied the performance of water-based nano-PCM emulsion flow and heat transfer. With higher heat transfer and lesser pressure drop compared to parallel one, a divergent rectangular MCHS was selected in this study. According to the influence of Reynolds number, heat flux, and nano-particle composition, a figure of merit (FOM), effectiveness, and coefficient of performance (COP) were evaluated. N-eicosane PCM was microencapsulated and suspended in water that worked as a cooling fluid and passed through the system with the help of a centrifugal pump. As Reynolds number increased, the heat transfer coefficient and flow velocity also increased, and thermal resistance was reduced. The small change was seen in thermal resistance at a large Reynolds number because of the completion of melting. As the composition of nano-particles increases, a decrease in FOM occurs. From the results, at Reynolds number 100, maximum effectiveness and COP were found.

Baby and Balaji (2012) experimentally determined the fin geometry effects in a heat sink filled with Phase Change Materials. With n-eicosane as the phase change material, the different fin geometry used was plate and pin fin which has the same volumetric fraction (8%). The material properties like specific heat and latent heat were found using differential scanning calorimetry (DSC). The experiments were conducted for different heat inputs, ranging from 2-7 W. The enhancement ratio expressed an increase in operating time with the addition of fins in the heat sink. The effect of the modified Stefan number to reach a specified temperature was represented graphically. Results show that the addition of fins to the heat sink stretched the operating duration. For a heat sink, an increase in the modified Stefan number decreases the time to attain a specified temperature.

For intermittent operations, Kandasamy et al. (2007) experimentally investigated the performance of PCM-based storage units in the thermal management of portable devices. A flat quad PCM package was tested for various power inputs and orientations under steady-state cyclic conditions. Paraffin wax was used as PCM, and power levels were 6 W, 9 W, and 12 W. Then 12 W input power was fixed by changing orientation vertically, horizontally, and in an inclined position (45^{o}). The results showed that a low thermal resistance heat conduction path from both sides of the heater could provide uniform

temperature distribution across the whole package. While designing the PCM package, the average value should be considered over the peak power level for the expected operating time. A numerical model was also simulated and agreed with the experimental results.

In the thermal management of electronic devices, PCM-based heat sink feasibility was investigated experimentally and numerically by Kandasamy et al. (2008). To remove entrapped air, PCM paraffin wax was poured inside the sink into a liquid state and allowed to solidify. Activation of melting in PCM was not found with a low power level of 2W. With the inclusion of PCM in a heat sink, the time to reach a steady state was increased, but the steady state temperature remains the same. 3-D numerical simulation results were in good agreement with experimental data. Cooling performance was increased with PCM inclusion heat sink than without PCM heat sink.

For the application of cooling electronic devices, a novel method of combining a liquid-metal phase change material (LMPCM) module and a flat heat pipe (FHP) thermal spreader was studied by Li et al. (2016). Both modules have similar external dimensions, and the total thickness of the module was 4 mm. Natural convection occurrence, even after the liquid metal gallium melts, was a mystery. Due to thin geometry, the phase change process inside the module has complicated behavior. From an experimental study, it was reported that FHP-LMPCM possesses a better solution for the thermal management of electronic devices.

Mahmoud et al. (2013) experimentally investigated the effects of PCM-based heat sinks with honeycomb-structured fins compared with machined fins. Different heat sinks were compared, like single cavity, 3, 6, 9, 36- cavities, and single cavity with honeycomb structure. PCM-HS29P, PCM-HS34P, PCM-OM37P, PCM-OM46P, PCM-HS58P, and RT42 with different phase change temperatures were used in the sink design. Increasing the number of fins enhances the thermal performance of heat sinks. At higher power levels, usage of PCM becomes more significant. Incorporating honeycomb structures provide comparable results, and due to its lightweight, it can be preferred over machined fins.

To maintain a low component temperature, Saha et al. (2008) focused on experimentally determining the optimal volume fraction of fins in TSU. The fins and the heat sink were made of aluminum, whereas PCM used eicosane. They also investigated fin shape and fin dimension effects with optimum volume fraction of TCE. 8% volume fraction with 36 fins was found to provide better performance than 0%, 2%, 18%, and 27%, and the corresponding number of fins were 0, 9, 81, and 121. Pin-fin heat sink performs better than plate-fin heat sinks due to their uniform distribution. A larger contact area between the fin results in a lower heater temperature. Higher the fin thickness, the higher the heater temperature for the same volume fraction of fins. For the interpretation of the experiment results, a numerical model was developed and matched with the experiment results.

Boudali Errebai et al. (2018) investigated the effect of PCM applications in buildings. Thermal management of PCM plasterboard with perforated holes instead of plasterboard panels without a hole was presented. Micronal DS 5001 in dry powder form was formed by paraffin wax encapsulated in a polymethyl methacrylate microcapsule shell. As the panel thickness increases, the phase shift value also increases; hence smaller thickness was recommended. Spacing between holes also affects the system, where a decrease in spacing increases the phase shift.

Ghosh and Guha (2019) have done experiments and simulations to study the dynamic behavior of PCM melting inside a spherical shell cavity. Melting of paraffin wax RT-27 was captured using high-speed digital cameras during experiments. The volume of fluid (VOF) model and the enthalpy porosity method were used to track the solid-liquid interface of PCM during melting. Simulations were done for various cavity materials such as glass, aluminum, and copper at constant Stefan number 0.18. Rather than the Nusselt number, thermal diffusivity affects the average heat flux inside the cavity. With a higher Stefan number, velocity was maximum and natural convection controls the melting process. Results show that materials with high thermal diffusivity should be considered for energy storage purposes.

2.3 NUMERICAL STUDY BASED ON THE PCM INCLUSION

Akhilesh et al. (2005) presented a proper sizing composite heat sink (CHS) thermal design procedure for maximizing energy storage and operation time. High conductive base material and PCM were essential for designing a CHS. The walls were assumed insulated for design purposes and were also valid for a convective condition at walls. Between the fin and the heater, providing a base material layer that could act as a heat spreader was necessary. Natural convection was not included in the design approach. Sensible heat contribution was also neglected. Constructing a heat sink with critical dimensions before it reaches set point temperature (SPT) ensures the complete melting of PCM.

Ghosh et al. (2019) numerically studied the unconstrained solidification process in different cavities. Rectangular and spherical shape cavities were used, and paraffin wax RT-27 was inserted inside the cavity. The presence of air was included in the simulation by the VOF model. By keeping Stefan's number as 0.12, 0.18, 0.28, melt fraction and heat flux variation inside the cavity were plotted for both cavities. From the results, solidification in the spherical cavity was faster than in the rectangular cavity. Poor thermal conductivity of PCM and lesser natural convection effects inside the cavity reduce the solidification rate more than the melting rate.

A numerical investigation of PCM in micro-channel heat sinks was presented by Hasan and Tbena (2018). Air was used as the cooling medium as a baseline comparison, then four PCM Paraffin wax, n-eicosane, p116, and RT41 were used as cooling mediums in different setups. A mixed (convection and radiation) boundary condition was applied at the top of a heat sink, and constant heat flux was given at the bottom. Seven different arrangements of PCM in microchannel heat sinks were modeled. A decrease in the Nusselt number was found when increasing the ambient temperature. From the results, it was observed that PCM placement in channels and base provides better thermal management by lowering sink temperature.

Abdulateef et al. (2019) numerically investigated the effect of optimized fin and dispersion of nanoparticles in PCM-based systems under simultaneous charging and discharging

(SCD). The optimum fin array was found by using Response Surface Method (RSM). RT82, Copper, and Al_2O_3 were used as PCM, fin material, and nanoparticles, respectively. Fins were attached on both sides of cold and hot fluid tubes for SCD. The addition of Al_2O_3 nanoparticles with PCM shows a less significant effect in the storage system. From the results, it was observed that there was an enhancement in attaining the final steady liquid fraction with the addition of fins.

Nayak et al. (2006) numerically investigated the effectiveness of thermal storage units (TSU) with PCM and the TCE. Two types of heat sink designs are made, one porous matrix with PCM and the other fins with PCM. A numerical model with different volume fractions of TCE was studied. A finite transient volume method was applied to find the optimum proportion of TCE in a TSU. The metal matrix insertion diminishes convection and enhances conduction. Melting onset of PCM was delayed with more addition of fins. Results show that a higher volume fraction of TCE material is lesser the latent heat storage since the amount of PCM volume decreases. There was a significant increase in thermal conductivity and melting rate with the addition of TCE materials.

Saha and Dutta (2015) developed a mathematical model to evaluate the effectiveness of PCM-based storage units. The mode of the heating condition is cyclic loads, and the performance is evaluated by varying the design parameters such as heat flux, heat transfer coefficient, and PCM properties. One dimensional model was presented to evaluate the melting-freezing phenomena of PCM in the preliminary design of PCM-based storage units. During melting and solidification, several parameters were evaluated, such as heat transfer coefficient, heat flux, thermo-physical properties of PCM, and the physical dimensions of storage units. A computational fluid dynamics (CFD) model was developed and compared with the results of an analytical model. No significant effect of the heat transfer coefficient was found, and the amount of PCM was directly proportional to the melt duration.

In a plate fin, PCM-based heat sink characterization of the melting process was studied numerically by Saha and Dutta (2010). The effect of an aspect ratio of different enclosures,

such as shallow, rectangular, and tall enclosures, was made and investigated. On the basis of characteristic length scales for each type of enclosure, correlations were derived. The numerical study neglected the contact resistance between PCM and the aluminum surface. It was observed from the results that convection strength diminishes with an increase in aspect ratio. Different correlations were identified for each enclosure for an appropriate characteristic length, and Nu-Ra relations based on these lengths were developed.

Srivatsa et al. (2016) numerically developed a PCM-based heat sink module without any thermal conductivity enhancer. Assumptions were made to estimate the overall heat transfer coefficient for heat loss in experiments. Numerical results were matched with experimental results by the Least Square Approach (LSA). The effect of natural convection inside the heat sink was discussed with velocity plots. The optimal heat sink geometry that maximizes the melting time was determined using the artificial neural network and genetic algorithm (ANN-GA) technique. By the assumption made from the surface of a heat sink to the surrounding, a value of U=1.81 W/m^2K was found. Reducing the heater area does not affect the system. Numerical simulation was done for optimum heat sink configuration, and the melting time was matched with the ANN-GA hybrid technique.

Luo et al. (2008) established a thermal resistance network for analyzing a mobile phone system with experiments and numerical results. A resistor was inserted to function as a heat source, and a mobile phone model Samsung SPH E2500 was used. The air gap inside the sealed case wall was small, and the flow inside the enclosure was negligible. Only conduction was the mode of heat transfer in the enclosure, and radiation was neglected. A network was formed for two heat paths, one from the chip through the keyboard and to the atmosphere & other from the chip through a battery and bottom case. To reduce the chip temperature, the biggest resistance and biggest branch should be targeted first. High thermal conductivity materials could be used to reduce the resistance offered to avoid overheating of the chip inside mobile phones.

Alshaer et al. (2015) numerically investigated the thermal characteristics of saturated carbon foam with PCM and multi-wall carbon nanotubes (MWCNT), which act as thermal

management modules. Using the volume average technique obtained mathematical model was validated with previous experimental results. Paraffin wax RT-65 was used as PCM and integrated with a high thermal conductivity CF-20, where CF-20 provides support for an efficient system. Three modules considered for simulations were 1. CF-20 module 2. CF-20+RT65 module, and 3. CF-20 + RT65/MWCNT. There was a reduction of thermal conductivity in the CF-20+RT65 module because of PCM's poor thermal conductivity, but the addition of nano carbon tubes with PCM overcame this. Surface temperature and uniform melting were found to be better in CF-20 + RT65/MWCNT module than in the other two modules.

Hu et al. (2015) proposed a PCM enclosure for storage purposes with frustum-shaped fins. Multiple PCM was incorporated into the storage system, and their melting behavior was investigated numerically. Three different PCM were arranged in series and parallel ways according to their increasing or decreasing order of melting temperature from top to bottom or from left to right of the enclosure. An optimal length ratio was found, and PCM should be filled more on the top side of the frustum-shaped enclosure. It was observed that increasing the order of PCM melting temperature from top to bottom enhances the melting inside the system.

Table 2.1 Summary of the PCM-based heat sinks during experimental investigations.

Authors	Year	Heat sink type	Investigation	Observations
Avci and Yazici	2018	Flat type	Effect of orientation	The increase in orientation angle maximizes the operating time of the heat sink
Ali et al.	2018	Square pin-fins	Different volume fractions of PCM	A less significant effect of PCM was found at lower heat flux, and by increasing the number of cycles, PCM was beneficial.
Ho et al.	2020	Water based nano-PCM	Microencapsulation of PCM	A reduction in thermal resistance was found within the enclosure when the emulsion was used.
Baby and Balaji	2012	Plate and Pin fins type	The fin volume fraction of 8 %	The enhancement ratio of fin type heat sink was better, and the pin fin type enhanced the melting/solidification more than plate fins.
Mahmoud et al.	2013	Honeycomb structured fin	Six different PCM was incorporated	Due to its less weight, the honeycomb structure possesses better enhancement compared to the machined plate fins.
Saha et al.	2008	Cylindrical pin fins	The optimal volume fraction of fins	Based on the volume fraction of fins 2%, 8%, 18%, and 27%, the number of fins also varies between 9, 36, 81, and 121. Among those, 8 % volume of fins appears to be optimal.
Errebai et al.	2018	PCM plasterboard with holes	Micro capsulation	The spacing between the perforated holes increases the phase shift by decreasing its space. Also, a smaller thickness board was recommended for enhanced performance.

Table 2.2 Summary of PCM-based heat sinks during numerical investigations

Authors	Year	Heat sink type	Investigation	Observations
Ghosh et al.	2019	The rectangular and spherical cavity	Unconstrained solidification	The presence of air during the completion of melting was considered using the VOF model, and the results illustrate that spherical cavities accelerate solidification more than rectangular.
Hasan and Tbena	2018	Microchannel	Mixed boundary conditions employed	When there was an increase in ambient temperature, the outcome had a decrease in the Nusselt number.
Mahdi et al.	2019	Combination of fins and nano additives in PCM	Simultaneous charging and discharging	The addition of fins to the walls of cold and hot tube surfaces maintains a uniform temperature distribution, and the addition of nano-particles had insignificant effects.
Luo et al.	2008	Samsung SPH E2500 model	A resistance network	The network displays a high thermal conductivity booster to be placed at the targeted spots where the peak temperature of the chip is higher.
Alshear et al.	2015	PCM with foams and nanotubes	A mathematical model based on volume average technique	The surface temperature of the heat sink is reduced, and uniform melting throughout the system was found to be better with the developed heat sink design.
Hu et al.	2015	Frustum fins	Arrangement of multiple PCM and their impact	The PCM can be filled in from the top side of the unit in increasing order of melting temperature resulting in accelerated melting.

2.4 INVESTIGATIONS OF FINS INCORPORATED PCM-BASED STORAGE SYSTEM

Ashraf et al. (2017) experimentally studied the effect of in-line and staggered fin arrangements in a PCM-based TSU. The influence of fin geometries like round and square types was investigated. The study used six PCM, namely RT-54, Paraffin wax, RT-44, RT-35HC, SP-31, and n-eicosane, with different thermal properties. Without the PCM case, the staggered arrangement performs better because the development of natural convection currents occurring by disturbance was greater. The PCM case inline arrangement shows better results than the staggered. Results show that circular inline was a better arrangement when different PCM was used in the TSU except for n-eicosane. This was because the circular shape arrangement shows uniform temperature distribution inside the heat sink. It was observed from the results for low power levels, low melting temperature PCM can be used, whereas high melting temperature PCM can be used for high power levels.

Ali et al. (2018b) designed a setup with various pin fin configurations like rectangular, circular, and triangular. Input power levels from 5 W to 8 W with six different PCM are used (RT-54, Paraffin wax, RT-44, RT-35HC, SP-31, and n-eicosane). Results recorded that triangular was an effective configuration for both PCM and without PCM cases. More fin number and a larger surface area was the reason behind the effective triangular configuration. The storage ratio was examined for triangular pin fin heat sink with different PCM, and RT-35C has the highest ratio of 68% at 5 W and 63% at 5 W. In the enhancement ratio case, effective PCM options to attain an SPT of 45^{o}C and 60^{o}C were SP-31 and RT-54.

Desai et al. (2021) analyzed the effect of fin geometry, the number of fins, and the volume of fins in electronic devices to control the peak temperature in electronic devices. In this numerical investigation, the input to the enclosure was considered as pulsed heat load conditions. Eight unique fin geometries are selected: triangle and star-shaped prism; triangle and star-shaped frustum; circular, square, triangular, and star-shaped inverted frustum. The fin number increases from 1-100, and a minimum peak temperature value was observed at 100 fins. The inverted fin geometry provides a high surface area and

increases heat dissipation. The prism fin configuration with a 20 % mass of fins provides the lowest peak temperature, and the inverted fin configuration with a 25 % mass of fins. Considering the heat dissipation from the fin surface area, the lowest peak temperature of 331.41 K was observed at star-inverted fin geometry, which was the best design.

Ji et al. (2018) investigated the effect of double-fin length in a PCM storage unit. The setting of the internal double-fin design is to provide a melting enhancement in a PCM storage unit. The fin was placed internally on the vertical sidewalls, and the effect of fin length variation on the liquid fraction was noted. A constant temperature condition of $70^{o}C$ is applied as heat input to the PCM unit. The contours show that the natural convection was bolstered when the length ratio was below 1. At the same time, increasing the length ratio above 1 diminishes the natural convection. The results reveal that the shorter upper fin and longer lower fin accelerates the melting by high heat absorption. A total melting time of 25 % was saved when considering the fin ratio as 0.25. Additionally, an optimum double-fin length setting can be obtained by reducing the length ratio further to 0.11, and maximum time saving is noted.

A 2D numerical model for the thermal management of electronic units was presented by Arshad et al. (2021). A plate-fin heat sink filled with RT-35HC as PCM was considered for the investigations. The fin volume fraction is varied by 10 % and 20 %, and fin height is varied by 10 mm, 15 mm, and 20 mm. The inclusion of fins reduces the base temperature by extracting heat from the base to the ambient. Moreover, the addition of fins provides uniform melting, and fin height of 20 mm and 20 % volume fraction fins provide better uniform melting. But with the increment of fins, there was a delay in PCM melting time, and the PCM latent heat stage was delayed by increasing the fin volume fraction. The lower temperature of the heat sink was observed in the heat sink with a higher volume fraction and fin height. A better thermal energy storage was observed with a fin height of 20 mm which is equal to the height of the PCM cavity.

During the charging/discharging cycles, the effect of fin spacing, fin volume, and cavity orientation was studied by Kasper et al. (2021). An aluminum-finned rectangular enclosure

was considered for cavity orientation investigation. A significant effect on orientation was observed during the charging cycle, whereas during discharging cycle negligible effect on orientation was observed. In an upwards-oriented enclosure, the convective flows are found dominant with an increase in fin spacing. Although, for downward-oriented enclosures, the convection flow was found to be less significant with an increase in fin spacing. An optimal fin ratio of 10-15 % with fin spacing of 25 mm provides a faster charging rate and storage capacity. On different orientations with lesser fin spacing, the heat absorption was higher, and the melting/solidification time was reduced.

Ji et al. (2018b) proposed an angled fins-based heat sink to enhance the charging cycle of the PCM enclosure. A rectangular container acts as a heat sink filled with RT42 PCM, and the heater was at the vertical side wall. Heat sinks with 0^o, $+15^o$, $+30^o$, -15^o, and -30^o, and angled parallel fins were numerically modeled. The contours of the melt fraction and the temperature were obtained to visualize the natural convection flow and heat distribution. Among all the angles, -15^o shown enhanced melting inside the heat sink than in other cases because of its orientation towards the bottom of the heat sink. Moreover, the melting time saved using -15^o was about 62 %. At the same time, the positive angle fins shows no improvement in melting and were not useful. Better suppression of non-uniform heating and better temperature distribution was noted at $-15^{o,}$ even at lower heat flux.

The combination of two different fractal fins added to the PCM storage unit was investigated by Luo et al. (2022). Lauric acid was used as the PCM, where the melting simulation was done using the enthalpy-porosity approach. The design of combined fractal fins has a better temperature distribution within the PCM, and the completion of melting time was also found to be 68 % lesser than the conventional fractal fins. By curve fitting, it was indicated that the completion of melting time is correlated with the coefficient parameter in negative exponential. The thermal conductivity of the fins was reduced when the width was minimized, and this resulted in higher heat transfer resistance between the PCM and the fins.

Xie et al. (2019) numerically presented an optimized metal fin PCM enclosure for an improvement of thermal conductance in the system. The fin structure was redesigned as a tree shape to improve the PCM enclosure's uniform melting and better thermal diffusion. An optimized tree shape fin with 20% and 30% volume fractions was designed to study the thermal performance of the PCM storage unit. A developed 2-D model with varying orientations of fins based on the enthalpy porosity technique and VOF method was studied. During the PCM melting stage, a lower source temperature and higher melt fraction are encountered using the tree-shaped fin settings. Uniformity of temperature within PCM and efficient heat diffusion were observed in the enclosure with optimized fins. Optimized tree shapes provide enhanced thermal performance than baseline comparison which was made of plate fins during upward and downward orientation heating.

Enhancement of discharging process by inserting innovative fin structure was studied by Sheikholeslami et al. (2016). The structure used was inspired by nature which was a snowflake crystal structure. Using Standard Galerkin Finite Element Method, the discharging process of the PCM-filled storage system was investigated. Initially, the fin geometry was changed to find the best suitable one, and later copper as a nanoparticle was added with PCM in a storage system to find its efficiency. The discharging process completes 4.5 and 7.8 times faster with longitudinal and snowflake fins than a case with no fins. A slight improvement in efficiency was found by adding nanoparticles. Results illustrate that employing an appropriate fin shape to the PCM system can be a better approach than nanoparticle dispersion for maximum energy storage capability and acceleration during the solidification process.

Lohrasbi et al. (2017) employed a novel V-shaped fin configuration for higher energy storage and quicker energy retrieval in a PCM-based enclosure. The fin configuration was determined using the Response Surface Method (RSM) for both charging and discharging cycles. The optimum finned structure was compared with conventional fin arrays, and results were obtained through numerical investigations. The energy storage capacity is higher during charging cycles when the fin branch angle and fin branch length are increased. During the discharging cycle, the energy storage capacity remains constant for

different fin branch angles, but energy storage capacity increased with an increment in fin branch length. Similarly, there was no considerable improvement in energy storage capacity for different fin branch thicknesses during both cycles. The phase change rate behavior was found to be faster for both cycles when a V-shaped fin structure was incorporated.

2.5 INVESTIGATIONS OF FOAMS EMBEDDED PCM-BASED STORAGE SYSTEM

Baby and Balaji (2013b) experimentally analyzed the effect of orientation on porous matrix combined PCM module. A tracking system was developed to change the orientation of the heat sink. A porous copper matrix with a porosity of 0.86 and 10 pores per inch (PPI) was press fitted in an aluminum heat sink. To examine the effect of metal foam in the PCM cavity, two enhancement ratio was determined. The first enhancement ratio was to define the metal foam effect, and a reasonable improvement is noticed with higher power levels. Whereas the second enhancement ratio was to define the effect of PCM, and it was observed that there is a negligible impact with varying power levels. Orientation angles were varied from 0^{o} to $210^{o,}$ and the PCM used was n-eicosane. From the results, it was perceived that the orientation does not have significant effects on the metal matrix-filled PCM-based heat sinks.

Chen et al. (2014) did an experimental study on PCM based heat sink filled with metal foams. Aluminum open-cell metal foams were used, and PCM used was paraffin wax. Melting of PCM behavior was observed at the pore scale by an infrared camera and optical microscope. A 2-D Lattice Boltzmann model was developed to simulate the melting of PCM in foams filled heat sink. An inclined melt front was found in the case of the PCM heat sink without foams, and a straight melt front was found in the case of the PCM heat sink with foams. It shows that there was a uniform distribution of heat inside foam immersed PCM heat sink. From the results, the influence due to convection was less with metal foams since conduction dominates the whole melting process. Further, the melting rate decreased with an increase in porosity. The 2-D model agreed qualitatively with experimental observations.

The performance of PCM-filled copper foam thermal storage was investigated experimentally by Rehman and Ali (2018). Copper foams with different porosity and PPI are used in this paper. First, copper foam with a porosity of 0.95 and pore density of 15 PPI, and second, copper foam with a porosity of 0.97 and 35 PPI. Varying PCM volume fractions 0, 0.6, 0.7, 0.8 under a heat load of 8-24 W were investigated. Heat transfer was reported to be faster for lower porosity due to its conduction-dominant nature. The reduced base temperature was also observed with lower porosity during solidification. The volume fraction of PCM dictates the duration of the phase change process. Hence, copper foam with a porosity of 0.95 with 0.8 volume fraction shown a good reduction in base temperature.

Zhu et al. (2018) experimentally studied the performance of PCM-based heat sinks filled with copper foams. The influence of filling of copper foams according to height ratio and effects of pore size were investigated. With an increasing filling height ratio, the thermal performance was enhanced. When high heating power input was applied, foams with larger pore sizes shows better results. Whereas for low heating power levels, the pore size effect was insignificant. Increasing the filling height ratio increases the cost and the performance gain. For effective thermal performance, partial filling of foams was found to be sufficient and feasible. A new parameter called filling effectiveness was introduced to assess the performance gain and saving cost. From this parameter, 2/3 partial filling of metal foams can be more economical than fully filled metal foams. The partial filling can reduce the weight of the PCM unit, along with a minor loss in thermal performance.

Similarly, another author, Zhao et al. (2021), studied the effect of PCM-based heat sinks using a partial filling of metal foams. In this study, they incorporated graphite foam into a 2D rectangular PCM storage unit. The heating condition was applied from the left side wall of the enclosure. Four porosities, namely, 0.8, 0.85, 0.9, and 0.95, were compared, and results were obtained. Their results interpret that fully filled foams with higher porosity are preferred for an effective heat sink with a fixed volume of foams. 0.9 porosity exhibited a better heat transfer behavior within the storage system among the four porosities. Later, the 0.9 porosity was fixed for partial filling, and four cases were examined. The foams filled

closer to the heat input side cases manifest a better melting and solidification process compared to the other layouts.

Mahdi and Nsofor (2018) employed multiple-segment metal foam and also discussed the effect of different heat sink arrangements. They also developed a mathematical model corresponding to charging and discharging cycles, with the inclusion of non-Darcy effects. Four different arrangements of metal foams were considered with a fixed porosity of 0.95. The energy stored during both cycles were enhanced when the cascaded metal foam was arranged in the heat flow direction. Non-uniformity of temperature distribution was suppressed by cascading of metal foams by eliminating the temperature differences within the PCM. But, the convection flow is strongly impeded, and the conduction was found to be dominant by the employment of metal foam. As the number of cascading foam regions increases, there is an acceleration of melting and solidification rate.

Dinesh and Bhattacharya (2020) developed a numerical model to study the effect of pore size in a PCM-filled heat sink. The pore size variation notably affected the energy absorption rate and melting behavior. The complete melting period was shorter for smaller pore radii for both high and low porosity values. Lower porosity for similar pore size provided higher energy absorption in a heat sink. With the presence of large pores, a higher melting rate was seen initially, and at the later stage of melting, the melting rate deteriorated.

An experimental study of the melting behavior of PCM with the addition of metal foams was presented by Zheng et al. (2018). They included the copper foam to study the effect of heating position on the melting rate with paraffin as PCM. They also developed a numerical model based on the one-dimensional temperature volume averaging method. Using this approach, they explored the influence of foam-filled PCM during the charging process. Adding copper foams reduced the thermal resistance and the melting time by 20.5 % compared with pure PCM. In different heating scenarios, the top wall heating provides a slower melting with a 10 % higher melting time, and a bigger temperature difference of

10^{o} C is detected. The numerical model developed coincided with experimental results and can be better for designing a PCM storage system embedded with metal foams.

Mancin et al. (2015) investigated the effect of a PCM-based heat sink with the addition of metal foams. They incorporated three paraffin waxes with different melting temperatures, and the heat input considered were 6.25, 12.5, and 18.75 kWm^{-2}. The foam porosity is fixed at 0.95, but the pore sizes were varied by 5, 10, and 40 PPI. The experiment results illustrate that the heat sink's surface temperature is lowered, and the presence of metal foams provides a uniform temperature distribution. But there was only a slight difference in output when three different pore sizes were inserted. From the video recorded, it was clearly visualized that the onset of PCM melting was delayed, but the completion of melting was faster. This is because of the strong influence of the copper foams, which provide a higher heat transfer path within the PCM.

For a copper-embedded PCM enclosure, a two-equation non-equilibrium numerical model was developed by Tian and Zhao (2011). In this investigation, they coupled both heat conduction and convection in the developed model during phase transition. The inclusion of foams in the RT58 PCM increases the heat transfer performance by ten times. The natural convection due to buoyancy force was weaker and did not impact the heat transfer within the PCM. The reason for this weak convective flow observed is the high viscosity and poor thermal expansion coefficient of the PCM. The numerical results manifest that the foams with less pore size and porosity can provide high thermal performance.

2.6 INVESTIGATIONS OF PCM-BASED ENCLOSURES WITH OTHER ENHANCERS

Joseph and Sajith (2019)mixed graphene fillers with PCM to improve thermal conductivity. The experiments were carried out under uniform and pulsed heat input under passive and forced cooling modes. The graphene filler was synthesized, and the blending was done for various concentrations. The thermo-physical parameter of the synthesized PCM was measured using differential scanning calorimetry, thermo-gravimetric, Rheometer, and thermal constant analyzer The added fillers enhance the thermal conductivity of the composite. When the heat sink was under passive cooling, the rise in

the temperature between a heat sink and paraffin was reduced. During their forced cooling analysis, the fan onset temperature was prolonged for a considerable time at any type of load. Their study also indicated that an 11-23 % enhancement in energy savings for a hybrid heat sink was noted.

A 3D numerical model was developed by Du et al. (2019) to examine the effect of PCM combined with nano additives. A spiral coil exchanger was designed with a combination of paraffin wax and copper nanoparticles to enhance effective conductivity. They observed that the melting rate was increased and saved 19.6 % of the melting time compared with a pure PCM-based heat sink. The inclusion of copper nanoparticles attenuated non-uniformity. A flow rate above 0.75 m^3/hr is not recommended while designing a similar heat exchanger due to the higher energy utilization of the pump. Increasing the heat transfer fluid inlet temperature and flow rate can minimize the melting time by 34.68 % and 9.29 %, respectively.

The effect of adding graphite particle fillers was evaluated by Srinivasan et al. (2017). Dispersing graphite particles in the n-eicosane, the thermal conductivity and viscosity were measured as a temperature function. As a result of filler usage, the thermal conductivity, and viscosity had been drastically improved. A 3.5 % volume of additives increases thermal conductivity by 450 % and viscosity by 1200%. The increment in viscosity reduced the mobility of PCM during the liquid state and reduced the convection flows. Furthermore, enlarging the concentration of nano additives lead to the agglomeration of PCM into clusters.

Sadrameli et al. (2019)experimentally investigated the addition of nano-diamond particles to paraffin wax in microencapsulation. The preparation of microcapsules was carried out by a complex method called coacervation, and the efficacy of capsules was determined by a heating test. A microcapsule with a spherical shape was tested using differential scanning calorimetry to obtain its thermo-physical properties. The measurements show that the composite has an enhanced thermal conductivity of 50% and can be an appropriate filler for PCM-based enclosures. In microencapsulation, an optimum amount of addition of

nano-diamond was found to be 5%, and further addition decreases the stability of the composites. The encapsulation efficiency was found to be decreased with an increment of the additive amount and emulsification time.

During the melting process, a non-dimensional parametric investigation was carried out by Faraji et al. (2021). They performed a numerical analysis to evaluate the hydrodynamic behavior of a PCM when it is dispersed with copper nanoparticles. The results summarized that the increase in an aspect ratio of enclosure and decrease in Rayleigh number provides the same result. i.e., there was a rise in steady-state temperature. The operating maximum temperature and time can be prolonged by extending the substrate thickness. Further addition of PCM or the nano-particles can decrease the plateau temperature. So, an optimum amount of PCM and nano-fillers should be determined while manufacturing PCM-based heat sinks.

Cheng and Zhai (2018) developed a three-stage cascaded cold storage unit. The storage unit is filled with three different PCMs named PCM-1, PCM-2, and PCM-3 with a freezing temperature of 13^{o}C, 14.5^{o}C, and 17^{o}C, respectively. These three PCM are comprised of capric-lauric acid eutectic and unlike mole fractions of oleic acid. A mathematical model was developed, and it was validated with experimental data. Their observations summarize that even though less exergy storage was observed in a cascaded unit, the cascaded unit acquired higher exergy efficiency than the single cascaded storage unit. When the heat transfer fluid flow rate decreases, the solidification rate is improved by 35 %-19 %, and the exergy efficiency is enhanced by 2.4 %-4.8 %.

A brief analysis of multiple PCMs incorporated into the storage system was presented by N. (2019). According to his review, multiple PCMs yield faster charging and discharging rates than single PCM, and also uniform exit temperature was noticed with multiple PCM storage units for a heat exchanger. Also, in multiple PCM storage systems, an optimal melting temperature, optimal PCM volume, and optimal melting temperature difference between the adjacent PCM should be considered. These factors can help in better thermal performance and better efficiency than the single storage unit. Thermodynamic

irreversibilities can be minimized by employing multiple PCMs. But, incorporating multiple PCM reduces the energy storage capability of an enclosure due to the different thermal properties of the PCM. Another limitation was finding PCM with a narrow melting temperature range, high latent heat, and high thermal conductivity.

Elsanusi and Nsofor (2021) evaluated the melting process of a storage unit with multiple PCMs. A Navier-strokes dependent computational model was developed, and the arrangement of multiple PCM in series and parallel was compared. The multiple PCM unit defines that the PCM is not mixed but placed in a different layer next to each other. The series arrangement of multiple PCM enhances the convective flow whereas the parallel arrangement improves the conduction slightly and diminishes the natural convection. The series arrangement with both conduction and natural convection modes of heat transfer impart a shorter melting time than the other cases. The multiple PCM arrangements also increased the energy storage capacity by 25 %.

Mahdi et al. (2020) investigated the solidification of PCM in different arrangements. The hybrid system consists of only multiple PCM, multiple PCM with metal nanoparticles, and multiple PCM with cascaded metal foams. The PCM employed in the storage unit are RT-55, RT-60, and RT-65, and aluminum was the material used for nano additives and metal foams. The uniform temperature distribution was found with an increasing number of PCM layers. The energy retrieval was found to be higher when the multiple PCM is bonded with nano-additives and metal foams. The two-PCM and three-PCM units provide a solidification rate of 5.2 % and 8.7 % higher than the one-PCM units. A hybrid system with metal foam and multiple PCM has shown a drastic discharging rate which is 17 times faster compared with others.

Incorporating multiple PCMs in a solar still to increase productivity was investigated by Vigneswaran et al. (2019). It was observed that multiple PCM-based solar still produces higher yields while their efficiency is favorably higher. The existence of multiple PCM in solar still improves the temperature difference between the water and glazing surface. Also, it favored maintaining the still at a higher temperature for an extended period of time. The

yield for multiple PCM compared with single PCM and no fin was found to be 19 % and 9.5 % higher. Multiple PCM's efficiency and exergy efficiencies are 46.29 % and 3.52 %, which is higher than the conventional and single PCM still.

Ezra et al. (2016) numerically analyzed the effects of multiple PCM incorporated in a storage unit. The melting time of PCM extends with an increase in the number of tube rows and shortens with a decrease in the mass flow rate of heat transfer fluid. Also, when the tube rows are kept closer to the entry, they melt slower than the tube rows kept closer to the exit. In multiple PCM storage units, there was a uniform temperature difference between the PCM and heat transfer fluid over the entire length. Additionally, in their mathematical model, sensible heat capacities of tubes and molten PCM were also considered, which leads to comprehensive relations. Those relations provide an optimal configuration for any number of materials and their melting temperature span, leading to shorter melting.

Table 2.3 Summary of different enhancers used in the PCM storage unit.

Authors	Year	Enhancer type	Investigation / Approach	Observations
Ashraf et al.	2017	fins	In-line and staggered fin arrangements.	The staggered fin arrangement was preferred for the case without PCM, and the in-line fin arrangement was a favorable choice for the case with PCM. Moreover, the circular fins display uniform melting.
Ali et al.	2018	fins	Fin shapes- rectangular, circular, and triangular	The triangular fins exhibit better melting and solidification rate among the three shapes exerted. Based on the critical temperature, the PCM can be selected accordingly.
Desai et al.	2021	fins	Fin geometry and number of fins	The inverted fin arrangements, which possess higher surface area, appears to be effective structure. Similarly, the maximum reduction in peak temperature was observed in the case with more fins.
Ji et al.	2018	fins	Double-fin length	When the fin ratio was below 1, there was a more heat absorption rate. This defines that shorter upper fins and longer lower fins expedite the melting operation.
Jinlong et al.	2019	fins	Tree shaped fins	The optimized tree shape fin design boosts a storage system's energy supply/retrieval corresponding to the upward and downward orientation heating.

Sheikholeslami et al.	2016	fins	Snowflake crystal structure	The uniform melting within the PCM and high heat absorption was observed with the innovatively developed snowflake design.
Baby and Balaji	2013	foams	Porosity 0.86 and PPI 10	The orientation of metal foam comprised heat sink was examined, and negligible influence of orientation was deduced under different heat loads. The presence of solid metal foams impedes natural convection.
Rehman and Ali	2018	foams	Porosity-0.95, 0.97 PPI-15, 35	By varying the amount of PCM with different heat inputs of 8-24 W, it was explored that there was a reduction in base temperature with lower porosity. The uniform temperature distribution within PCM was also spotted.
Zhu et al.	2018	Foams	Partial filling-0.96 fixed porosity and 15,30 PPI	In conclusion, 2/3 partial filling of metal foams can be selected because of its less weight. Besides, a minor loss of thermal outcome was also noted.
Zhao	2021	Foams	Partial filling with porosity of 0.8,0.85,0.9, and 0.95 & 10 PPI is fixed	When the foams are packed full, 0.9 porosity PCM enclosure enhances the heat transfer rate. With this 0.9 porosity, partial filling of metal foams was investigated, and it manifests better charging and discharging cycles.

Mahdi and Nsofor	2018	Foams	Fixed porosity and PPI-0.95 and 10	Metal foams are arranged in different manners, and the grouping of metal foams in the heat flow direction enhances the stored energy capacity.
Mancin et al.	2015	foams	Fixed porosity and PPI-5,10, and 40	The maximum junction temperature was reduced with the presence of foams, but only a marginal difference was noticed with varying pore sizes.
Joseph and Sajith	2019	Nano additives	Graphene fillers	During natural and forced convection, the additives immersed in PCM reduced the peak temperature, and the fan onset temperature was also extended.
Du et al.	2019	Nano additives	Copper particles	A 19.6 % melting was saved when the fillers were bonded with the PCM. It also disturbed the non-uniformity within the enclosure.
Sadrameli et al.	2019	Nano additives	Nano-diamond particles	The diamond particles and n-eicosane were microencapsulated together. This encapsulation enhanced the thermal diffusivity rate by 50%.
Faraji et al.	2019	Nano additives	Copper particles	By extending the substrate thickness, the operating failure temperature was prolonged with the help of optimum nanofiller concentration.

Cheng and Zhai	2018	Multiple PCM	Mathematical model	From the mathematical model derived, the cascaded unit manifests less exergy storage and higher exergy efficiency. Also, the solidification rate was improved by 35-19%.
Narashimhan	2019	Multiple PCM	Critical review	The review summarized that the irreversibilities could be diminished by employing multiple PCM. Although, multiple PCM storage systems reduce energy storage capacity compared to a single PCM system.
Elsanusi and Nsofor	2021	Multiple PCM	Navier-stokes equation-based numerical formulation	The arrangements of multiple PCM impact on the heat sink was evaluated. When both conduction and convection were considered, the series arrangements impart a shorter melting time.
Mahdi et al.	2020	Multiple PCM	Enthalpy-porosity technique	The uniform temperature distribution was found with an increasing number of PCM layers in the storage unit. Compared to a two-PCM layout, a three-PCM layout provides a faster solidification rate.
Vigneswaran et al.	2019	Multiple PCM	Experimentation	In solar still, incorporating multiple PCM escalates the temperature difference between the water and glazing surfaces, and the yield was also elevated.

2.7 DIFFERENT OPTIMIZATION TECHNIQUES EMPLOYED IN PCM INVESTIGATIONS

Nagose et al. (2008) used a Genetic algorithm approach to find the optimal configuration of PCM-based heat sinks to extend the operating time of the sink. This operating time is the critical temperature of the electronic circuit temperature. The PCM employed was n-eicosane, and a constant heat flux boundary condition was applied at the top wall. The numerical results yield an excellent energy balance, i.e., the energy entering the heat sink is equivalent to the energy stored in the base material and PCM. The amount of PCM in the heat sink initially impacts the sink operating time, and over a maximum limit, there was a decrement in operating time. In this study, to maximize the operating time and completion of PCM melting, GA was implemented. Based on the results, two correlations were proposed to relate the operating time to parameters such as the amount of PCM, heat spreader thickness, and heat sink height.

From the experimental results, Baby and Balaji (2013) used a hybrid optimization technique to maximize the operating time to reach a set temperature. Experiments were conducted by varying the number of fins (33, 72, and 120) in a pin-fin heat sink with the same volume fraction. Then different volume fractions of the PCM (ϕ=0.3, 0.6, and 1) were also used in the experiments to determine its effects. Paraffin wax and n-eicosane were used as PCM with different power levels. An ANN-GA combined algorithm was attempted to provide the optimum number of fins by keeping the volume fraction constant. From experimental results, using paraffin as PCM, the 72-pin fins perform better than the others. By hybrid algorithm keeping ϕ=0.95 as constant, the optimal number of fins for a PCM-based heat sink was 77.

A composite pin fin matrix heat sink with PCM was investigated experimentally by Srikanth et al. (2015). To stretch the operating time of the composite heat sink during the heating and cooling cycle, an optimized setup was determined. The heat sink and pin fin was made of aluminum heat sink inserted with n-eicosane as PCM. An ANN-GA based optimization technique was used, and inputs were fed into the algorithm from numerical simulation output. Multi-objective optimization was considered for this study, maximizing

melting time and minimizing solidification time. In the solidification process, spacing between fins should be less for effective cooling.

For a shell and tube heat exchanger, a density-based topology optimization was presented to accelerate the melting and solidification (Pizzolato et al. 2017). The objective was based on the structure of the fins provided in the enclosure. To provide an efficient geometry, no assumptions are considered for the fin structure. Results illustrated that for a melting process, the fins elongated toward the bottom of the shell provide a 27 % reduction in time. In solidification, an 11 % reduction in time was observed with the absence of fin bifurcation and fin branch length. Convective transport with an optimal fin shape can increase the charging and discharging cycles. They also found a modified version of the fin structure for easy manufacturing and conserves the original structure.

A straightforward approach to finding a reduced sink height in electronic devices was proposed by Levin et al. (2013). In this study, the number of fins, PCM percentage, and thickness of fins were varied, and the results were interpreted. A numerical investigation was performed to obtain the safe operating temperature limit neglecting the convection. It was shown that when the difference between the liquidus and sink temperature increases, thinner fins are preferred, and the PCM amount is increased. Similarly, decreasing the fin length and increasing the number of fins leads to a rise in the optimal amount of PCM. In their study, they concluded that the PCM does not melt entirely when the sink reaches critical time due to the wide melting range of PCM used. This leads to the partial filling of PCM can be found effective for a heat sink.

Augspurger et al. (2018) designed an optimal PCM-based system using a dynamic kriging approach. The optimization technique was based on a few numerical strategies: precise Cartesian grid mesh, profound coupled schemes, minor loss of accuracy in evaluating objective functions, and de-escalating the number of simulations. It was observed that the high aspect ratio heat sink provides high velocity within PCM. But the convective flow within the enclosure has very marginal effects on the heat sink design. Their discussions

disclosed that the overall configuration (aspect ratio) of the setup plays a more vital role in designing finned heat sinks than the internal structures.

A desirability function technique was introduced by Mozafari and Lee (2022) to optimize the dual PCM-filled enclosure. With different set point temperatures, the objective function considered was extending the melting time and shrinking the solidification time. The response surface method was used to find the relation between the objective functions and design parameters. Results indicated that the height of the fin is the most influencing design parameter, and base thickness was the least influencing design parameter. The validity of the obtained functions was checked using the employed variance analysis approach. The optimized design possesses a 7 % extended charging period and a 4.2 % shortened discharging period. For a compact cooling setup, the reference heat sink total volume was decreased to 23 % to achieve an efficient design.

Huang et al. (2022) employed a low melting point alloy in the PCM-based storage system to increase its efficiency. The comparison of three single PCM-filled enclosures and cascaded PCM enclosures is made experimentally. Under different heat inputs, the cascaded PCM enclosure prolongs the sink operating time about 7.2 % longer than the single PCM enclosures. As mentioned in the earlier interpretations, the melting temperature difference between the PCM incorporated enhances the thermal performance of a storage unit. The GA-optimized heat sink decreases the temperature-rising rate of the heat sink by more than 13.6 % of the original heat sink. The 1D numerical simulation exhibited a faster cooling rate using cascaded PCM in electronic cooling.

Based on the FOM approach, Singh et al. (2022) designed an optimal composite PCM-based heat sink. The balance between effective thermal conductivity and energy storage capacity was considered here. The design points considered are the total volume of composite and interfacial heat transfer area. The effective thermal conductivity of the composite was purely dependent on the enhancer used and not on the PCM added. The ability to store more energy depends on the latent heat of the PCM, and this effective

storage was formulated with an expression. The optimized heat sink design was compared with other models, and a maximum FOM was perceived with a nominal metal volume.

Table 2.4 Summary of different optimization approaches implemented on a PCM enclosure.

Authors	Year	Method	Observations
Nagose et al.	2008	GA	The GA technique was introduced to maximize the operational time and completion of melting. The correlation is derived based on the parameters such as the amount of PCM, heat spreader thickness, and heat sink height.
Baby and Balaji	2013	ANN-GA combined	With varying the number of fins and PCM volume fraction, the maximization of time to attain a set temperature was established. The combined algorithm provides the optimum results of a PCM volume percentage of 95 and fin numbers of 77.
Pizzolato et al.	2017	Topology optimization	A discrete evaluation was done for a beneficial heat exchanger with PCM. During the charging cycle, the fins elongated towards the shell bottom, reducing the operating time by 27 %. Whereas, in the discharging cycle, an 11 % reduction in time was observed with the absence of fin bifurcation and fin branch length
Augspurger et al.	2018	Dynamic kriging approach	From their outcome, it was understood that the optimum layout was dependent on the enclosure aspect ratio rather than the internal structures. Also, the convective flow was less vital in the heat sink design.
Mozafari and Lee	2022	Desirability function technique	Extending the melting time and shrinking the solidification time for different set temperatures was considered in a dual PCM-filled enclosure, and a relation was obtained. The optimized design possessed a 7 % extended charging period and a 4.2 % shortened discharging period

2.8 RESEARCH GAP

Building on the literature review, the authors have identified notable research gaps that warrant further investigation and form the basis for the current study.

Integration of Enhancer Types: Combining enhancer types can enhance heat transfer, but optimal integration is not well-understood, creating a research gap in electronic cooling.

Optimal Design Considerations: Designs aiming for improved thermal outcomes lack in-depth exploration, and trade-offs between parameters impacting heat transfer efficiency need further investigation.

Limited Parametric Investigation: The literature identifies parameters affecting PCM-based heat sinks, but there's a gap in a systematic investigation considering the simultaneous influence of multiple factors.

Lack of Discussion on Specific Enhancer Types: A research gap in providing a detailed analysis of enhancer types and their specific impacts on heat sink performance is observed.

Thermal Performance vs. Energy Storage Capacity: The trade-off between heat transfer enhancement and energy-storing capacity due to the use of enhancers is acknowledged. However, there is a need to identify a balanced design that optimizes both thermal performance and energy storage capacity.

The limitations of extensive experimentation due to high cost and time consumption is acknowledged and a solely experimental approach cannot comprehensively explore the parametric investigation on heat sink characteristics.

2.9 MOTIVATION AND SCOPE FOR THE PRESENT STUDY

Based on the apprehension from the available works of literature, it is understood that the numerical and experimental perceptions are required more to acknowledge the influence of thermal conductivity enhancers in a PCM storage unit. Besides, the PCM behavior and energy-storing capacity of the heat sink with enhancers need to be analyzed with numerical and experimental evaluation. But, the exploration of the parametric investigation on the

heat sink characteristics cannot be done extensively through only experimentation. Experimental research results in high-cost and consumes plenty of time. Hence, the numerical interpretation is convenient for providing the effect of enhancers on the heat sink along with a few experimentation analyses.

Furthermore, it is understood that the enhancement of heat transfer performance can be achieved with the help of combining two distinct enhancer types. Meanwhile, such design happens at the expense of a low amount of PCM, which leads to less energy-storing capacity. Therefore, many researchers reported an optimum heat sink design to attain better thermal outcomes and marginal reduction in PCM volume. Those designs considered the consequences of varying PCM volume, fin size, fin spacing, foam porous and porosity, enclosure aspect ratio, nano-additives concentration, and cascading more PCM. These parameters overall influence the heat transfer characteristics of PCM-based heat sinks with the presence of thermal enhancers. From this insight, the foremost investigation of this thesis emphasizes the numerical and experimental investigation of PCM-filled heat sink with different thermal enhancers. For electronic cooling, with the contemplation of the above-stated scope, the objective of the present study is listed below.

2.10 OBJECTIVES OF THE PRESENT WORK

1. To numerically investigate the effect of the hybrid enhancers comprised of horizontal fins and partially filled foams in a PCM storage unit during charging and discharging cycles.
2. To provide an optimum and effective design for a PCM-filled hybrid heat sink with the combination of fins and foams for prolonged charging and shortened discharging cycles.
3. To numerically examine the heat transfer performance of PCM-based heat sink with multiple PCM integration. Also, to obtain the outcome of fin orientation in multiple PCM enclosures for different heat fluxes and initial conditions.
4. To experimentally investigate the impact of variable height fin assembly over the constant height fin assembly under the constant and pulsating heat loads in a PCM stored enclosure.

2.11 CLOSURE

An elaborate discussion of the earlier studies and investigations by several authors into the problem considered was presented. The scope and objectives of the current study are listed in this chapter. The present objectives are incorporated in the forthcoming chapter, and numerical and experimental approaches carry out a detailed analysis. The next chapter elaborates the numerical investigations of combining fins and foams.

CHAPTER 3

INVESTIGATION OF THE HYBRID HEAT SINK WITH FINS AND FOAMS IMMERSED IN A PCM-BASED UNIT

3.1 INTRODUCTION

This chapter exhibits the numerical demonstration of a hybrid heat sink comprised of two types of heat sink, 1. vertical and horizontal fins combined together, and 2. Horizontal fins with partial foam filling. In this present chapter, two types of fin shapes - rectangular and tapered, are provided, and a heat sink with no fin case is used as a baseline comparison during melting. Further, the addition of tapered fins to a metal matrix with varying filling heights is investigated. For all the cases, the solidification process is also discussed. The temperature distribution within the system, convection role, melting, and solidification rate are investigated in detail.

3.2 SELECTION OF HEAT SINK SIZE

The dimensions used in the analysis of heat sink thermal performance for electronic cooling from the earlier studies are listed in Table 3.1. Based on the list, it is understood that the heat sink with dimensions of 100 x 50 mm can be selected. Since the chosen dimensions fall within the range of the already implemented heat sink dimensions.

Table 3.1 Heat sink dimension selected by different authors.

Authors	Title	Heat sink dimensions (mm)
Jalil et al. (2022)	Cooling performance investigation of PCM integrated into heat sink with nanoparticles addition	114 x 53 x 40
Rehman et al. (2018)	Copper foam/PCMs based heat sinks: An experimental study for electronic cooling systems	100 x 100 x 25
Wang and Yang (2011)	Three-dimensional transient cooling simulations of a portable electronic device using PCM in multi-fin heat sink	97 x 72 x 18

Kurhade et al. (2021)	Computational study of PCM cooling for the electronic circuit of smart-phone	150 x 80
Al Siyabi et al. (2018)	Multiple PCM Configuration for PCM-Based Heat Sinks—An Experimental Study	60 x 30 x 30 (PCM cavity)
Ghanbarpour et al. (2021)	Evaluation of heat sink performance using PCM and vapor chamber/heat pipe	90 x 40 x 8
Sheikh et al. (2022)	Heat transfer enhancement of a bio-based PCM/metal foam composite heat sink	106 x 96 x 8 (2 mm thickness)
Tharwan and Hadidi (2022)	Experimental investigation on the thermal performance of a heat sink filled with PCM	120 x 120 x 50
Zheng et al. (2018)	Thermal performance of copper foam/paraffin composite phase change material	100 x 100 x 30
Ling et al. (2020)	Performance study of phase change materials coupled with threedimensional oscillating heat pipes with different structures for electronic cooling	90 x 80 x 50
Ren et al. (2020)	Thermal management of electronic devices using pin-fin based cascade microencapsulated PCM/expanded graphite composite	112 x 112 x 27

3.3 COMPUTATIONAL DOMAIN

A rectangular 2D model with an aluminum enclosure of 104 x 52 mm is developed, as shown in Figure 3.1. PCM cavity dimension is 50 x 100 mm, and a 2 mm thickness of the aluminum substrate is provided, which acts as a thermal spreader. The heat source is kept at the bottom beneath the aluminum substrate. The PCM used in this study is n-eicosane, and the thermal properties of the PCM are listed in Table 3.2 Srivatsa et al. (2016).

Drawing from the commercially available materials within the specified temperature range, n-eicosane stands out for its high latent heat of fusion, rendering it an effective energy storage material during phase change. Although a few other phase change materials

(PCMs) also exhibit high latent heat of fusion within the considered temperature range, n-eicosane distinguishes itself as a more cost-effective and widely available option. Hence, these characteristics position it as a practical choice for selecting for the analysis.

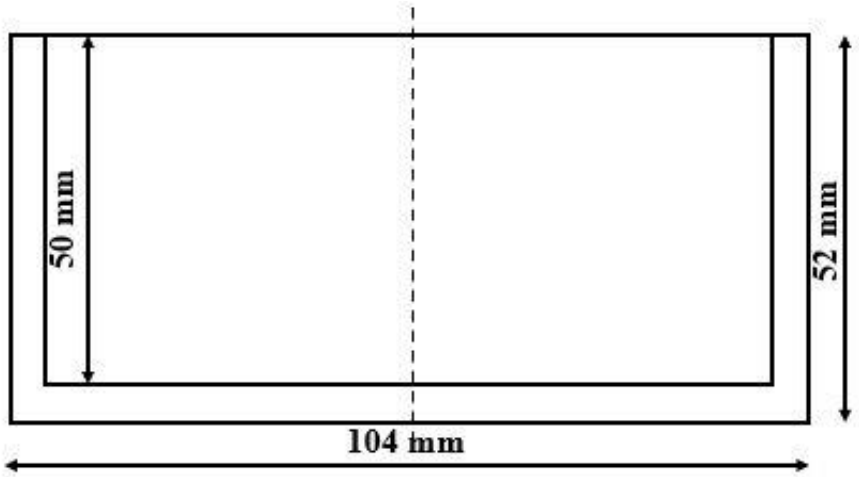

Figure 3.1 2D geometry of heat sink.

Table 3.2 Properties of materials used Srivatsa et al. (2016).

Material	ρ (kg/m^3)	k (W/mK)	c_p (kJ/kg K)	T_m (^oC)	β_0 (1/K)	L (J/kg)	μ (kg/ms)
n-eicosane	780	0.16	2200	36.5	0.001	237,000	0.00355
Aluminum	2719	202.4	871	---	---	---	---

Since it is symmetrical, only half of the side is taken for the study, which reduces the computational time. Five types of heat sinks are developed, keeping PCM with no fin as a baseline comparison. In the first case, rectangular fins with a fin thickness of 7 mm and 20 mm fin height and tapered fins with a bottom length of 10 mm, top length of 4 mm, and fin height of 20 mm are considered. Both fins are of the same cross-sectional area and protrude from the same positions. The area occupied by the fins is one-sixth of the area of the PCM cavity. The area of a single fin is 1.4×10^{-4} mm^2. Thus, the reduction in the volume of PCM percentage in the heat sink is 16.8 %. Detailed dimensions are given in Figure 3.2.

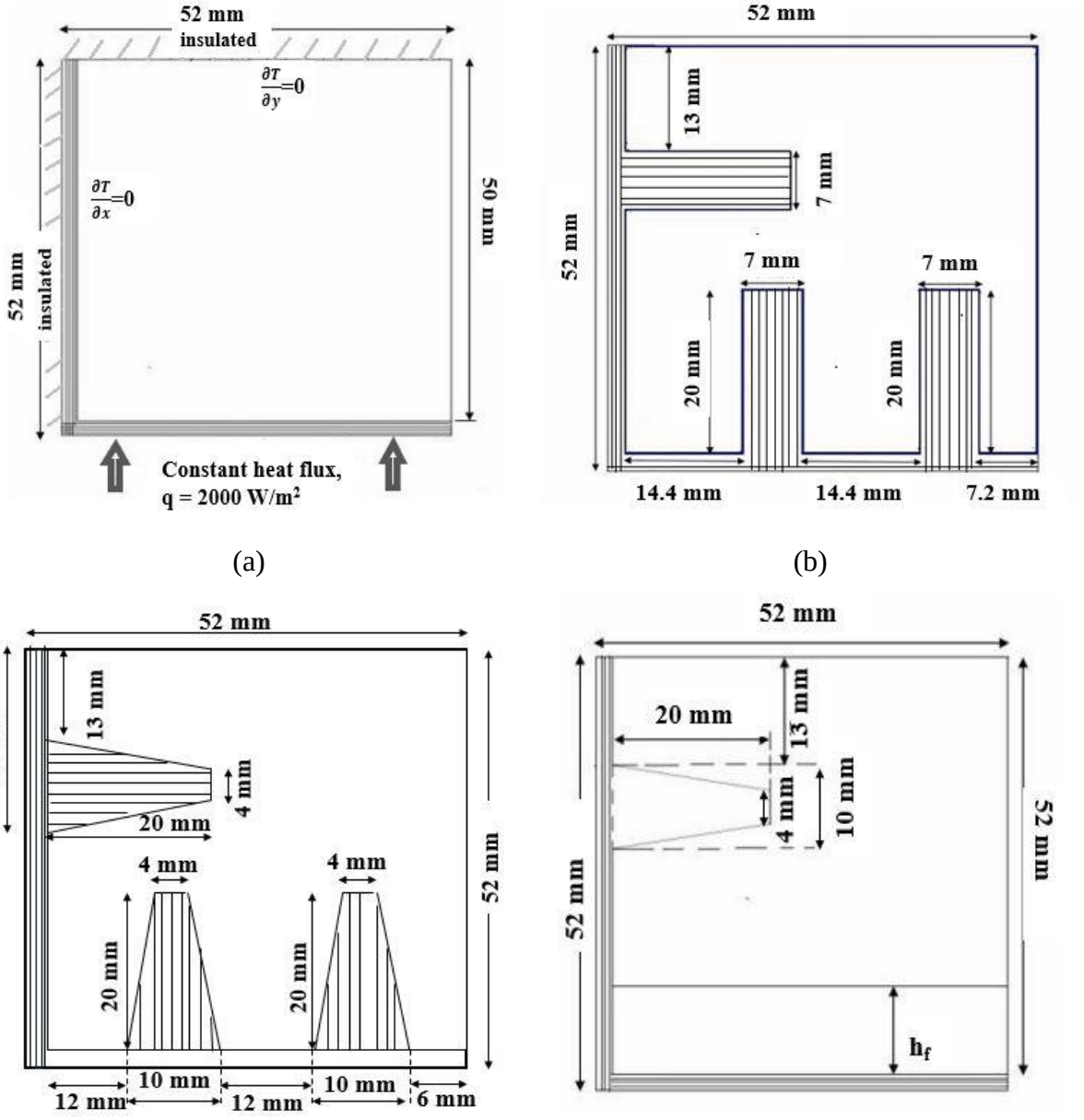

Figure 3.2 Heat sink with different geometry.

In the second case, foams with different heights are filled in the aluminum heat sink. Foam is made of aluminum with 90% porosity and 10 PPI. The filling height is varied from 10 mm, 15 mm, and 20 mm from the bottom of the sink. Foams replace the fins at the bottom wall, and at side walls, tapered fin is placed.

3.4 GOVERNING EQUATION

3.4.1 Enthalpy-Porosity Technique

Melting and solidification of PCM are done using ANSYS Fluent based on the enthalpy porosity technique. In this technique, the solid/liquid interface in the phase change process is not tracked explicitly. Alternatively, in the PCM domain, an amount of liquid phase is computed at each cell volume. This is called a liquid fraction and is derived from enthalpy balance. The liquid fraction of PCM is given by Φ; this gives how much the amount of PCM melts in a unit cell. Where 0 determines PCM is still in the solid phase, and one shows the PCM melted completely. The value between regions 0 and 1 leads to a mushy zone, where the PCM is semi-solid.

Continuity and Momentum equations:

$$\frac{\partial \rho_p}{\partial t} + \frac{\partial (\rho_p u)}{\partial x} + \frac{\partial (\rho_p v)}{\partial y} = 0 \tag{3.1}$$

$$\rho_p \frac{D\vec{v}}{Dt} = \mu \nabla^2 \vec{v} - \nabla P + \rho_p \beta_0 (T_m - T)\, \vec{g} + A\, \frac{(1-\Phi)^2}{(\Phi^3 + \lambda)} \vec{v} \tag{3.2}$$

where ρ_p is the density of PCM and β_0 is the coefficient of thermal expansion.The last term on the right side of Eq. (3.2) is the source term. It provides the effect of phase change in the equation. This source term is to account for the region between solid and liquid state. A is a mushy zone constant that measures the damping amplitude. This value varies from 10^4 to $10^{7,}$ and the value chosen for simulation is 10^5. Higher this constant value, the steeper the transition of velocity when it solidifies. In order to avoid zero in the division, a small value of λ=0.001 is used. The liquid fraction is given in Eq. (3 a-c).

$$\Phi = 0, if\ T < T_s \tag{3.3a}$$

$$\Phi = 1, if\ T > T_l \tag{3.3b}$$

$$\Phi = \frac{T - T_s}{T_l - T_s}\ if\ T_s < T < T_l \tag{3.3c}$$

Energy equation:

$$\frac{\partial}{\partial t}(\rho H) + \nabla \cdot (\rho \vec{v} H) = \nabla \cdot (k \nabla T) \tag{3.4}$$

In Eq. (3.4), H is enthalpy which comprises both sensible and latent enthalpy. It is given in Eqs. (3.5) and (3.6). where T_r is reference temperature and h_{ref} is reference enthalpy at T_r. L_l is the latent heat of PCM in a liquid state.

$$H = h_{se} + \Phi L_l \tag{3.5}$$

$$h_{se} = h_{ref} + \int_{T_r}^{T} c_p \mathrm{dT} \tag{3.6}$$

3.4.2 Darcy-Forchheimer law

The governing equations are modified when the cases with foams are introduced with the PCM. Two types of models are involved when the investigation is done on a porous matrix based heat sink. One is the local thermal equilibrium model (LTE), and the other is the local thermal non equilibrium model (LTNE). In the LTE model, there is an identical temperature between the foams and fluids is noticed. It explains that a single set of energy transport equations is employed for this model. Whereas for the LTNE model, two unique energy transport equations are applied. Accordingly, a dissimilar temperature is found between the foams and fluids within the enclosure. The equations are,

Continuity equation:

$$\frac{\partial \rho_p}{\partial t} + \frac{\partial (\rho_p u)}{\partial x} + \frac{\partial (\rho_p v)}{\partial y} = 0 \tag{3.7}$$

X-Momentum equation:

$$\frac{\rho_p}{\varphi}\left\{\frac{\partial u}{\partial t} + \frac{1}{\varphi}\left(u\frac{\partial u}{\partial x} + v\frac{\partial u}{\partial y}\right)\right\} = -\frac{\partial P}{\partial x} + \frac{\mu}{\varphi}\left(\frac{\partial^2 u}{\partial x^2} + \frac{\partial^2 v}{\partial y^2}\right) + \frac{(1-\Phi)^2}{\Phi^3 + \lambda}\,\mathrm{Au} - \frac{\mu}{K}u - \frac{1}{2}C\rho_p u|u| \tag{3.8}$$

Y-Momentum equation:

$$\frac{\rho_p}{\varphi}\left\{\frac{\partial v}{\partial t}+\frac{1}{\varphi}\left(u\frac{\partial v}{\partial x}+v\frac{\partial v}{\partial y}\right)\right\} = -\frac{\partial P}{\partial y}+\frac{\mu}{\varphi}\left(\frac{\partial^2 u}{\partial x^2}+\frac{\partial^2 v}{\partial y^2}\right)+\frac{(1-\Phi)^2}{\Phi^3+\lambda}\,\mathrm{Av}-\frac{\mu}{K}v-\frac{1}{2}C\rho_p v|v| + \rho_p\beta_0\,(T_m-T)\,\vec{g} \quad (3.9)$$

Energy equation:

$$\zeta\frac{\partial T}{\partial t}+\varepsilon(\rho c_p)_p\left(u\frac{\partial T}{\partial x}+v\frac{\partial T}{\partial y}\right)=k_{eff}\left(\frac{\partial^2 T}{\partial x^2}+\frac{\partial^2 T}{\partial y^2}\right)+\varepsilon\rho_p L_p\frac{\partial \Phi}{\partial t} \quad (3.10)$$

$$\zeta=\varepsilon(\rho c_p)_p+(1-\varepsilon)(\rho c_p)_{mf} \quad (3.11)$$

The effective thermal capacitance and composite porosity are indicated by ζ and φ. The terms 4 and 5 on the right side of the momentum equation determine the flow within the open porous medium. Darcy-Forchheimer law provides the darcy, non-darcy, and inertial effects in the metal foams. The main parameters in the metal foam structure investigations are interfacial surface area (a_{sf}), permeability (K), and inertia coefficient (C). The interfacial surface area in Eq. (3.12) is derived from Calmidi and Mahajan (2000) and is defined as the surface area ratio between the void and ligaments to the total unit cell volume. The pressure gradient developed when the fluid flows through the porous medium is given by permeability. The term inertia coefficient explains the resistance the metal foam offers due to its complex structure. The widely used correlations for permeability and inertia coefficient Calmidi (1998) are reported here in Eqs. (3.16) and (3.17). Since PCM and solid foams are employed, there is a need to find an effective thermal conductivity. Though numerous empirical and analytical correlations are proposed by the authors, in this study, K_{eff} is evaluated from the correlations proposed by Boomsma and Poulikakos (2011). The last key parameter is the interstitial heat transfer coefficient (h_{sf}), which evaluates the energy interaction between metal structures and PCM. This coefficient, along

with fiber diameter (d_f) and pore diameter (d_{pr}) in Eqs. (3.13-3.15) also derived from correlations of Zukauskas (1987).

$$a_{sf} = \frac{3\pi d_f(1 - exp - ((1-\varepsilon)/0.04))}{(0.59 d_{pr})^2} \tag{3.12}$$

$$\frac{h_{sf} d_f(1 - exp - ((1-\varepsilon)/0.04))}{k_f} = \begin{cases} 0.76 {Re_{df}}^{0.4} Pr^{0.37}, (1 \le Re_{df} \le 40), \\ 0.52 {Re_{df}}^{0.5} Pr^{0.37}, (40 \le Re_{df} \le 10^3), \\ 0.26 {Re_{df}}^{0.6} Pr^{0.37}, (10^3 \le Re_{df} \le 2 \times 10^5). \end{cases} \tag{3.13}$$

$$d_{pr} = \frac{0.0254}{PPI} \tag{3.14}$$

$$\frac{d_f}{d_{pr}} = 1.18 \sqrt{\frac{1-\varepsilon}{3\pi}} \times \frac{1}{1 - exp - ((1-\varepsilon)/0.04)} \tag{3.15}$$

$$K = 0.00073(1-\varepsilon)^{-0.224} (d_f/d_{pr})^{-1.11} {d_{pr}}^2 \tag{3.16}$$

$$C = 0.00212(1-\varepsilon)^{-0.132} (d_f/d_{pr})^{-1.63} \tag{3.17}$$

3.5 NUMERICAL PROCEDURE

The governing equations based on the finite volume method are solved using ANSYS Fluent 19. The method employed for pressure-velocity coupling is SIMPLE algorithm, and for the pressure correction equation is PRESTO! Scheme. The second-order upwind scheme is set for the discretization of momentum and energy equations. Values opted for under relaxation factors for pressure, momentum, liquid fraction, and energy are 0.3, 0.2, 0.9, and 1, respectively. The convergence criterion for momentum and continuity equations is 10^{-5}, and for the energy equation is 10^{-8}.

The volume expansion/shrinkage of PCM during melting and freezing is neglected in this study. Also, the bulk motion of solid PCM is not considered in this simulation. The assumption for the liquid phase PCM is unsteady, laminar, and incompressible. The

properties such as thermal conductivity, dynamic viscosity, and specific heat are considered to be constant. The Boussinesq approximation is applied to density variation to account for the effect of natural convection. For foam cases, the LTE model is applied here.

3.6 GRID STUDY AND INITIAL CONDITION

Numerical accuracy is investigated by considering the effects of the grid and time step size. A heat sink without fins is employed, and results are plotted in Figure 3.3. Three grid sizes of 10870 x 10681, 5027 x 4897, 17161 x 16900, and time step sizes of 0.06, 0.08, and 0.1 are considered. In order to reduce the computational time, these values are selected, and the average deviation is also less for the selected grids and time step size. The number of elements and time step size have similar trends. From the results, the chosen mesh and time step size are 10681 and 0.1, respectively.

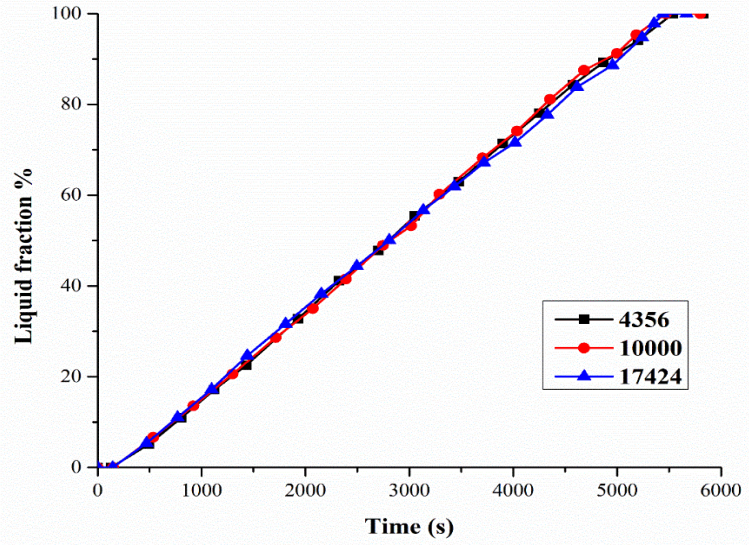

(a)

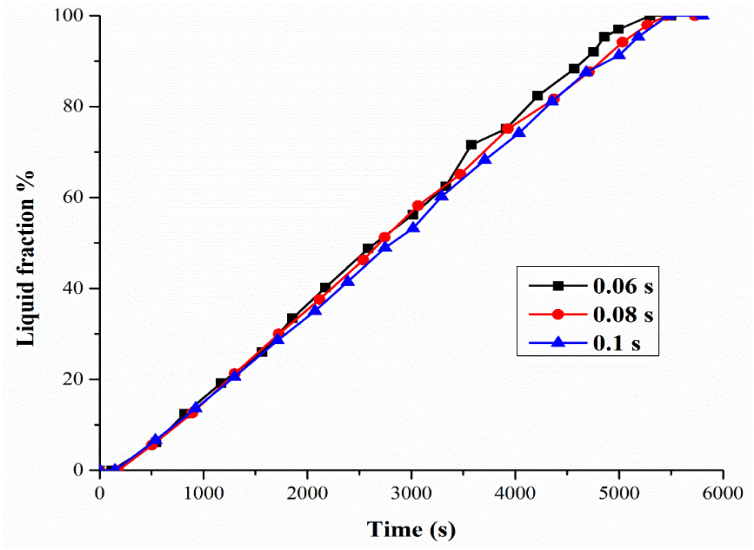

(b)

Figure 3.3 Grid independence study (a) at 0.1 time step size and (b) for 10000 elements. At t=0, the PCM, n-eicosane is in solid state. $T=T_s=T_{mf}=T_p=300$ K and $\vec{v}=0$. Constant heat flux boundary condition of 2000 W/m^2 is applied at the bottom side of the heat sink. The other side of the wall is considered to be an adiabatic condition, $-k\frac{\partial T}{\partial x}=-k\frac{\partial T}{\partial y}=0$.

3.7 VALIDATION

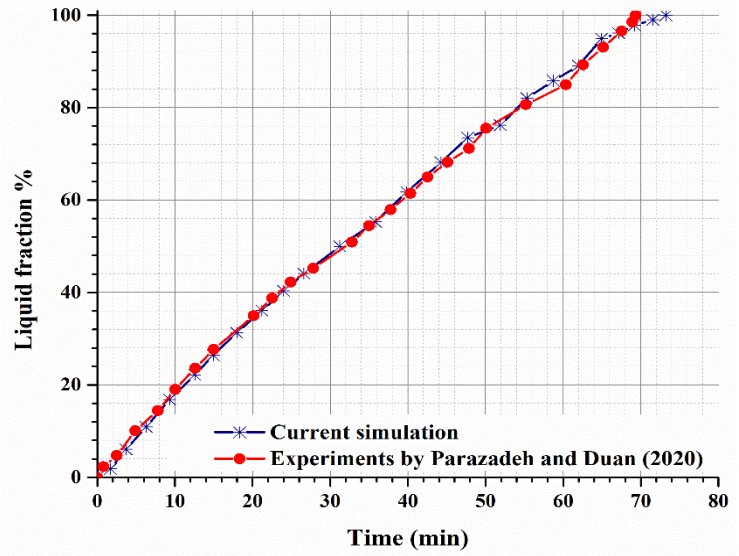

(a)

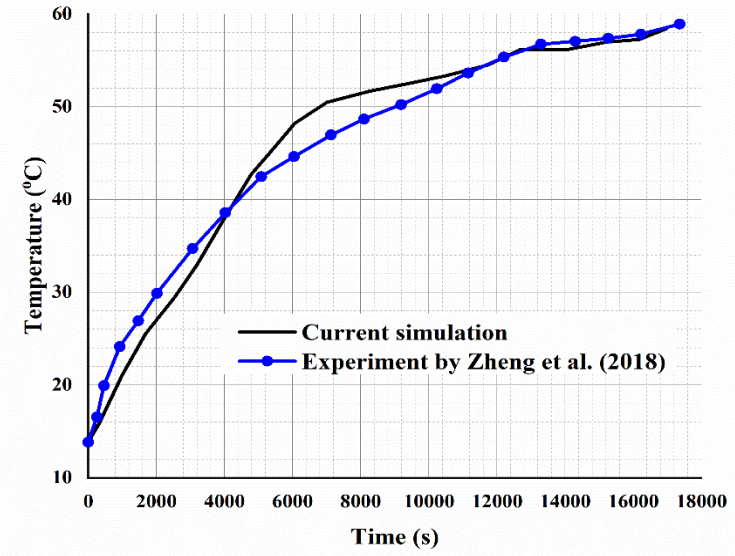

(b)

Figure 3.4 Validation of (a) Liquid fraction percentage from (Parsazadeh and Duan 2020) and (b) Temperature profile within PCM from (Zheng et al. 2018).

To validate the numerical model developed, the charging cycle simulations are compared with the experimental work of Parsazadeh and Duan (2020). Using coconut oil as PCM, its melting behavior with the presence of Rayleigh-Bernard convection was studied. A 60 x 60 mm square enclosure with PCM is heated isothermally at the bottom, with the rest of the walls insulated. PCM is kept at 15^{o}C initially, and the bottom wall is kept at a constant wall temperature of 55^{o}C. The liquid fraction percentage is plotted against time. From Figure 3.4(a), it is observed that the present simulation almost coincides with experiments except at the end. In Figure 3.4(a), when the melting is initiated, the PCM begins to melt, the phase change occurs, and PCM is in the mushy zone. The linear trend defines that there is a steady increase of liquid fraction with temperature over a period of time. In the mushy zone, for a time interval, there is always a uniform rise of liquid fraction with temperature until the phase change completes. When there is a transition of phase change for a PCM until it converts to a liquid phase, the graph tends to be linear. The average deviation found between the experiment and simulation is 4.56%.

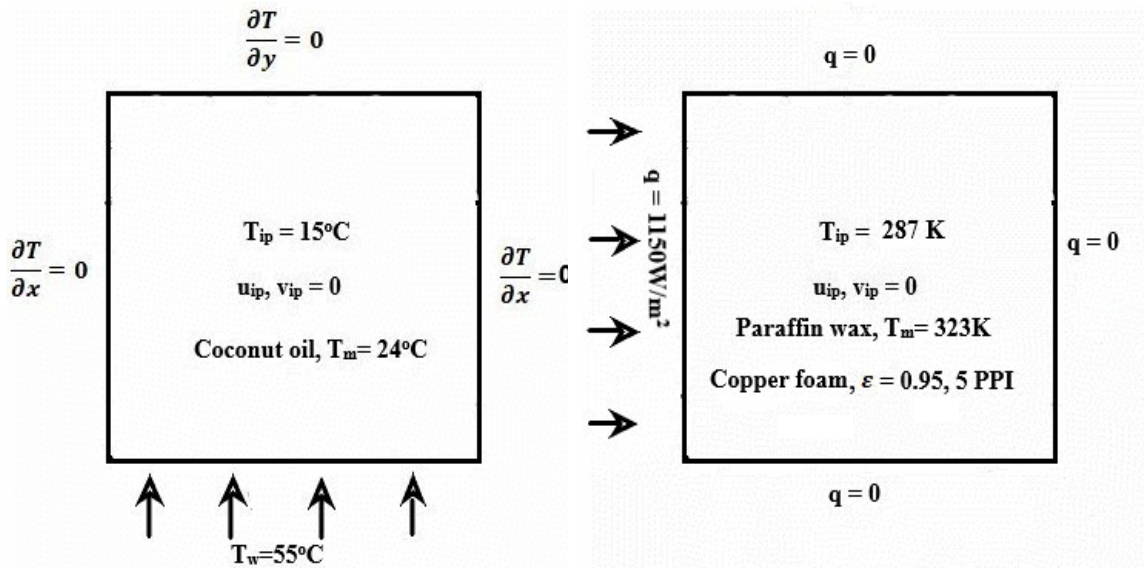

(a) (b)

Figure 3.5 Schematic of the computational setup used by (a) (Parsazadeh and Duan 2020) and (b) (Zheng et al. 2018).

For the validation of the present study with foams, a dimension of 100x100 mm is considered, according to Zheng et al. (2018). Copper foam of 0.95 porosity and 5 PPI are used, and constant heat flux is provided at the left side wall. Paraffin wax is used as PCM material. The temperature within PCM is taken into consideration. The inconsistent variations arise from a disparity in the treatment of phase change material (PCM) temperature between simulations and experiments. In the simulation, PCM properties are kept constant and do not vary with temperature, whereas PCM properties vary with temperature in experiments. The maximum deviation is found to be around 6000s which is 8%. A schematic of both the simulation study, including initial conditions and boundary conditions, is summarized in Figure 3.5.

3.8 RESULTS AND DISCUSSION

3.8.1 Case with Fins

The significance of incorporating fins on both vertical walls and horizontal walls is shown in Figure 3.6. From the figure, it is understood that single-side fins provide accelerated melting, but the solidification is decelerated. In contrast, the introduced hybrid heat sink

design possesses slower melting and faster discharging. Since the solidification time is much lesser in hybrid heat sink and it leads to the option of choosing the hybrid heat sink for further analysis.

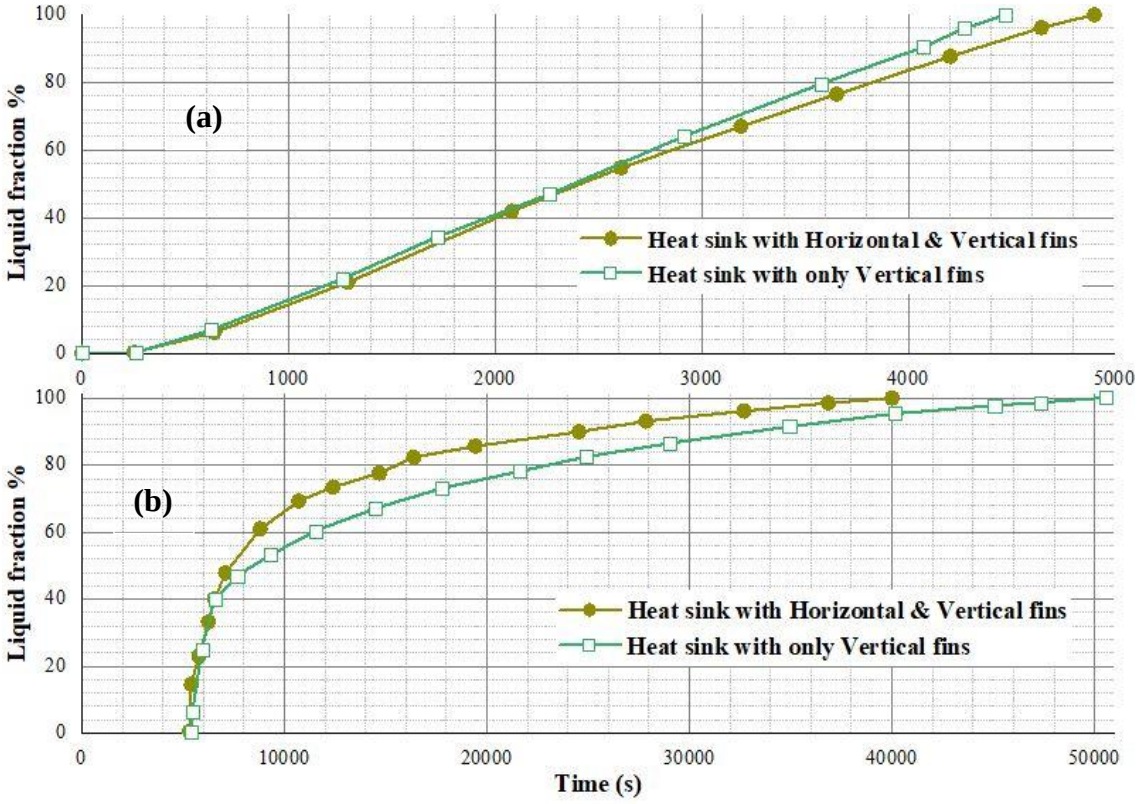

Figure 3.6 Comparison of vertical fins heat sink and combination of vertical and horizontal fins heat sink (a) melting and (b) solidification.

The liquid fraction percentage is plotted in Figure 3.7. The detailed geometry is given in Figure 3.2. It can be seen that the melting begins early for the case without a fin, and the time taken is 70 s. In the fin case, it takes some time to initiate the melting. For rectangular and tapered fins, it takes 250 s and 230 s, respectively. This is because the heat is absorbed by the fins first due to its higher thermal conductivity than PCM. Then, the melting rate for both cases with fins increases and completes melting at around 4900 s, whereas heat sink without fin completes melting at 5400 s.

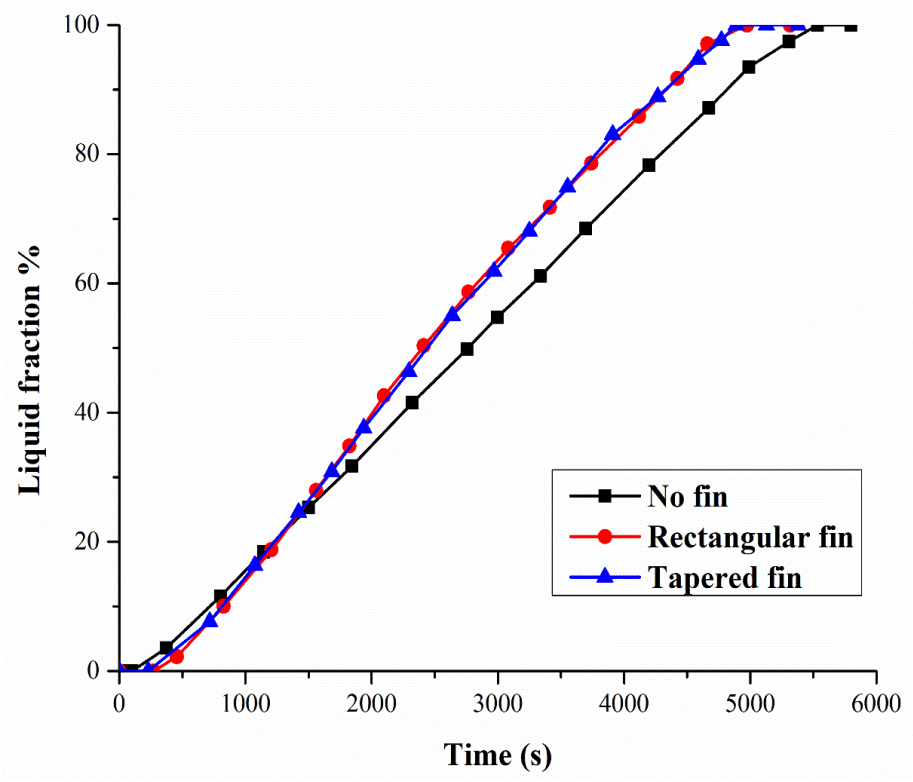

Figure 3.7 Liquid fraction percentage with no fin, rectangular, and tapered fins.

The contours of temperature distribution are shown in Figures 3.8 and 3.9. As mentioned by Parsazadeh and Duan (2020), at 600 s, there are local hotspots for the case without fins which may damage the heat sink. But, by adding fins, the local hotspots are reduced. The tapered fins reduce these spots more than rectangular fins, which are seen at 1200 s. Due to the increase in the surface area of tapered fins near the base, the tapered fins absorb the thermal stress and reduce these local hotspots. Thus the local hotspots are less for tapered fins than the rectangular fins. Hence, the local hotspots can be eliminated by increasing the surface area near the heater side. At transient or cyclic heat loads, these spots can impact the system.

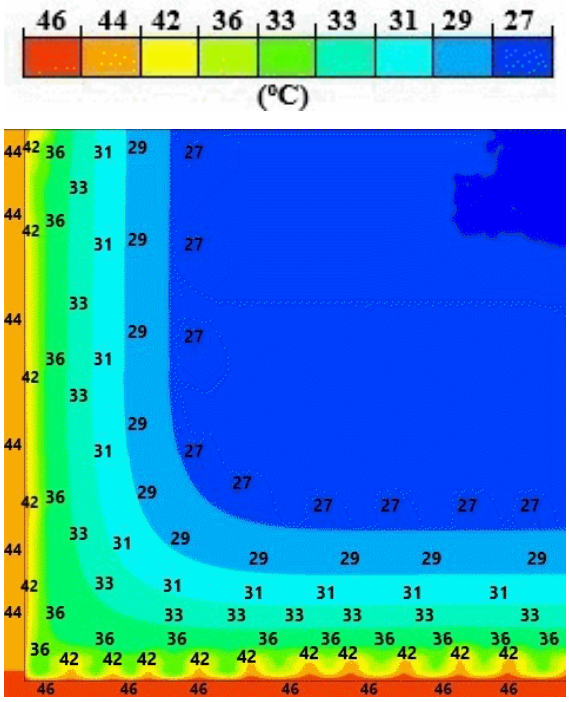

(a) 600 s

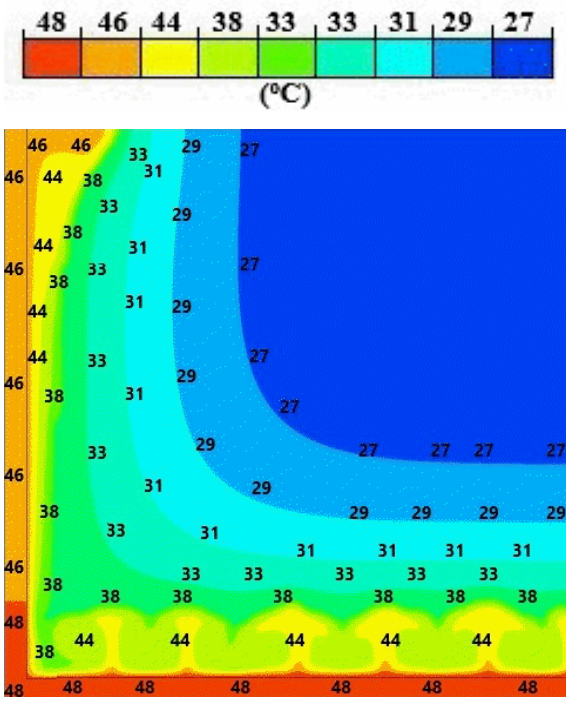

(b) 1200 s

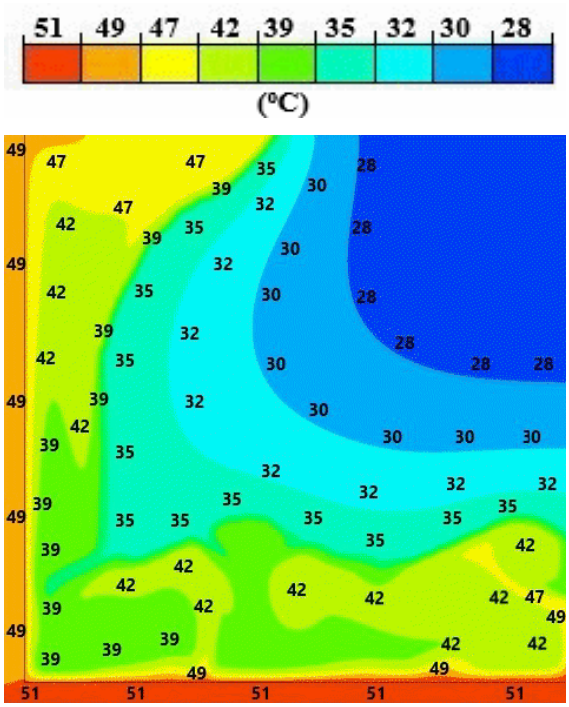

(c) 2400 s

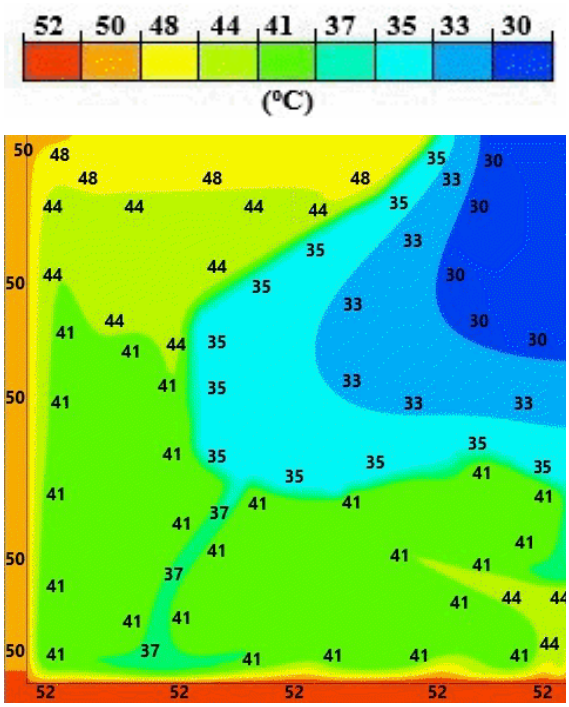

(d) 3600s

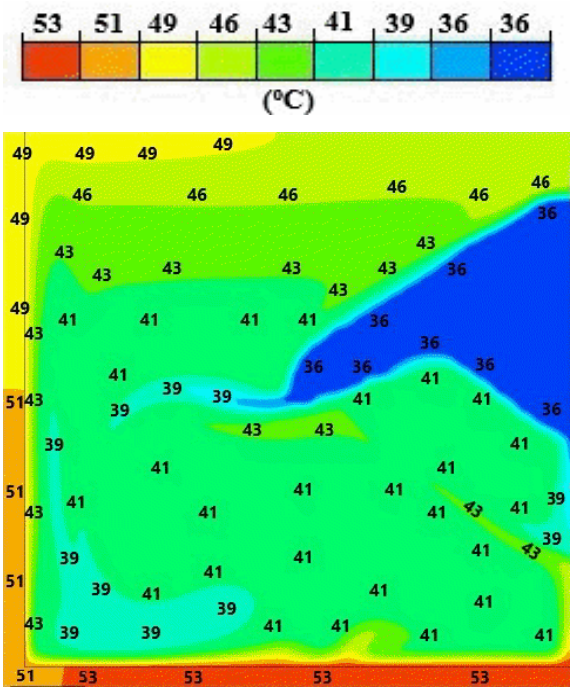

(e) 4800 s

Figure 3.8 Temperature distribution contour for no fin case at various times: (a) 600 s, (b) 1200 s, (c) 2400 s, (d) 3600 s, and (e) 4800s.

At the bottom, left and mid positions of the heat sink, the temperature distribution is faster in the tapered fins. At the top right corner position, the type of fins does not influence the melting, and the temperature distribution is similar. Figure 3.10 shows the contours of the melting interface. Similar to Parsazadeh and Duan (2020), in the no-fin case, the liquid near the bottom wall has a wavy nature because of the hotspots induced. Once the melting time increases, it is clear that the intensity of the wavy nature increases. But the number of waves is reduced when the intensity of waves enhances. This is mainly due to the effect of buoyancy, where the solid PCM tries to move down with higher density. This behavior is not seen in the fin cases at the early stages. This is because the conduction effect dominates at the early stages when fins are introduced. This restricts the natural convection at early stages for fin cases. Hence less wavy nature is found at the early stages for fin cases. The melting interface is similar for both fin cases. But at 2400 s, in between the fins and side walls, there is a discontinuity in the interface for rectangular fins.

Rectangular fins **Tapered fins**

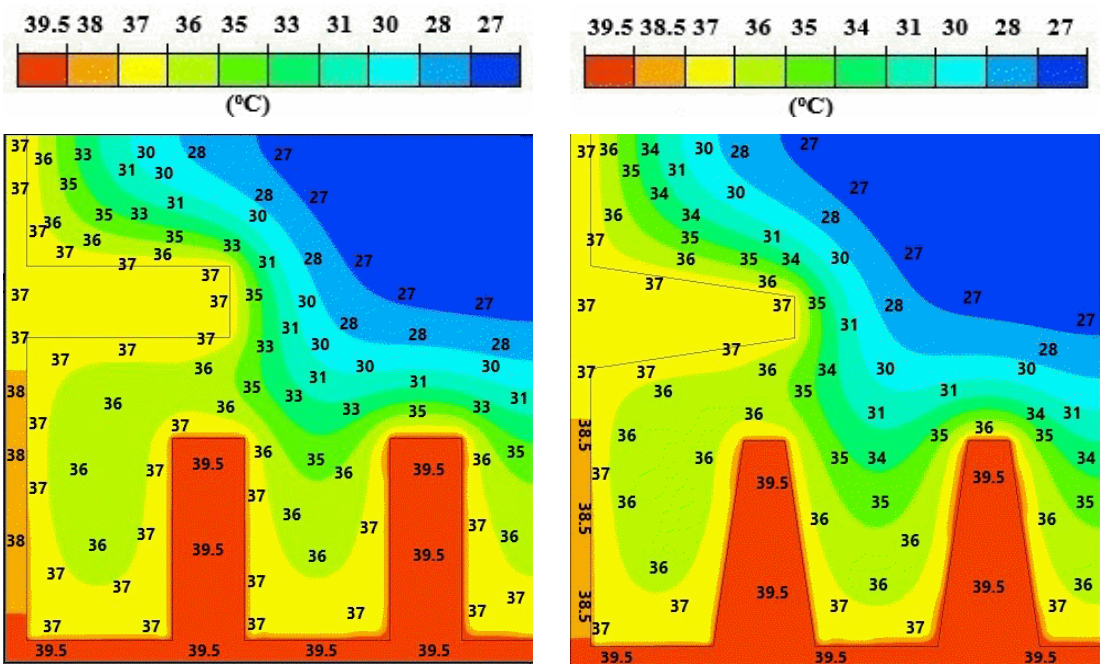

(a) 600 s

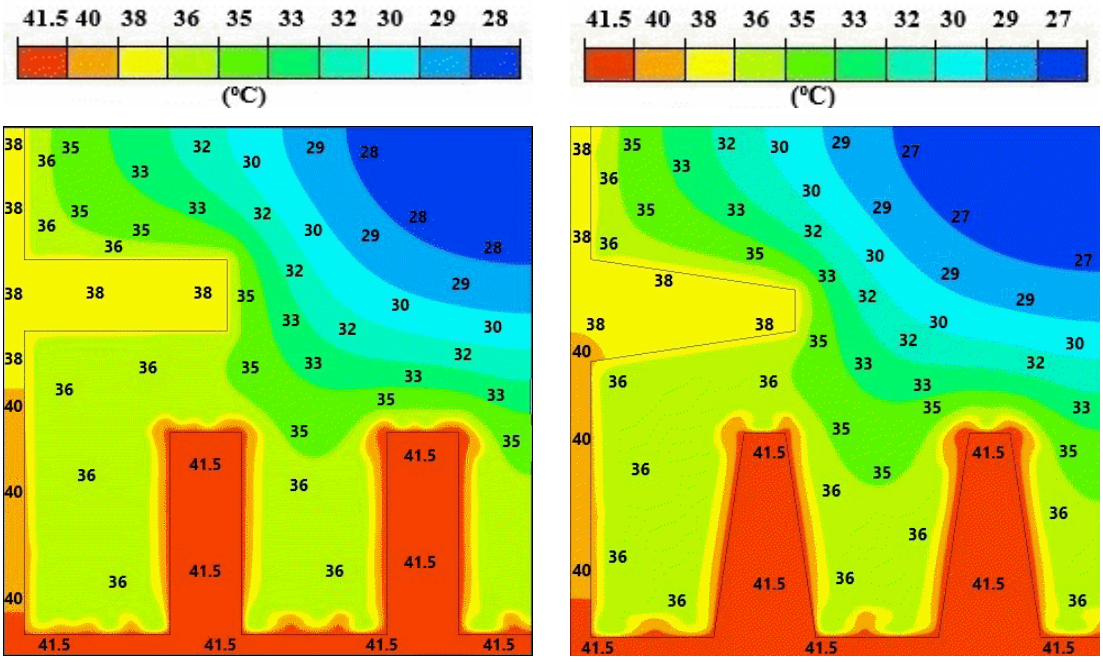

(b) 1200 s

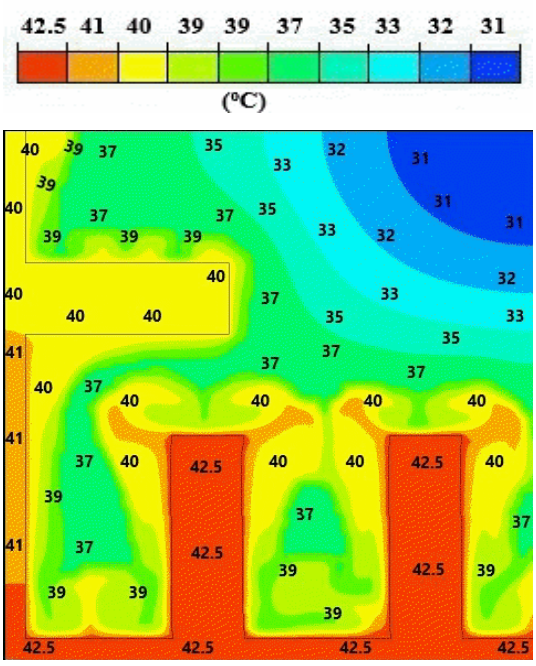

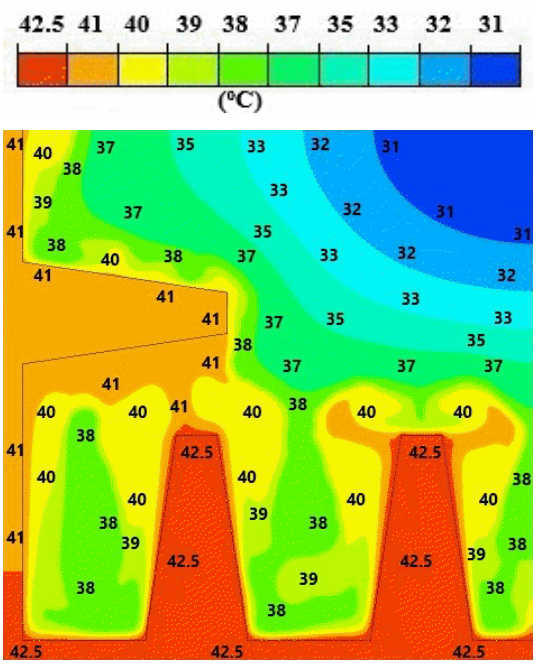

(c) 2400 s

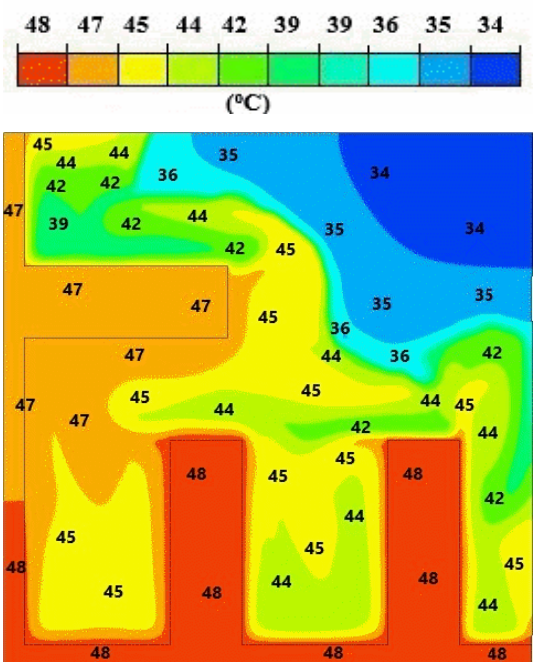

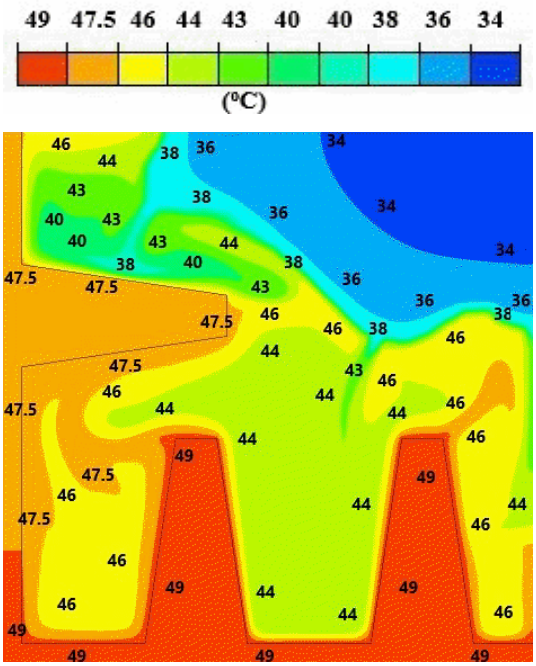

(d) 3600 s

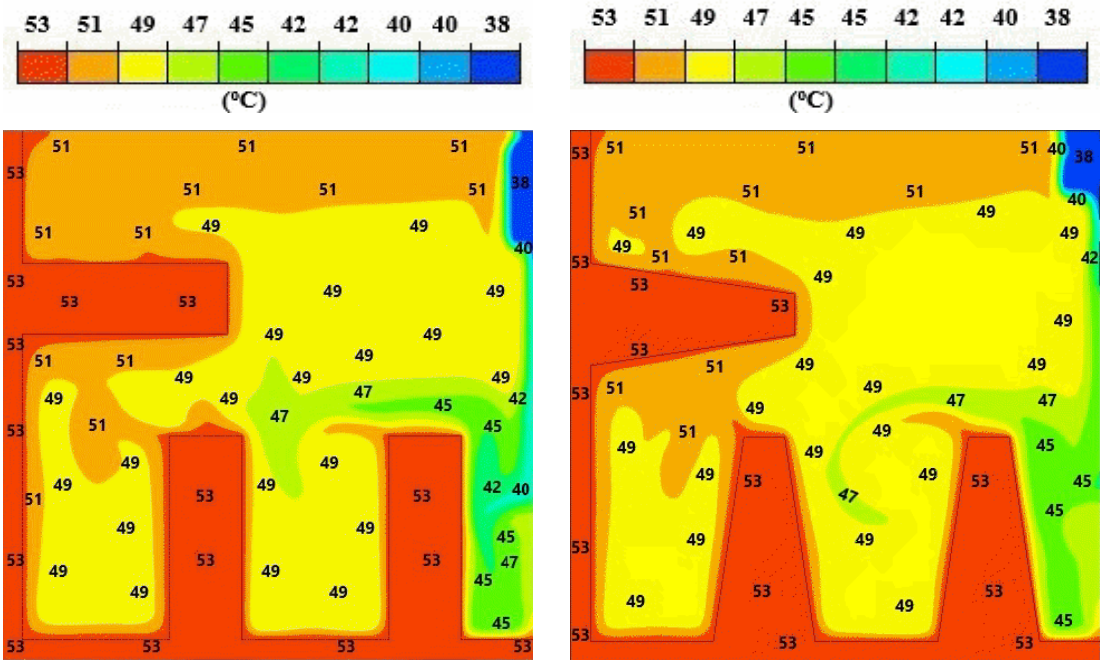

(e) 4800 s

Figure 3.9 Temperature distribution contour for Rectangular and Tapered fins at various times: (a) 600 s, (b) 1200 s, (c) 2400 s, (d) 3600 s, and (e) 4800s.

The reason behind the discontinuity found in Figure 3.10 (c) for the rectangular fin is due to the interruption of the heat flow path offered by the fins. For no fin cases, it is clear that heat flow is towards the top right corner from the bottom and left wall substrate. The melt front of liquid PCM is also uniformly distributed towards the corner. But the heat flow path is disturbed when the fins are added to the heat sink. The melt front of liquid PCM was also found to be mixed up. Since the thermal conductivity of the fins is immense than the PCM, the PCM near the fin walls gets melted quicker. Thus the heat flow path is disrupted, and the melt front is disoriented. This disoriented melt fraction forms the gap between the fins and walls. The heat absorbed is more towards the fin surfaces due to higher thermal conductivity, and less heat is oriented towards these gaps due to the poor thermal conductivity of PCM. Hence, there is a discontinuity found on fins cases at that time interval.

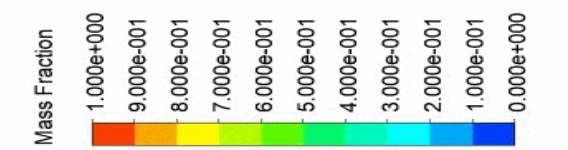

No fin Rectangular fin Tapered fin

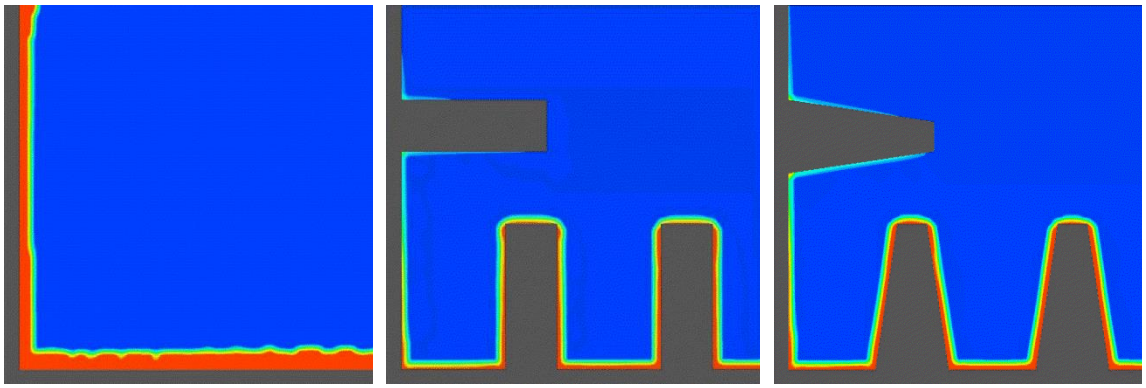

(a) 600 s

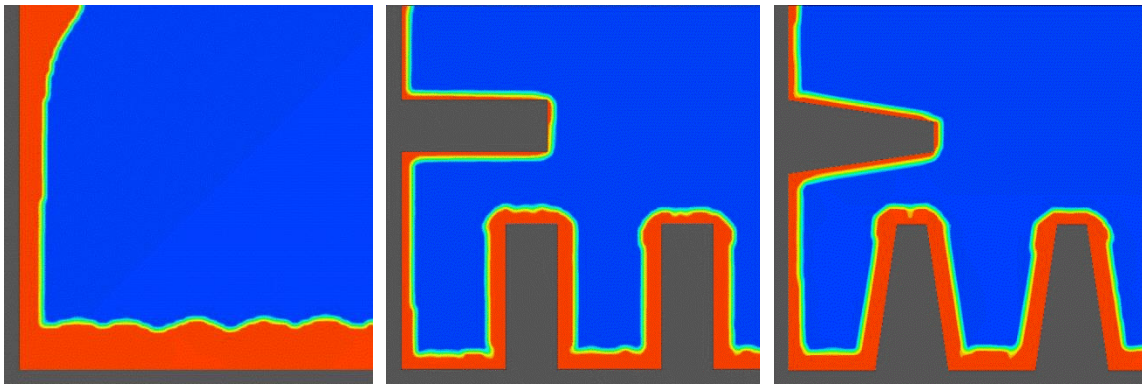

(b) 1200 s

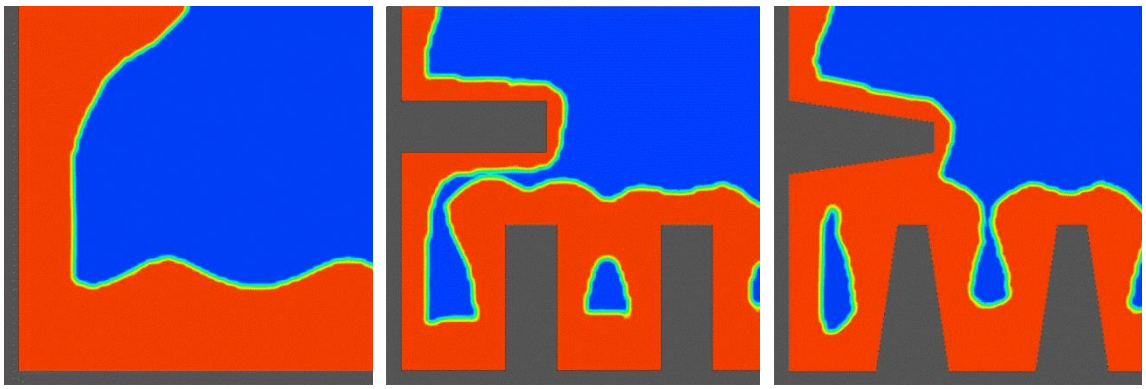

(c) 2400 s

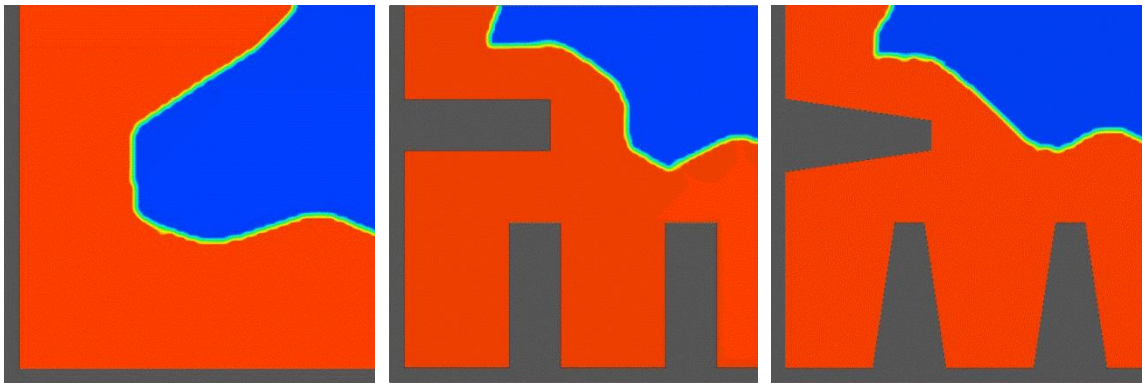

(d) 3600 s

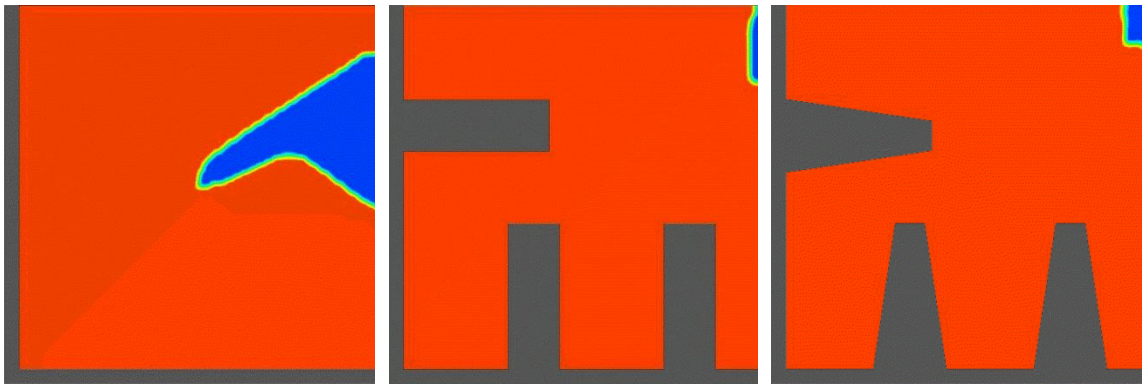

(e) 4800s

Figure 3.10 Contours of melt fraction at various times: (a) 600 s, (b) 1200 s, (c) 2400 s, (d) 3600 s, and (e) 4800s.

The maximum velocity found at different time intervals is plotted in Figure 3.11. The maximum velocity in the figure shows the influence of natural convection in the system with the presence of fins and without fins. The plot shows that natural convection plays a major role in heat sinks without fins. Because of the vortex motion with waves observed near the bottom side influences the natural convection. These vortices, in turn, increase the magnitude of velocity for the case with no fin. But in the case of fins, initially, it is dominated by conduction, and later on, only convection influences the melting. The reason behind this is that adding fins to a heat sink disturbs the liquid PCM flow. As mentioned earlier, the wavy nature is reduced for the fin cases, which restricts the vortex motion of PCM near the base. Which further reduces the magnitude of velocity at the early stages.

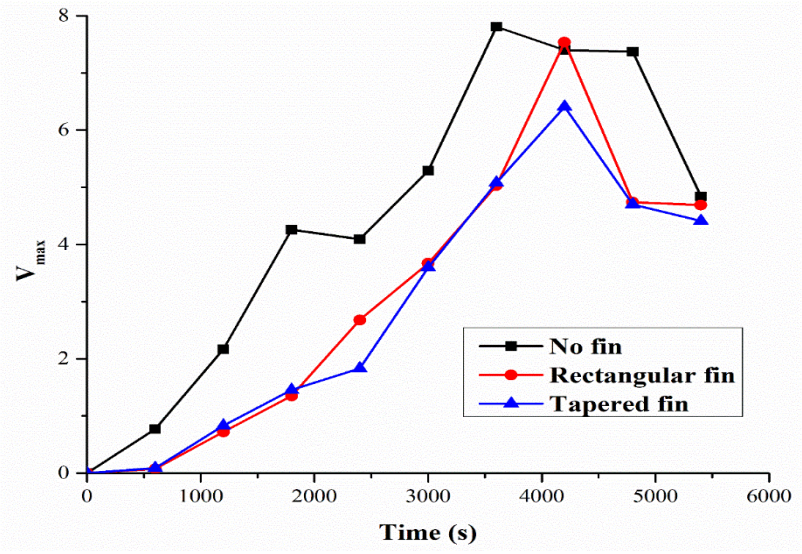

Figure 3.11 Maximum velocity for no fin, rectangular, and tapered fins.

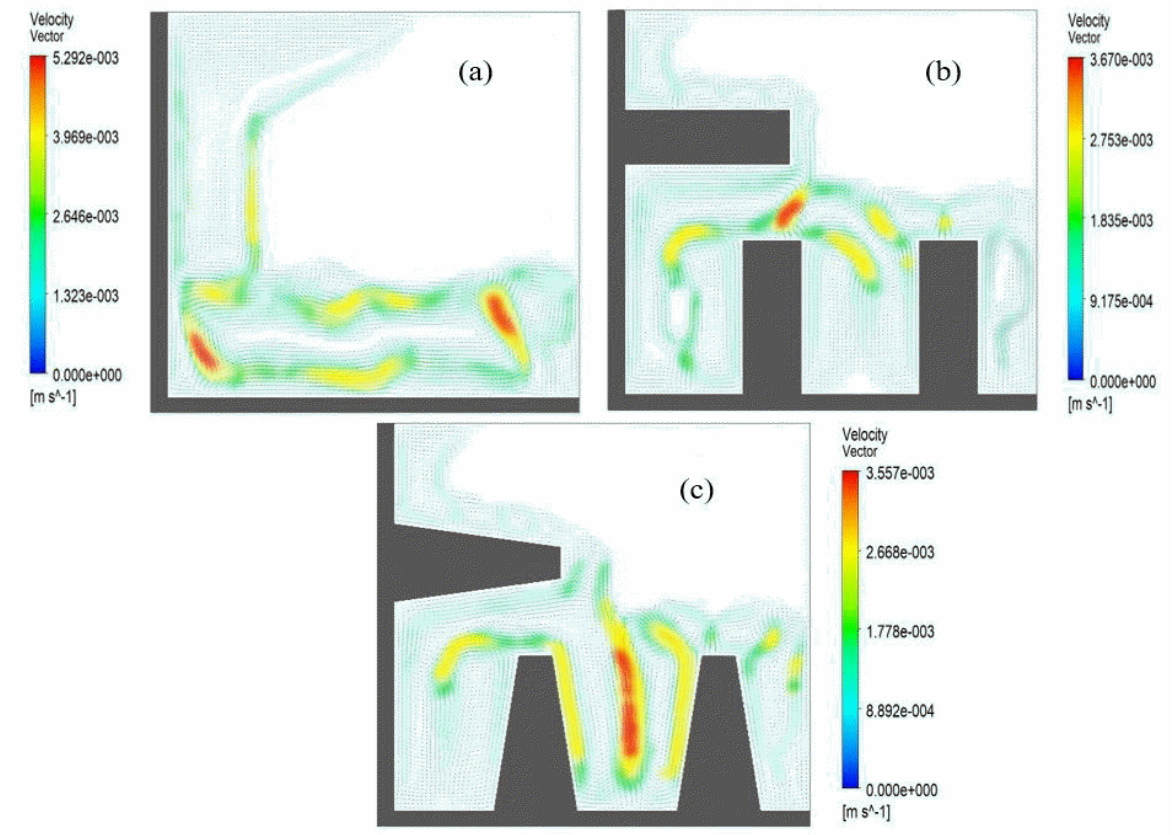

Figure 3.12 Velocity vectors at 3600 s for (a) no fin, (b) rectangular, and (c) tapered fins.

The average maximum velocity for heat sink without a fin, rectangular fin, and tapered fin is 4.41 mm/s, 3.06 mm/s, and 2.86 mm/s, respectively. The peak velocity of 7.81 mm/s was found at 3600 s for the heat sink without fins. For rectangular and tapered fins, the peak velocity was found at 4200 s which is 7.54 mm/s and 6.41 mm/s, respectively. The peak velocity for the fin case is found at 4200 s, whereas for the no-fin case, it is found at 3600 s. This 600 s lag for fin cases is due to the delay of initiation of melting at the initial stage. At the end of the melting stage, the peak velocity falls, showing that the solid PCM is converted to the liquid phase. The velocity vector of cases with fins and no fin case is displayed in Figure 3.12.

3.8.2 Case with Foams

The geometry of foam integrated with the finned PCM heat sink is given in Figure 3.2 (d). The liquid fraction percentage is plotted in Figure 3.13. The trend of the graph of the 10 mm foam-filled heat sink lags behind 15 mm and 20 mm filling height. 15 mm and 20 mm foam-filled heat sinks have a similar trend.

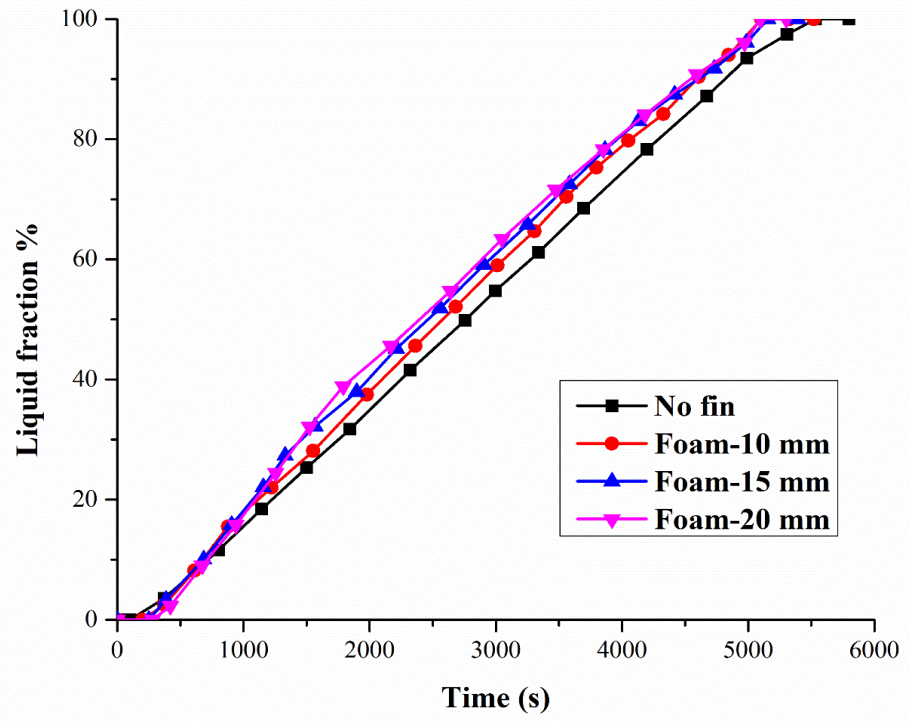

Figure 3.13 Liquid fraction percentage for varying filling heights of foam.

The initiation of melting is delayed slightly by increasing the filling height. Similar to fin cases, in foam cases also, the heat is initially absorbed by the foam. After that, heat is distributed to the PCM; therefore, melting is delayed. By increasing the filling height, the heat flow towards the PCM is restricted further due to the increase in foam size. The addition of foams shows an accelerated melting rate than no fin case. The conduction effects dominate the convection effects for foam cases, also. For 10 mm, 15 mm, and 20 mm heights, the melting begins at 200 s, 250 s, and 280 s, respectively. But the completion of melting takes place around 5100 s.

Figure 3.14 shows the temperature distribution at different positions of a heat sink. The temperatures are measured at four different places. Location 1 is at the heater, location 2 at x = 10 mm and y = 15 mm from the base, location 3 at x =30 mm, y = 25 mm from the base, and location 4 at x = 40 mm, y = 45 mm from the base. The heater temperature depends on the filling height, and it depends on the amount of PCM present. The amount of PCM indicates the phase change transition period of a PCM from the solid to the liquid phase. The time taken for the heater to attain the steady-state temperature is early for 10 mm and late for 20 mm. The duration of the heater steady state temperature is longer for 10 mm height and least for 20 mm. This is due to the amount of PCM, which is more in the case of 10 mm filling height, providing a longer phase transition period of PCM. Within PCM, the filling height does not affect the temperature distribution other than location 2. The temperature distribution is almost the same for all cases at locations 3 and 4. At location 2, for a filling height of 10 mm, there is a deviation between 15 mm and 20 mm. The reason behind this is that the presence of foam at location 2 provides smooth distribution for 15 mm and 20 mm. Whereas, for 10 mm, location 2 is above solid material, and convection arises more than conduction.

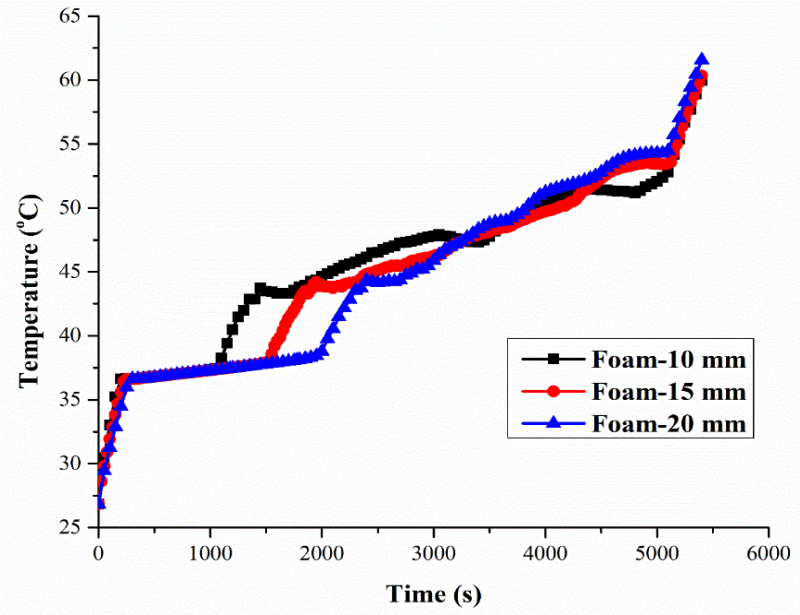

(a) Temperature distribution at location 1.

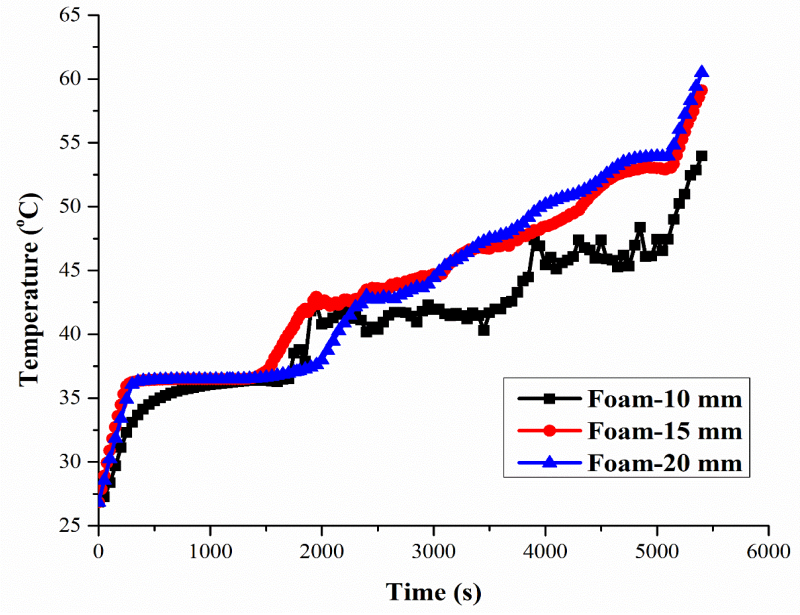

(b) Temperature distribution at location 2.

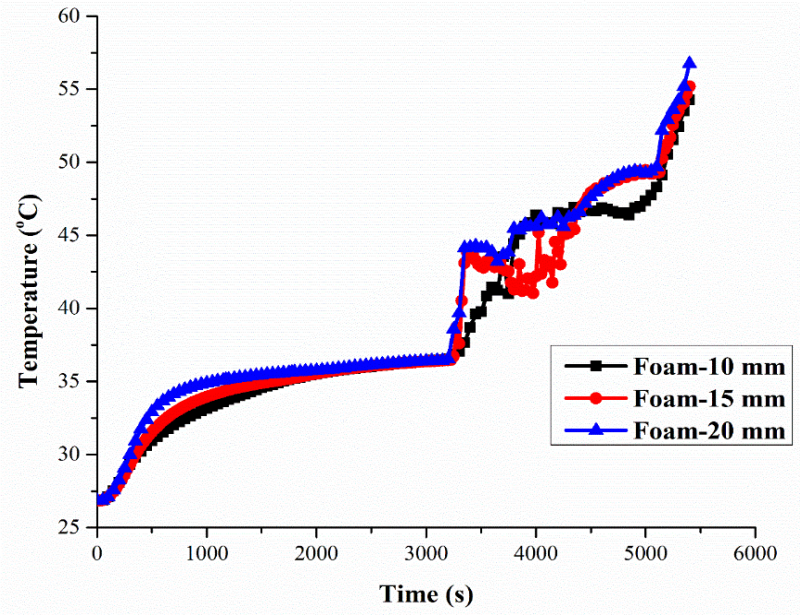

(c) Temperature distribution at location 3.

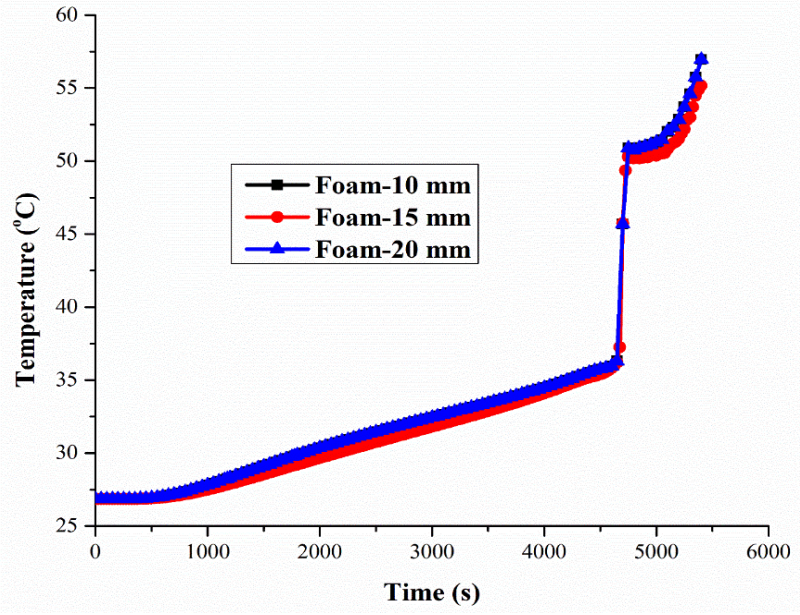

(d) Temperature distribution at location 4.

Figure 3.14 Temperature distribution within the system for the case with foams.

Figure 3.15 shows the maximum velocity for different filling heights. As the filling height increases, the initiation of convection delays and the average maximum velocity also decrease. The average maximum velocity for filling heights 10 mm, 15 mm, and 20 mm is

3.01 mm/s, 2.91 mm/s, and 2.02 mm/s, respectively. Though the velocity magnitude of 15 mm foam height is found to be higher at several stages, the average velocity is less. It is because the velocity has magnitude only after 1800 s. Similarly, for 20 mm foam height, only after 2400 s velocity has a magnitude. The reason is the foam's domination of the conduction effect by absorbing the heat at early stages, so initially, velocity is not found at that stage.

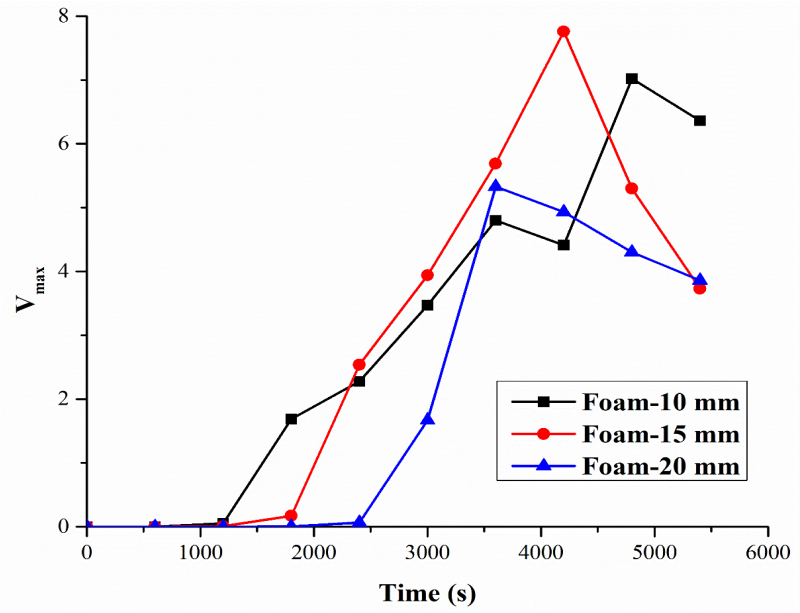

Figure 3.15 Maximum velocity for different foam heights.

The peak velocity for 15 mm is 7.76 mm/s at 4200 s. The peak velocity for 10 mm and 20 mm is 7 mm/s at 4800 s and 5.33 mm/s at 3600 s. It is also noted that the time required to attain peak velocity decreases with an increase in filling height. This is due to the delayed effect of natural convection with increasing filling heights. Once the melting starts, the peak velocity is found at the later stages of melting for all the cases, where all the PCM is almost at the liquid phase. Thus, the natural convection influences the velocity at the later stages of melting for foam cases. The velocity vector of the foams is given in Figure 3.16.

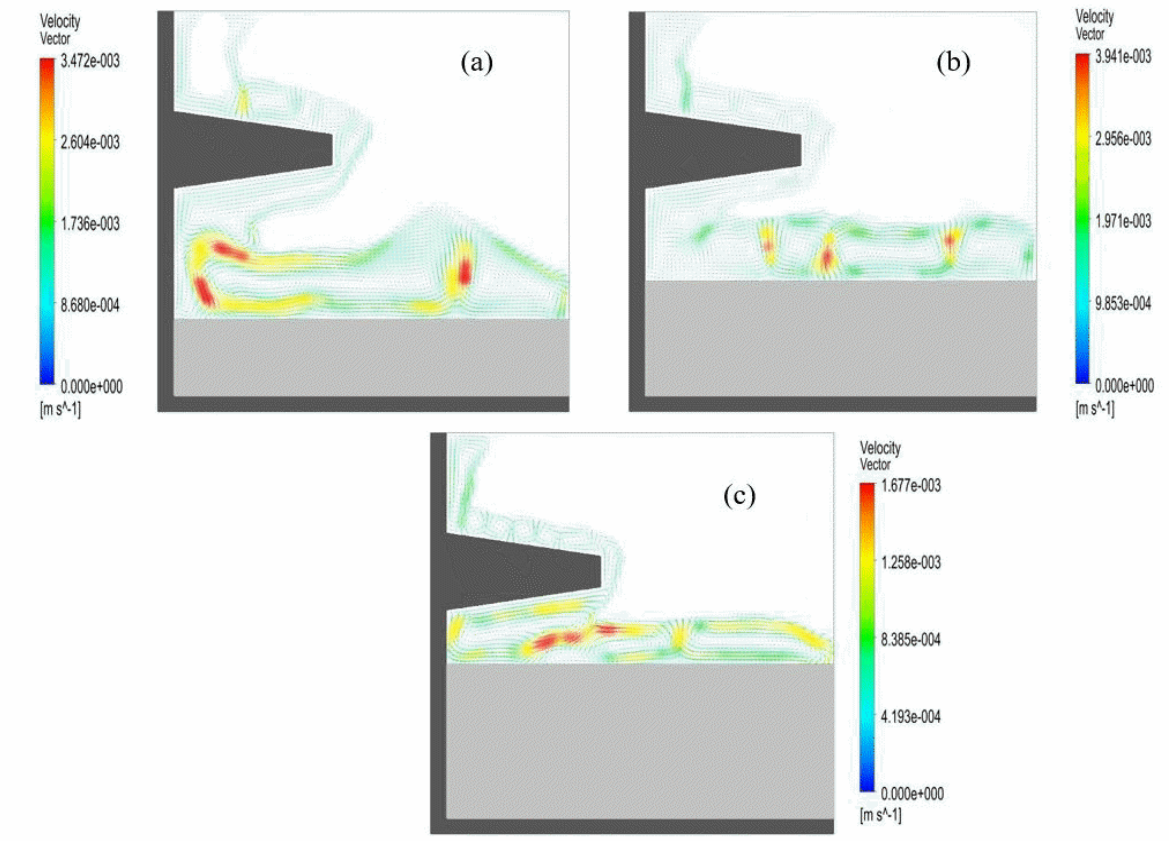

Figure 3.16 Velocity vector at 3600 s for varying filling heights (a) 10 mm, (b) 15 mm, and (c) 20 mm.

3.8.3 Solidification

The boundary condition is changed for the solidification process, and PCM is at the liquid stage. The heater wall boundary condition is changed from constant wall heat flux to constant wall temperature 300 K. The solidification boundary condition is set from 5400 s for all cases except the no-fin case. But for heat sink without fins, the solidification time starts at 6000 s since the melting completes later than in other cases, and the boundary condition is kept the same as in other cases. The remaining walls are insulated like the charging process. The percentage of solid fractions for all the cases is plotted in Figure 3.17. The solid fraction of a Phase Change Material (PCM) represents the proportion or fraction of the material that exists in a solid state at a specific point in time. In ANSYS Fluent, contours are obtained through liquid fraction graphs. However, to extract the solid

fraction values, the 100-liquid fraction at respective times is considered, and this value represents the solid fraction.

The solidification rate is 15 times longer than the melting rate of the no-fin case. The solidification rate is 15 times longer than the melting rate for no fin cases, mainly due to the property of the PCM and applied boundary condition. The poor thermal conductivity and high PCM latent heat increase the discharging cycle's completion time. The amount of heat required to extract is more for no-fin case, and the heat dissipation rate is poor for PCM because of high thermal resistance.

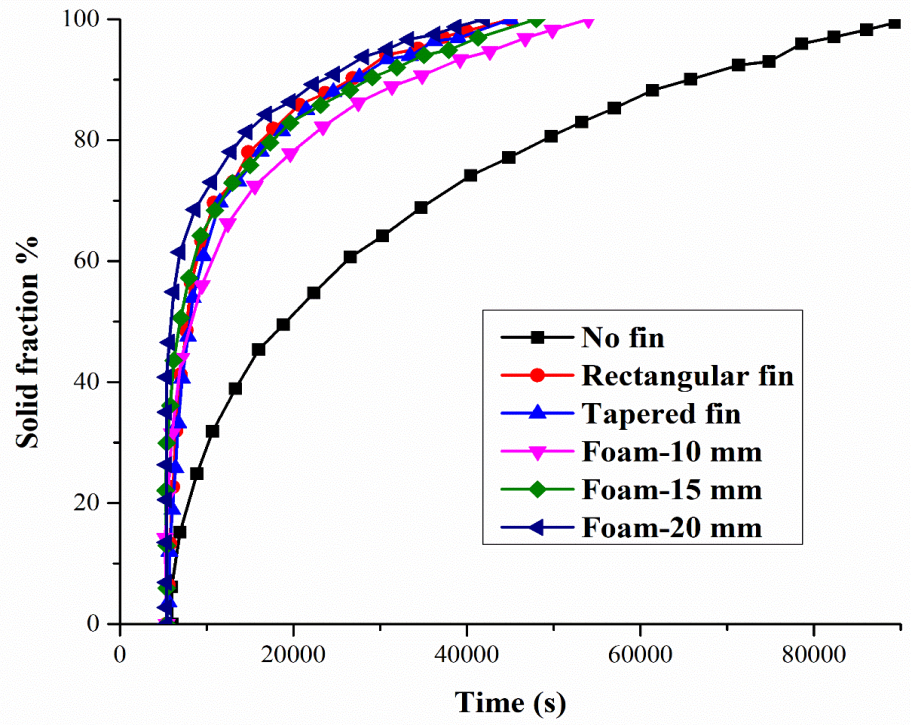

Figure 3.17 Solid fraction percentage comparison with all cases.

Whereas the addition of fins/foams reduces the resistance offered by the PCM and increase the heat dissipation. Thus, there is an enhanced solidification rate for fin and foam cases. Secondly, since the boundary condition is applied at the bottom, the heat flow will be from bottom to top. During solidification, the liquid PCM near the walls and bottom gets solidified first. Also, the buoyancy effect will be eliminated. Since there is no convection found within the heat sink, there is no movement of PCM, unlike melting. If the boundary

condition is applied at the top side, the buoyancy effect comes into the picture, and there is a chance of an increase in the solidification rate, but the melting rate will be affected by that boundary condition. The time taken to complete solidification for no-fin case is 85000 s. The type of fin shape does not have a considerable effect during the discharging cycle, unlike the charging cycle. The solidification time taken for rectangular and tapered fins is 39710 s and 39680 s, respectively.

With foam cases, the filling height does not have much impact on the charging cycle. But during discharging cycle, filling height affects the solidification rate remarkably. This is due to the strong conduction effect which takes place within the foams. The increase in filling heights increases the volume of foams, thus reducing the amount of PCM. The reduced amount of PCM solidifies faster compared with other cases. Thus provide an accelerated solidification rate for foams with increasing filling heights. For 10 mm, 15 mm, and 20 mm, the time taken for solidification is 49600 s, 42200 s, and 36500 s, respectively. With the increase in filling height, the time taken to complete solidification decreases, which shows that conduction is the dominant mode of heat transfer during discharging. The enhancement percentage for all cases with no fin as baseline comparison is calculated by Eq. (3.18) and is given in Table 3.3.

$$Enhancement\ percentage = \frac{t_{S_b} - t_{S_f}}{t_{S_b}} * 100\ \% \tag{3.18}$$

Table 3.3 Enhancement percentage for all cases.

Cases	Enhancement percentage (%)	
	Melting	Solidification
Rectangular fin	12.57	53.28
Tapered fin	12.75	53.33
Foam with 10mm height	8.06	41.64
Foam with 15mm height	9	49.88
Foam with 20mm height	9.56	56.94

3.9 SUMMARY

A simplified 2D model with both horizontal and vertical fins and horizontal foam with vertical fins was developed. The numerical models were validated with previous experimental results. Two types of fin shapes are used rectangular and tapered fins. Then a hybrid case was chosen, which has tapered fins attached horizontally and combined with metal foams for better performance. The foam filling height varied from 10 mm, 15 mm, and 20 mm. Both charging and discharging cycles for all cases were considered in this study.

- The initiation of melting of PCM was delayed with the insertion of fins because the fins absorb the heat initially before heat dissipates to PCM. For the case with fins, when compared with no fin case, the local hotspots were reduced by the addition of fins. Tapered fins provide better temperature distribution within PCM than rectangular fins.
- Maximum velocity and an average of maximum velocity were found to be highest with no-fin cases that are 7.81 mm/s and 4.1 mm/s, respectively. This shows that natural convection plays a major role in the case of no fins.
- For foam filled with horizontal fin cases, the filling ratio slightly affects melting initiation. The time taken for completion of melting was almost the same for different filling heights; however, the time taken to attain the steady-state temperature was delayed by increasing the filling height.
- The filling height of 15 mm has a higher peak velocity of 7.76 mm/s, and the average velocity is higher for the 10 mm fin case, which is 3.01 mm/s. The convection role was delayed with an increment of filling heights. It was found that as the filling height increases, the time taken to reach peak velocity increases.
- For the melting case, the type of fin shape and foam filling height does not have a significant effect at the top right position. This, in turn, reduces the melting rate, so further optimization is required for fin heights, fin spacing, and foam heights.
- The time taken for completion of solidification for no-fin case is 85000 s which is 15 times higher than melting. Both rectangular and tapered fins have similar

solidification rate. The filling height has remarkable effects on discharging. Increasing the order of filling height increases the solidification rate.

3.10 CLOSURE

This chapter explores the numerical investigation of PCM-based heat sink with fins placed on both horizontal walls and vertical walls. Further, the partial filling foam study was analyzed by placing a fin on the top side of the enclosure. The effects of this combination were evaluated during charging and discharging cycles, and results were compared with the PCM-filled case with no enhancers. The optimization study of the hybrid heat sink is conducted and discussed in the next chapter.

CHAPTER 4

OPTIMIZATION STUDY OF HYBRID PCM UNIT FOR EXTENDED MELTING AND SHORTENED SOLIDIFICATION

4.1 INTRODUCTION

This chapter combines metal fins with a porous matrix to provide a multi-objective optimization on a hybrid heat sink filled with PCM. The foam placed contains PPI ranging from 5-25 with varying porosity 0.8-0.95. Since foams are partially filled, the filling height of foams also varied by 10 mm, 20 mm, and 30 mm. The positioning of the horizontal fin from the top wall (p_f) and fin height (h_f) is also estimated initially and fixed later for the variation of foam analysis. A total of 60 cases were developed and analyzed for the charging and discharging cycle using Ansys Fluent. A constant hot wall temperature of 50^oC is applied at the bottom of a heat sink, with the rest of the walls insulated. From the studies, it is seen that the TOPSIS algorithm for a PCM-based heat sink is scarce. Maximizing melting time (M_{max}) and minimizing solidification time (S_{min}) are the objective functions considered during optimization. The outcome from the descriptions can provide a broad knowledge of picking the right porous structure when inputting partial filling.

4.2 NUMERICAL DOMAIN

A rectangular enclosure of 104 x 52 mm with 2 mm substrate thickness (b_s) is numerically developed from the past study (Nedumaran and Gnanasekaran 2022). For effective cooling performance, both the fin and foams are employed as thermal enhancers in the heat sink. As shown in Figure 4.1, fins are placed horizontally at the sidewall of the enclosure, and the metal foam is placed at the bottom. The solid material chosen is aluminum for fins, foams, and substrate. A heat spreader is imparted to the PCM cavity as a substrate for uniform heat dissipation. PCM used in the current study is n-eicosane, and the PCM cavity dimensions are 50 x 100 mm. The properties of the PCM used are listed in Table 3.2. Due to its symmetrical nature, only half of the enclosure is considered to reduce computational time. A computational domain for the numerical study is provided in Figure 4.2.

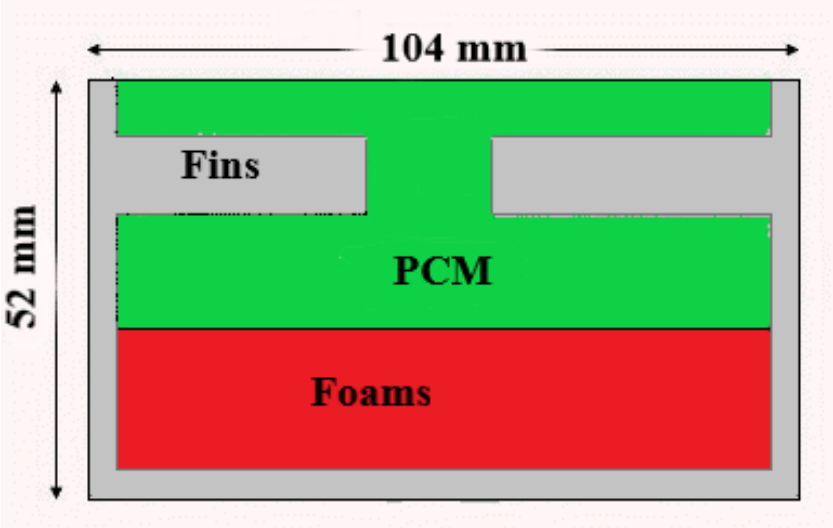

Figure 4.1 2D Enclosure with fins and foam.

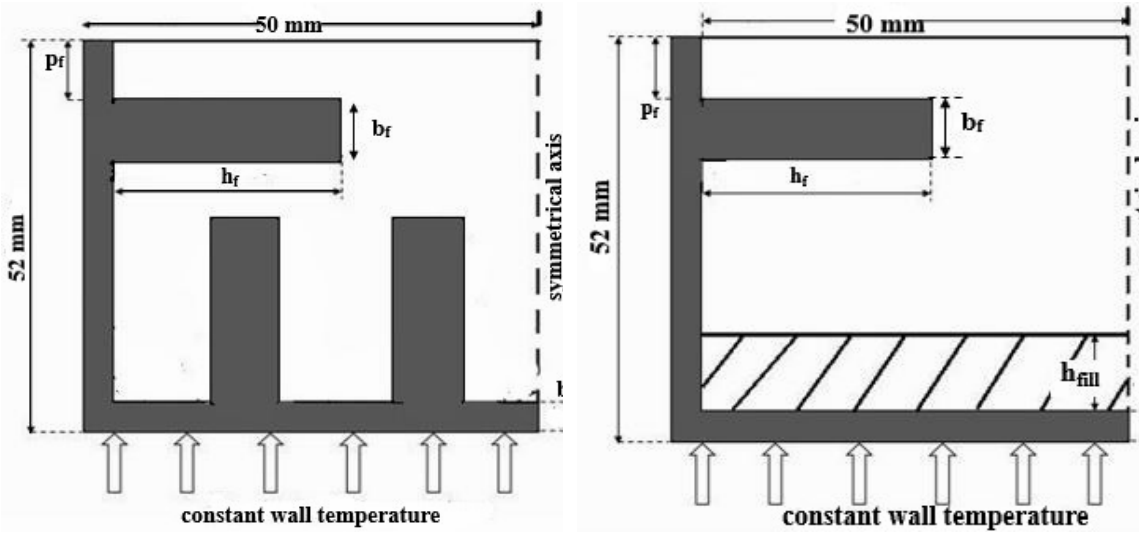

(a) (b)

Figure 4.2 Computational domain of hybrid heat sink (a) with only fins and (b) with fins and foams

Overall, 60 cases are considered in this study to select an optimum design by varying the parameters. The parameters accounted for are filling height (h_{fill}), foam porosity (ε), and

foam density. The heights of the foam-filled in the heat sink are 10 mm, 20 mm, and 30 mm. The range of the porosity of foam is 0.8-0.95 with increasing order of pore density from 5 PPI to 25 PPI. Based on the completion of the charging and discharging cycles, the study is undertaken from these parameters.

4.3 NUMERICAL DESCRIPTION

Here, LTNE is preferred with enthalpy porosity formulation for a porous filled PCM-based heat sink. Boussinesq approximation in the liquid state of PCM with density variation to account for natural convection is employed. The fluid is considered Newtonian and incompressible. A laminar and unsteady state for the fluid flow with homogenous and isotropic properties for PCM and foam is considered. During the phase change, the properties such as thermal conductivity, specific heat, and viscosity are kept constant. The shrinkage of PCM volume during solidification and expansion of PCM volume during melting is neglected.

The influencing parameter are foam filling height, pore structure and fin configuration. The foam filling height, representing the vertical extent of a foam or filler material within a designated space, plays a critical role in determining the material's volume and thermal capacity. The pore structure of a material refers to the arrangement, size, and distribution of pores, often characterized by parameters like porosity and pore density. Porosity is a measure of the void spaces or open spaces within a material, often expressed as a percentage of the total volume of the material. It indicates the fraction of a material's volume that is not occupied by solid substances but rather by empty spaces or pores. Pore density refers to the concentration or number of pores within a given volume of material. It quantifies how densely packed the void spaces or openings are within the material structure. Pore density is often expressed in terms of the number of pores per unit area or volume, such as pores per square inch (PPI) or pores per cubic inch (PcI).

The geometric configuration of fins, known as fin shape, affects the flow of heat-transfer fluids and, consequently, the overall efficiency of the system. Fin height, representing the vertical dimension of these extended surfaces, influences the available surface area for heat

exchange. While higher fin heights often provide increased surface area, they may introduce additional resistance to fluid flow. Optimal fin placement, defines the positioning of fin within the enclosure, is determined by factors such as the heat distribution pattern and the desired uniformity of temperature across the system. The performance parameters considered for the optimization encompass solidification time and melting time.

4.3.1 Governing equations

The governing equation when only fins are considered with PCM at first and their governing equations are elaborated in chapter 3.4.1.

When the cases with foams are introduced with the PCM, the governing equations are modified. In combination of both PCM and metal foams (mf) are derived below ANSYS FLUENT (2009),

Continuity equation:

$$\frac{\partial \rho_p}{\partial t} + \frac{\partial (\rho_p u)}{\partial x} + \frac{\partial (\rho_p v)}{\partial y} = 0 \tag{4.1}$$

X-Momentum equation

$$\frac{\rho_p}{\varphi}\left\{\frac{\partial u}{\partial t} + \frac{1}{\varphi}\left(u\frac{\partial u}{\partial x} + v\frac{\partial u}{\partial y}\right)\right\} = -\frac{\partial P}{\partial x} + \frac{\mu}{\varphi}\left(\frac{\partial^2 u}{\partial x^2} + \frac{\partial^2 v}{\partial y^2}\right) + \frac{(1-\Phi)^2}{\Phi^3 + \lambda}\,\mathrm{Au} - \frac{\mu}{K}u - \frac{1}{2}C\rho_p u|u| \tag{4.2}$$

Y-Momentum equations

$$\frac{\rho_p}{\varphi}\left\{\frac{\partial v}{\partial t} + \frac{1}{\varphi}\left(u\frac{\partial v}{\partial x} + v\frac{\partial v}{\partial y}\right)\right\} = -\frac{\partial P}{\partial y} + \frac{\mu}{\varphi}\left(\frac{\partial^2 u}{\partial x^2} + \frac{\partial^2 v}{\partial y^2}\right) + \frac{(1-\Phi)^2}{\Phi^3 + \lambda}\,\mathrm{Av} - \frac{\mu}{K}v - \frac{1}{2}C\rho_p v|v| + \rho_p \beta_0 (T_m - T)\,\vec{g} \tag{4.3}$$

Energy equation:

$$(1-\varepsilon)\left(\rho c_p\right)_{mf}\frac{\partial T_{mf}}{\partial t}=k_{eff_{mf}}\left(\frac{\partial^2 T_{mf}}{\partial x^2}+\frac{\partial^2 T_{mf}}{\partial y^2}\right)+h_{sf}a_{sf}\left(T_P-T_{mf}\right) \tag{4.4}$$

$$\begin{aligned}\varepsilon\left(\rho c_p\right)_P\frac{\partial T_P}{\partial t}+\varepsilon\left(\rho c_p\right)_P\left(u\frac{\partial T_P}{\partial x}+v\frac{\partial T_P}{\partial x}\right)\\ =k_{eff_p}\left(\frac{\partial^2 T_P}{\partial x^2}+\frac{\partial^2 T_P}{\partial y^2}\right)+\varepsilon\rho_p L_p\frac{\partial \Phi}{\partial t}+h_{sf}a_{sf}\left(T_{mf}-T_P\right)\end{aligned} \tag{4.5}$$

The composite porosity is indicated by φ. The terms 4 and 5 on the right side of the momentum equation determine the flow within the open porous medium. The Darcy, non-Darcy, and inertial effects of metal foam are provided by the Darcy-Forchheimer law. The main parameters in the metal foam structure investigations are briefly explored in Chapter 3.4.1.

4.4 GRID INDEPENDENCE STUDY AND VALIDATION

The numerical simulations are carried out in ANSYS Fluent 19, which is based on the finite volume method. A grid size study and a time step size study are performed to obtain numerical accuracy. The liquid fraction is plotted in Figure 4.3 for the hybrid heat sink with varying time periods by fixing filling height 30, porosity 0.8, and 5 PPI. For the grid size study, the time step size is fixed at 0.5 s, and the element size considered is 15000, 20000, and 25000. Element size is set at 20000 by varying time step size from 0.25 s, 0.5 s, and 0.75 s. The time step size and the number of elements selected for the forthcoming simulations are 0.5 s and 20000.

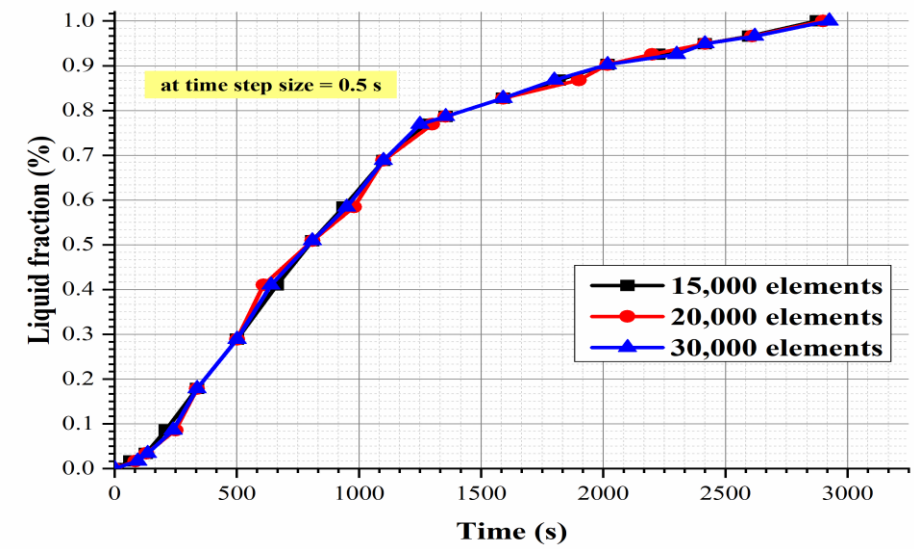

(a)

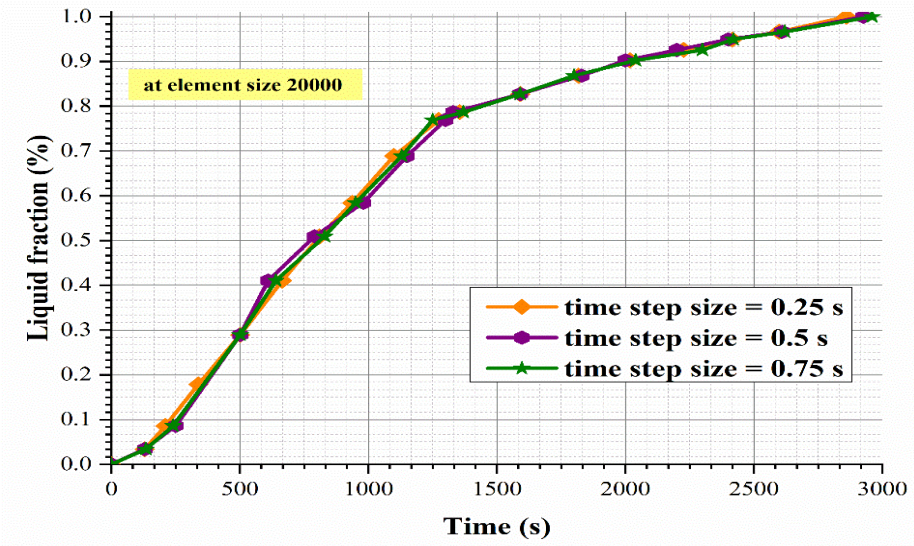

(b)

Figure 4.3 Grid independence study (a) Element size study and (b) Time step size study.

The validation of this numerical methodology is done by comparing the work carried out by Zheng et al. (2018). Paraffin wax is filled in an enclosure with copper metal foams. The porosity of 0.95 and pore density of 5 PPI of copper foam are kept constant, and studies

are done. The temperature variation within the PCM in the enclosure results is compared in Figure 4.4. The left side of the enclosure is heated at a constant heat flux of 1150 W/m^2. The remaining walls are kept in adiabatic conditions, apart from the heating side. Initially, the paraffin PCM is at the temperature of 15^{o}C under no-slip conditions. The experiment was repeated twice under the same conditions to ensure accuracy. The total uncertainty of the experiment was around 7.04 %, including power inputs (2 %), thermocouples (0.4 %), and heat loss (4.6 %). A maximum deviation of 8% around 6000s is found when simulation results are compared with the experimental study. This deviation is due to the thermal properties of the materials used. In experiments, the thermal properties vary with time, but these properties are kept constant in numerical studies.

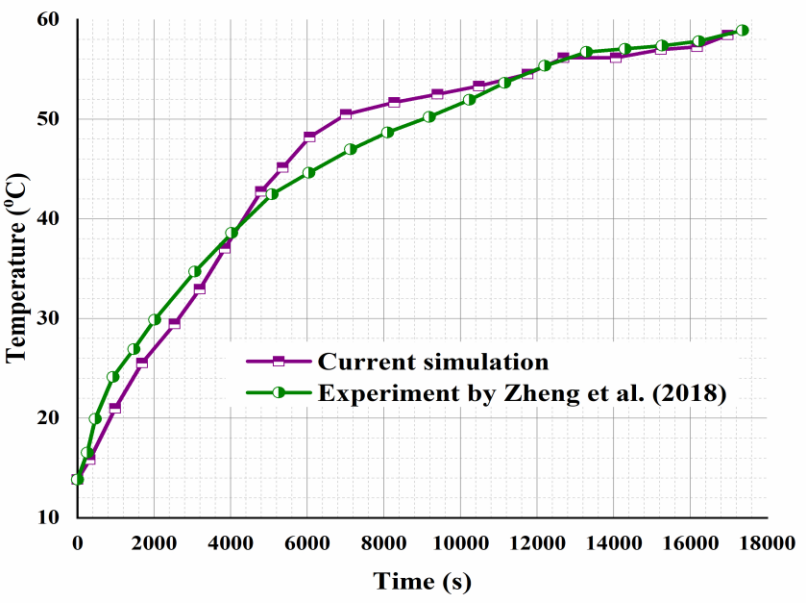

(a)

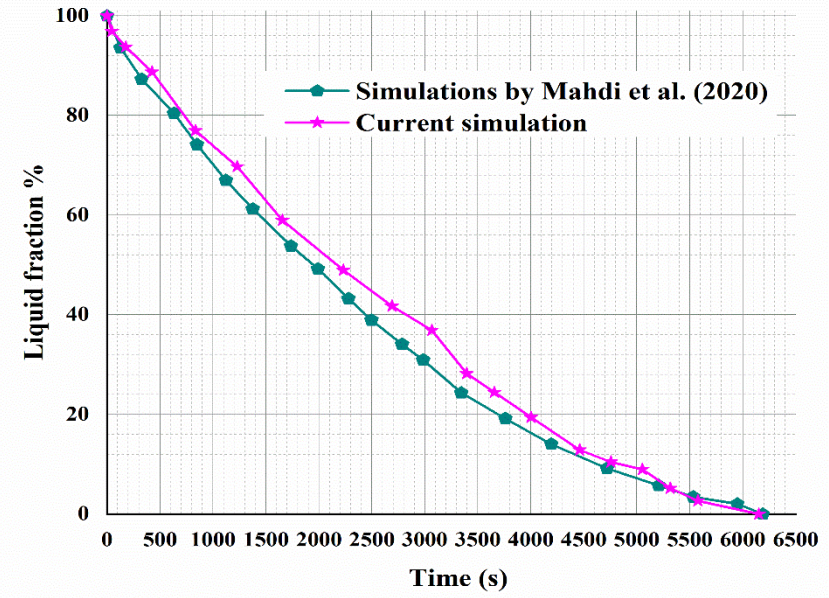

(b)

Figure 4.4 Numerical validation (a) melting process (Zheng et al. 2018) and (b) solidification process Mahdi et al. (2020).

Next, a multiple PCM case is considered to validate the solidification process. The freezing process results from numerical studies by Mahdi et al. (2020) are compared with the present numerical work. The heat sink is filled with three different PCM of RT-55, RT-60, and RT-65. The simulations are carried out in the shell and tube heat exchanger, with an initial temperature of 353 K and leaving the surface temperature to ambient. The remaining walls are kept at adiabatic conditions. From the results, the liquid fraction is plotted for various time intervals, and an average deviation of 3.2 % is observed.

4.5 TOPSIS

Technique for order performance by similarity to ideal solution (TOPSIS) is a versatile multi-objective tool that eases the analysis under circumstances where both desired, and undesired outcomes are accompanied. Previous studies have successfully applied it to comprehensively analyze various tradeoffs between heat transfer maximization and flow resistance minimization in metal foams G and N (2021a); Jadhav et al. (2022). This method permits various weightages on the ability to maximize the desired outcome and on the

ability to minimize the undesired outcome, thereby allowing comprehending the effect of introduced variable conditions.

The present study shows that the advantage of a decrease in solidification time with the use of metal foams with PCM as a result of enhanced heat transfer comes with the disadvantage of decreased melting time. However, the key point lies in the optimal solidification and melting time. In the present study, various parameters such as fin height, positioning of fins, and metal foams of altered structural combinations (porosity and pore density) are considered, and variations in melting and solidification time are witnessed. However, the tradeoff between melting and solidification time must be well understood to comprehensively analyze the outcomes. Techniques like TOSPIS enable one to analyze such conditions where introducing/variation in individual parameters results in both desired (reduction in solidification time) and undesired (reduction in melting time) phenomena mainly due to enhanced heat transfer. Through the TOPSIS method, the outcomes of the present work, i.e., melting time and solidification time with variation in considered parameters such as varying porosity and pore density combinations of metal foams and fin height, are analyzed and subjected to various criteria. Each criterion is adopted based on different weightages placed on maximizing the desired outcome, which is enhancing melting time and minimizing undesired effect, which is reducing solidification time. In the present work, varied parameters such as metal foam properties, fin height, and positioning of the fin are analyzed in combination with PCM, and the TOPSIS method is implemented to comprehend the tradeoff between melting time and solidification time

Various steps involved in implementing the TOPSIS method are as follows G and N (2021):

- Step 1:

Compute columns comprising values of melting time (Mt_{i1}) and solidification time (St_{i2}). Then extend it to two more columns, each comprising normalized magnitudes of values in the first two columns ($\overline{Mt_{\iota 3}}$) and ($\overline{St_{\iota 4}}$) respectively using Eqs. (4.6) and (4.7).

$$\overline{Mt_{\imath 3}} = \frac{Mt_{i1}}{\sqrt{\sum_{i=1}^{n} {Mt_{i1}}^2}} \tag{4.6}$$

$$\overline{St_{\imath 4}} = \frac{St_{i2}}{\sqrt{\sum_{i=1}^{n} {St_{i2}}^2}} \tag{4.7}$$

Where, i = 1, 2, ... , n, implying the rows and 'n' referring to a total number of values (corresponding to all variable conditions).

- Step 2:

Various weights are added to the weighted normalized values using Eqs. (4.8) and (4.9). The distributed weight varying from 0 to 1 is assigned to the previously computed normalized values of melting and solidification based on desired tradeoff scenario.

$$V_{i5} = \overline{Mt_{\imath 3}}.W_m \tag{4.8}$$

$$V_{i6} = \overline{St_{\imath 4}}.W_s \tag{4.9}$$

W_m and W_s are 0 and 1 for criteria I, 0.25 and 0.75, 0.5 and 0.5, 0.75 and 0.25, and 1 and 0 for criteria II, III, IV, and V, respectively.

- Step 3:

Compute ideal worst and ideal best values. Since solidification time is considered a non-beneficial parameter as it is expected to be minimized while melting time is considered the beneficial parameter as it is expected to be maximized, the highest value from the weighted normalized values of solidification time is treated as the ideal worst, while the lowest value from the weighted normalized values of solidification time is treated as ideal best. On the other hand, the highest value from the weighted normalized values of melting time is considered as ideal best, while the least value from the weighted normalized values of melting time is considered as ideal worst, as expressed in Eqs. (4.10-4.13).

$$V_m{}^{+} = \max\,(V_{i5}) \tag{4.10}$$

$$V_s{}^{+} = \min\,(V_{i6}) \tag{4.11}$$

$$V_m{}^{-} = \min\,(V_{i5}) \tag{4.12}$$

$$V_s{}^{-} = \max\,(V_{i6}) \tag{4.13}$$

- Step 4:

Compute Euclidean distance, which refers to the relative distance of individual values in a weighted normalized column from the ideal values identified (best or worst). Positive Euclidean distance corresponds to the distance of each value in the weighted normalized column from the ideal best value and is calculated as given in Eq. (4.14). Similarly, negative Euclidean distance is the distance of each value in the weighted normalized column from the ideal worst value and is calculated as given in Eq. (4.15).

$$S_i{}^{+} = \left[(V_{i5} - V_m{}^{+})^2 + (V_{i6} - V_s{}^{+})^2\right]^{0.5} \tag{4.14}$$

$$S_i{}^{-} = \left[(V_{i5} - V_m{}^{-})^2 + (V_{i6} - V_s{}^{-})^2\right]^{0.5} \tag{4.15}$$

- Step 5:

Performance scores of each variable condition are evaluated using Eq. (4.16). It ranks the considered varying states based on their closeness in meeting the fixed weighted criteria.

$$P_i = \frac{S_i{}^{-}}{S_i{}^{+} + S_i{}^{-}} \tag{4.16}$$

4.6 EVALUATION OF FIN PLACEMENT AND HEIGHT

The steps involved in the numerical procedures are represented as a flow chart in Figure 4.5. The governing equations comprising PCM are solved using finite volume method based ANSYS Fluent software. In this simulation, the methods applied for pressure-velocity coupling are the SIMPLE algorithm and PRESTO! Scheme for pressure correction equation. A second-order upwind scheme is specified in consideration of the discretization

of momentum and energy equations. The relaxation factors default values are set for the pressure, momentum, liquid fraction, and energy. A constant value of 10^{-6} is assorted for both continuity and momentum equations. Whereas for the energy equation, a value of 10^{-8} is specified. Initially, to determine the height of the fin and positioning of the horizontal fin, a few cases were selected and given in Table 4.1.

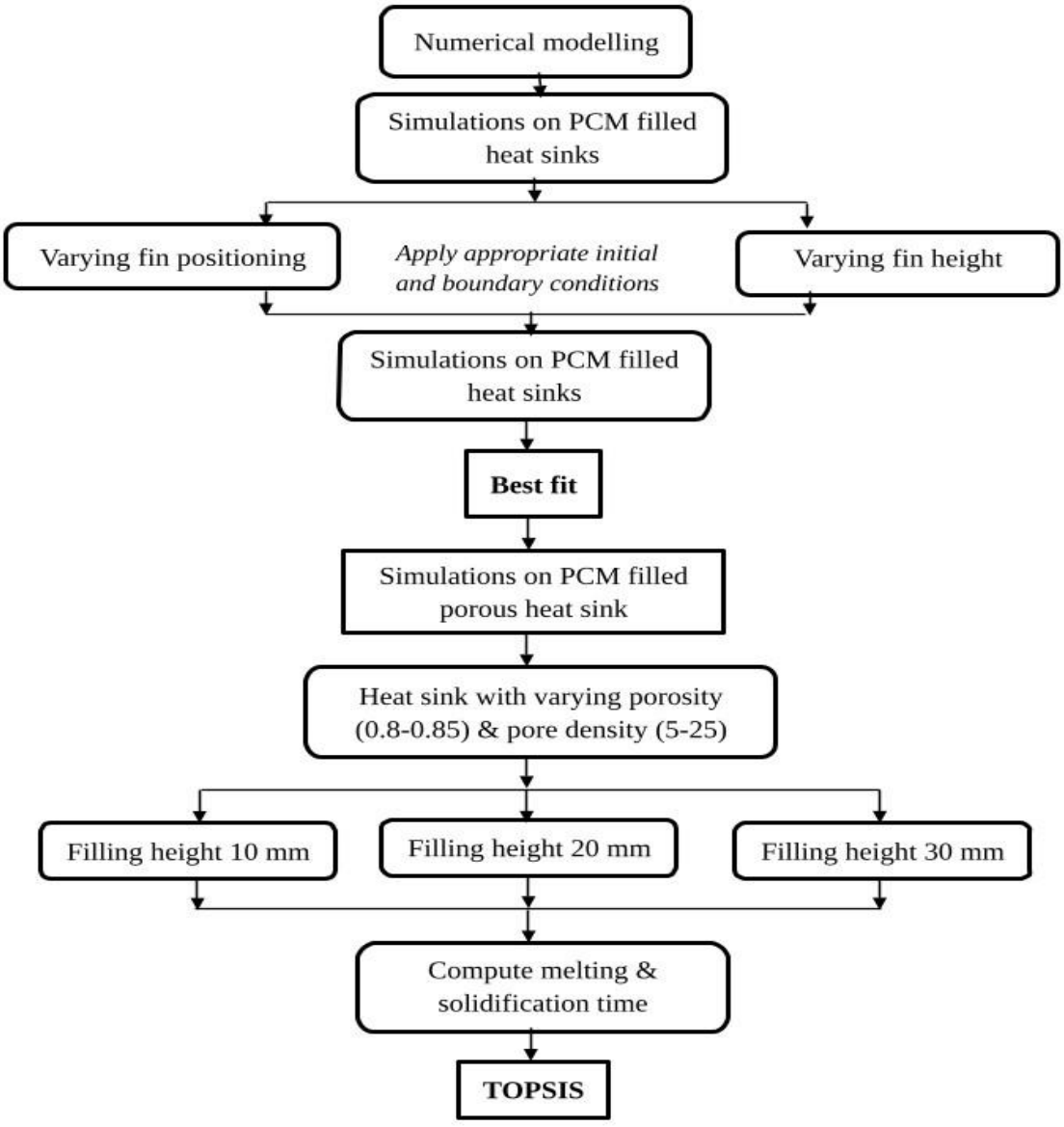

Figure 4.5 Flowchart with the numerical procedure.

Table. 4.1 Case study with only finned PCM heat sink.

Cases	Rectangular Fins		
A (p_f = 13 mm)	1	2	3
	h_f = 16 mm	h_f = 20 mm	h_f = 25 mm
B (h_f = 20 mm)	1’	2’	3’
	p_f = 11 mm	p_f = 13 mm	p_f = 15 mm

In these cases, only fins were selected to acquire the behavior of PCM, and foams were neglected. Since the fin height varies, the thickness of the fin also varies accordingly, but the area of the fin remains constant. The selected geometry is given in Figure 4.2 (a). Three conditions are selected; first, importance is given to the minimization of solidification time completely. In the second condition B, the importance is shared equally between both the objective function of maximizing melting time and minimizing solidification time. And finally, in condition C, the importance is set entirely for the maximization of melting. TOPSIS algorithm is applied to find the best fit among the different cases. The fin positioning and fin height are varied for rectangular shapes, and results are obtained.

Table 4.2 Responses for fin positioning and fin height.

Weightage	Parameters	Best fit	Worst fit
Condition A	p_f	11 mm	13 mm
M_{max} : S_{min} =0:1	h_f	25 mm	16 mm
Condition B	p_f	11 mm	13 mm
M_{max} : S_{min} =0.5:0.5	h_f	25 mm	16 mm
Condition C	p_f	13 mm	15 mm
M_{max} : S_{min} =1:0	h_f	16 mm	25 mm

From the results for all weightages in Table 4.2, it is clear that the rectangular fin shape impacts the system significantly. This is because rectangular fin shapes have a uniform thickness (t_f) throughout the enclosure, which dissipates uniform heat flow. Hence, heat flow is enlarged for rectangular fins within the PCM and accelerates the process. Similarly, considering a fin height of 25 mm for the first two conditions yield better results. This is due to the increased fin height; the amount of heat conducted within PCM also increases, thus accelerating the process. But for condition C, when the importance is solely set to maximization of melting, a lesser fin height delivers a greater outcome because its lesser amount exists within the PCM cavity. Subsequently, setting the horizontal fins from the top wall, for the first two conditions 11 mm, significantly influences the process. When the fin is near the top wall, it affects the natural convection remarkably; as a result, the process is expedited. Inversely, when the fins are placed away from the top wall, it decelerates the melting. Therefore, when the weightage is prolonged melting, 13 mm delivers an extended melting time.

The statement above conveys a clear idea of the placement of horizontal fins at 11 mm from the top wall and the height of fins to be 25 mm. With the variation of fin height, fin thickness also varies; at 25 mm height, the thickness is 5.6 mm. Following this, our main goal to obtain optimized partially filled metal foam with a finned heat sink is assessed. Zhu et al. (2018) studied the effect of partial filling of foams in a PCM-based heat sink. Their communications stated that the fully filling of foams could be uneconomical, and the weightage of the heat sink also became critical. Hence, this work examines a feasible strategy of encompassing the partial filling of foams with fins on a PCM-based enclosure.

4.7 RESULTS AND DISCUSSION

4.7.1 Initial and boundary conditions

The heat is dissipated from the bottom side, and the rest of the side walls are insulated. During the charging cycle, the PCM is initially at the solid phase, and the temperature of foam (T_{mf}) and the temperature of PCM (T_p) are at 27^{o}C. The hot wall side is at a constant wall temperature condition of 50^{o}C. Similarly, during the discharging cycle, the bottom wall is kept at 27^{o}C. The PCM is at the liquid state, and the T_{mf} and T_p are at 50^{o}C.

Table 4.3 Weightage ratio for each criteria.

Weightage ratio	Criteria-1	Criteria-2	Criteria-3	Criteria-4	Criteria-5
M_{max}	0	0.25	0.5	0.75	1
S_{min}	1	0.75	0.5	0.25	0

Performance scores define the score based on their results from TOPSIS. These scores give the importance of each parameter and how it contributes to the objective function. The performance scores range from 0 to 1 for different weightage inputs. For any condition, the parameter closer to value 1 has the best fit for a function, and the parameter closer to value 0 has the worst fit. From Table 4.3, in the first two criteria, the weightages are towards minimizing solidification time. This table is based on the geometry with only fins, which are represented. Likewise, for the last two criteria, the importance is set to maximize melting time. Especially on criteria-1 and criteria-2, the weightage is solely specified to minimize discharging time and maximization of charging time. Finally, the weightage is distributed only for a prolonged charging cycle at criteria-5.

The aim of the present paper is to obtain better thermal enhancement for melting and solidification. In order to compare the variations in parameters during both cycles, it is required to consider this as a separate process. Only if this is treated as a separate process one can come to know which are the beneficial and non-beneficial parameters from the results obtained.

4.7.2 Criteria-1

All the criteria (1-5) and their corresponding Figures (4.6-4.10) are derived from geometry 2 (b), where both fin and foams are placed. In criteria-1, the weightage is mainly set to minimize solidification time and no weightage for melting. The filling height is varied as 10 mm, 20 mm, and 30 mm for different porosity and pore densities, and the results are plotted in Figure 4.6. It is clearly visible from the plots that an increment in filling height leads to the desired effect of solidification, and the performance score is also above 0.88,

according to Figure 4.6 (c). This is because the amount of foam volume within the heat sink is higher, accelerating solidification. Whereas a filling height of 10 mm has more PCM volume and a lesser volume of foams than other filling heights. So there is a longer solidification period, and hence least performance score below 0.07 is observed for 10mm filling height.

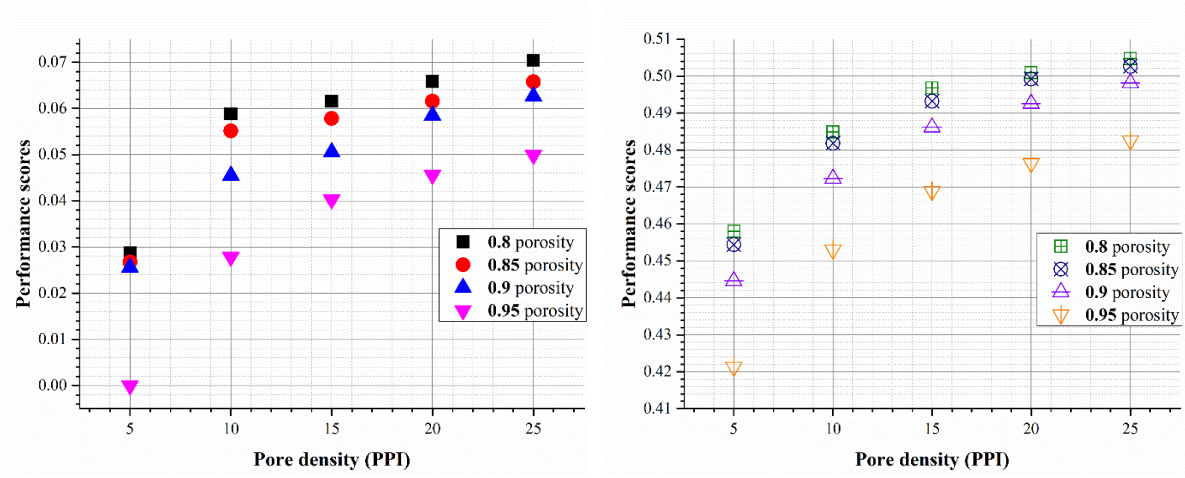

(a) (b)

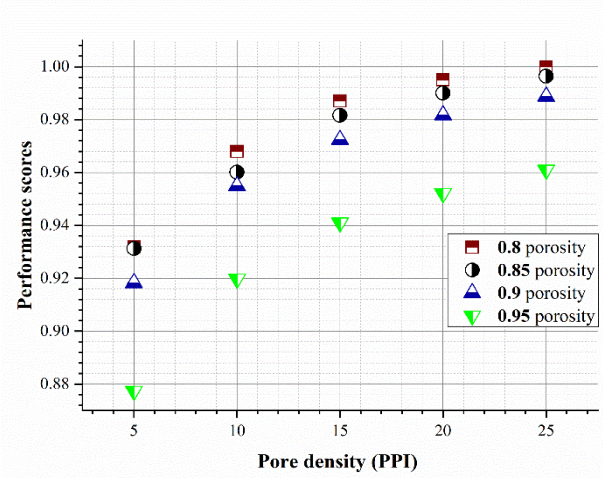

(c)

Figure 4.6 Performance scores of Criteria-1 for filling heights (a) 10 mm, (b) 20 mm, and (c) 30 mm.

When considering porosity and pore density, 0.8 porosity with 25 PPI provides a better outcome. This is the same for all filling height cases. The reason is that compared to 0.95 porosity, 0.8 porosity has a lesser amount of PCM. An increase in void space can fill a larger amount of PCM. Though the difference between scores for 0.8, 0.85, and 0.9 is less, the difference of 0.95 porosity compared with other porosity is large. Similarly, for pore density considering a single unit, the solid structure is higher for higher density. Therefore, 25 PPI yields better results than the other PPI. The trend for all PPI is almost similar at any height.

4.7.3 Criteria-2

In criteria-2, the weightage is mostly inclined towards minimizing solidification time and less towards maximizing melting. Similar to criteria-1 in Figure 4.7, with an increment in filling height, the solidification time is less. But, here quarter amount of weightage is towards the melting time; hence there is a rise in the score for 10 mm filling height and a fall in scores for 30 mm filling height. This explains that when importance is given to both, the objective function filling height considerably impacts the heat sink at these heights. Despite a change in scores for filling heights 10 mm and 20 mm, the performance scores for 20 mm height for both criteria-1 and criteria-2 remain the same.

Correspondingly for varying porosity at 10 mm filling height, except for 0.95 porosity, the trend for remaining porosity increases first and then decreases with an increase in PPI. Besides porosity, the change in PPI does not alter the trend. In parallel to the 10 mm case with varying PPI, for 30 mm filling height apart from 0.95 porosity, the remaining all have an increasing trend at the beginning, and then there is a slight decrement towards the end. 0.95 porosity at 25 PPI yields a higher performance score for both cases. But with PPI cases, 0.95 has the lowest score at 5 PPI, and after that, score is suddenly increased. When the weightage of prolonged melting is considered, 0.95 plays a major role. Irrespective of changes found in the 10 mm and 30 mm filling trends, the trend remains the same for all porosity and PPI for 20 mm filling height. Unlike the other two cases, in this 20 mm filling height, 0.8 porosity with 25 PPI has better performance scores.

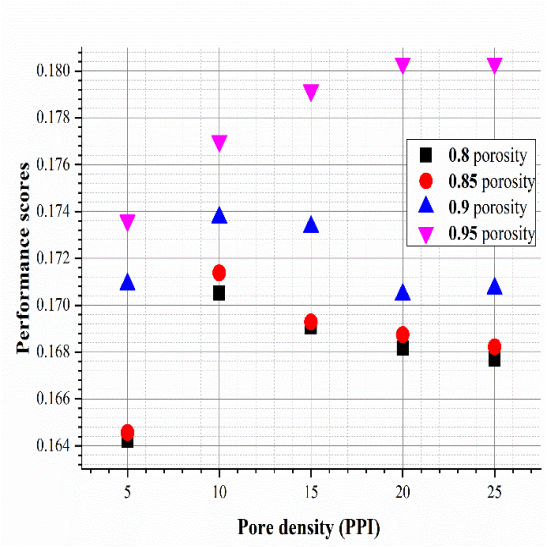

(a)

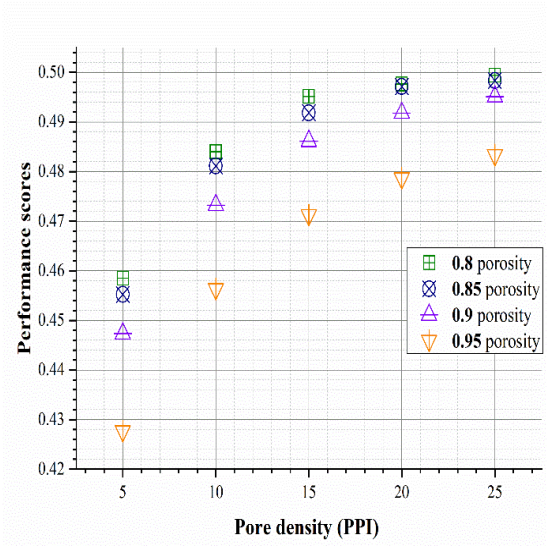

(b)

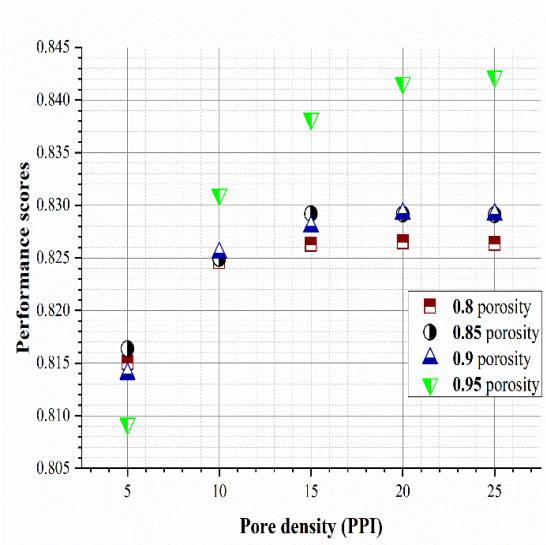

(c)

Figure 4.7 Performance scores of Criteria-2 for filling heights (a) 10 mm, (b) 20 mm, and (c) 30 mm.

4.7.4 Criteria-3

Equal importance is given to both objective functions in criteria-3. Here, an aforementioned discussion is applied, i.e., the higher filling foams affect the solidification significantly. But the performance scores observed from the first three criteria show that

the outcome score is influenced by different weightage applied. The least performance score has been increased from 0 to 0.6 for the filling height of 10 mm in Figure 4.8. Inversely for 20 mm filling height, the maximum performance scores decreased from 1 to 0.606. This shows that the weightage for the given objective function varies, and the performance outcome also gets affected. Despite this occurrence, the performance scores of filling height with 20 mm remain almost the same for the first three criteria.

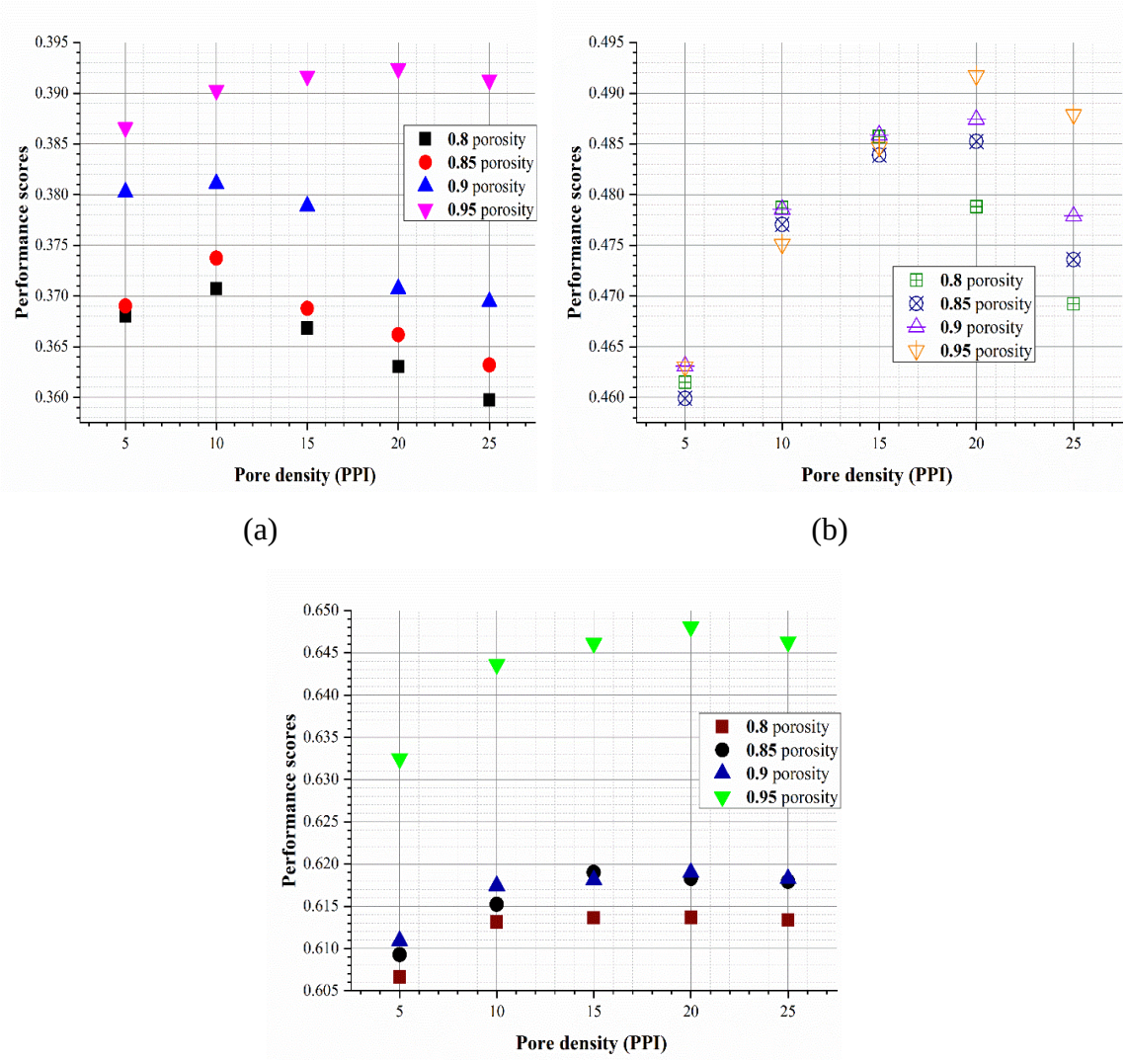

Figure 4.8 Performance scores of Criteria-3 for filling heights (a) 10 mm, (b) 20 mm, and (c) 30 mm.

A porous structure with 0.95 porosity at 20 PPI has higher performance scores for all three cases. In addition to it, the graph shows a rise initially and then falls for all porosity at 10 mm when there is a change in PPI. There is a slight decline at 30 mm filling height at the later end of the plots. A non-identical plot is observed for a filling height of 20 mm; the score increases up to 5 PPI, and it drops down at 25 PPI. The cause of this drop is due to the increase of pore density after 20 PPI becomes significant for 20 mm porous height.

4.7.5 Criteria-4

Low-filling foams try to dominate when the weightage is shifted slightly towards the maximization of melting time. The performance scores are higher for 10 mm than the other two cases. The explanation for this change is when the filling height decreases, the volume of PCM increases. So, the heat transfer within PCM decreases. Therefore the higher amount of PCM leads to a longer melting period. The maximum performance score is observed in Figure 4.9 at 10 mm, and the least performance scores are noted at 30 mm. Whereas, for the case of 20 mm, the performance scores do not alter highly. But, a slight improvement in the maximum performance score is spotted at 0.54.

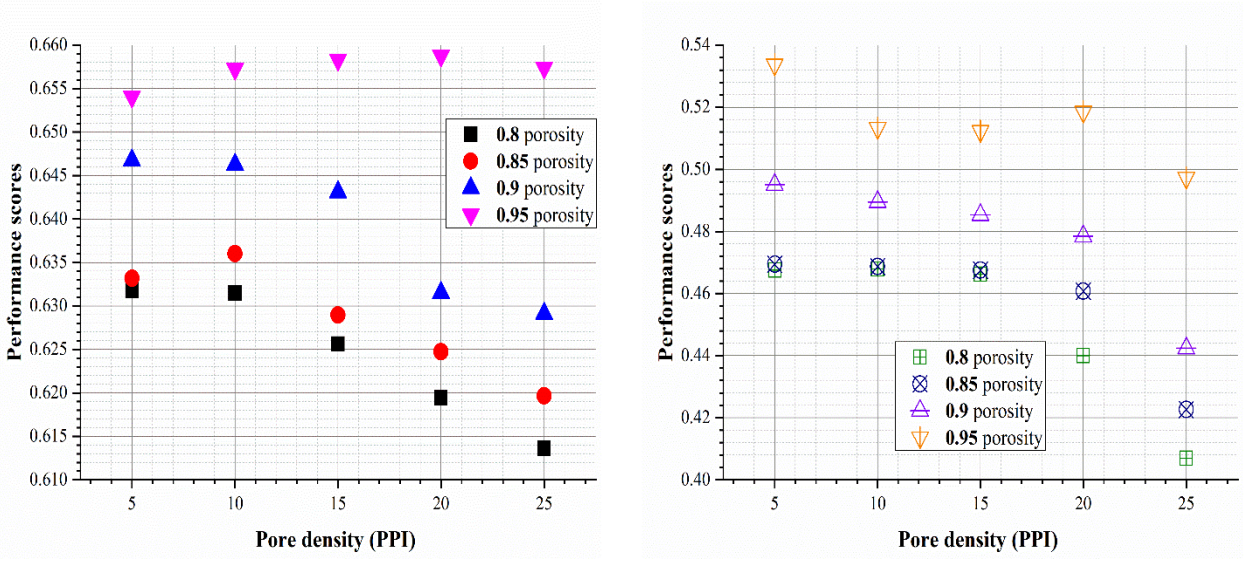

(a) (b)

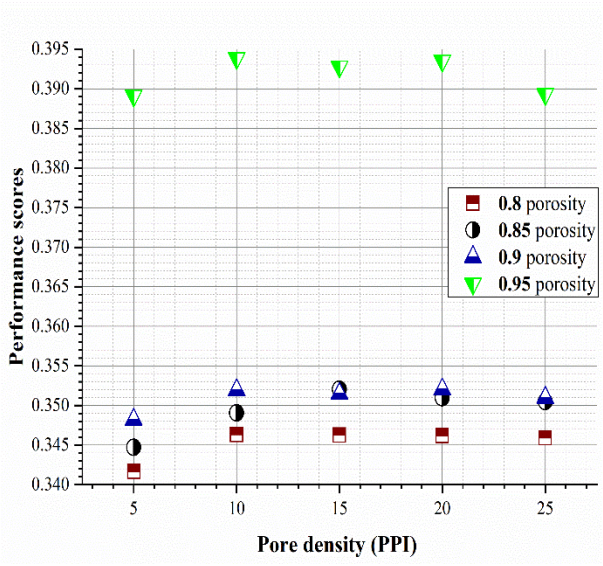

(c)

Figure 4.9 Performance scores of Criteria-4 for filling heights (a) 10 mm, (b) 20 mm, and (c) 30 mm.

A better response is observed in accounting for the porous structure in criteria-4. For all 3 cases, 0.95 porosity has a desirable outcome with varying porosity. However, when there is a change in PPI, distinct results are observed for each filling height case. When the foams are filled to 10 mm, 20 mm, and 30 mm, 20 PPI, 5 PPI, and 10 PPI induce higher scores, respectively.

4.7.6 Criteria-5

The sole weightage is specified for the melting period elongation at criteria-5. Contrarily to criteria-1, here, null weightage is defined for shortening of solidification time. Consequently, it leads to a large PCM volume in the heat sink for a preferable effect. From Figure 4.10, it is noticed that with an increase in filling height, the performance score decreases. A decrease in foam height leads to a lesser amount of foam, and a longer melting period is observed. 10 mm filling height is a higher performance score of 1, and the least score of 0 is spotted at 30 mm filling height. Whereas for 20 mm filling height, there is a slight improvement of the maximum score noted.

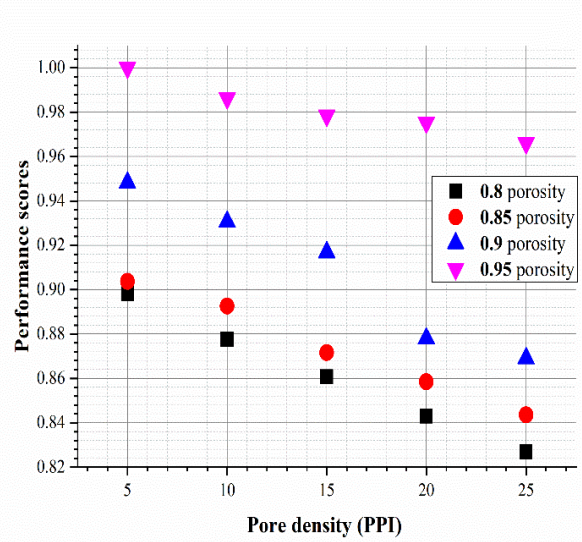

(a)

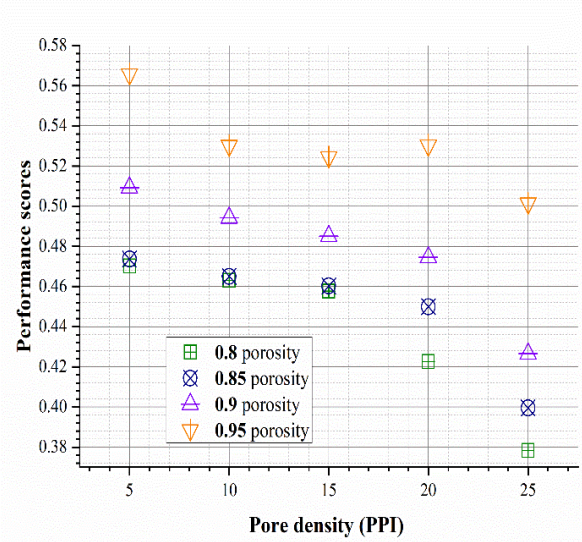

(b)

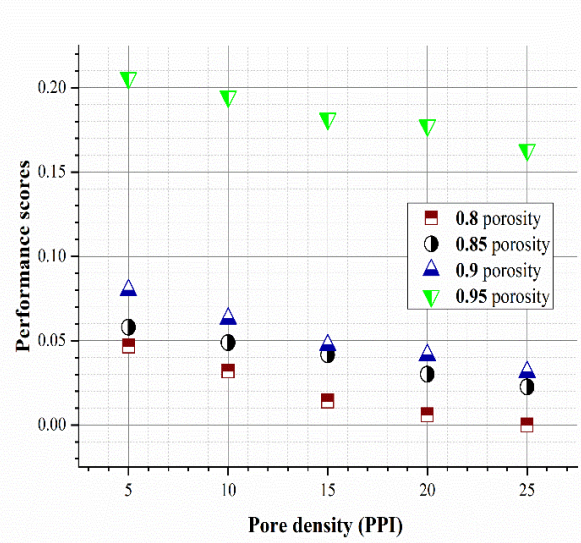

(c)

Figure 4.10 Performance scores of Criteria-5 for filling heights (a) 10 mm, (b) 20 mm, and (c) 30 mm.

When assessing the effects of porosity for filling height cases, there is a drop in performance with rising PPI. All other cases follow the statement above except for 20 mm filling height, with 0.95 porosity at 20 PPI. For all cases of foam height, 5 PPI with 0.95

porosity shows the best response. The reason behind this is with a decrease in PPI, a less solid structure is introduced to PCM. Hence a reduced heat transfer is observed, leading to extended melting.

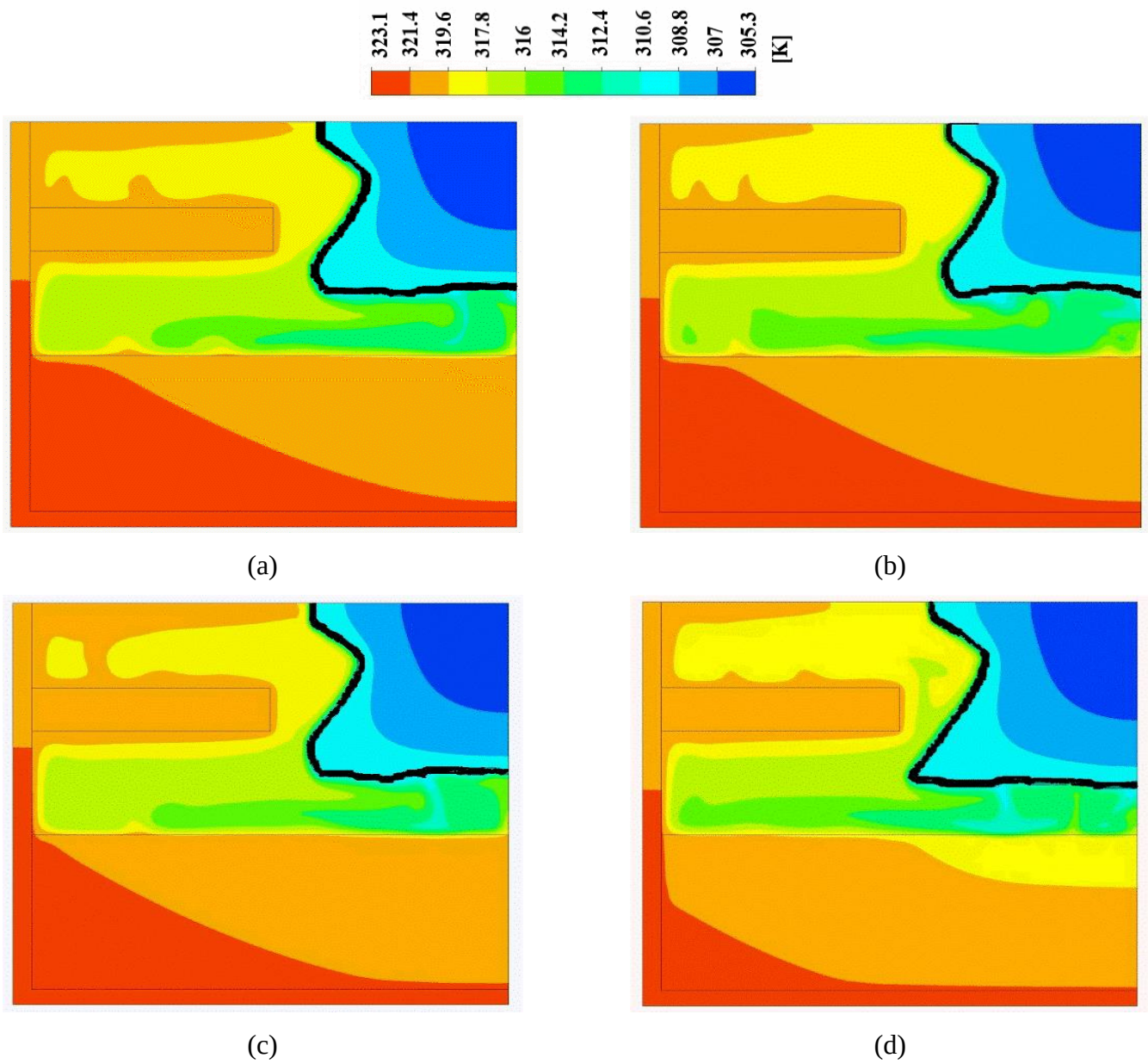

Fig. 4.11 Contours of the heat sink with filling height 20 mm at 25 PPI for different porosities (a) 0.8 (b) 0.85 (c) 0.9 (d) 0.95.

Table 4.4 Ideal solutions for all criteria.

Criteria	Melting/solidification time	Ideal positive/negative	Ideal solutions
Criteria-1	M_{max}	ideal positive	0
		ideal negative	0
	S_{min}	ideal positive	0.08
		ideal negative	0.168784354
Criteria-2	M_{max}	ideal positive	0.039381738
		ideal negative	0.02505625
	S_{min}	ideal positive	0.06
		ideal negative	0.126588266
Criteria-3	M_{max}	ideal positive	0.078763476
		ideal negative	0.0501125
	S_{min}	ideal positive	0.04
		ideal negative	0.084329177
Criteria-4	M_{max}	ideal positive	0.118145214
		ideal negative	0.075168751
	S_{min}	ideal positive	0.02
		ideal negative	0.042196089
Criteria-5	M_{max}	ideal positive	0.157526952
		ideal negative	0.100225001
	S_{min}	ideal positive	0
		ideal negative	0

The contours are plotted to better understand the temperature distribution and melt fraction curve. The heat sink with a filling height of 20 mm at different pore sizes and pore densities is considered in Figures 4.11 and 4.12 at a time interval of 2000 s. The time interval of 2000 s is selected, which shows a clear melt fraction and temperature plots. The melt fraction curve is displayed in black color, where liquid PCM is found below the curve, towards the heater surface, and solid PCM is found above the curve. In Figure 4.11, the pore density is fixed at 25 PPI, porosity is varied, and contours are obtained. It is clearly seen that with increasing porosity, the temperature distribution is found to be higher at low porosity. It is because, for low porosity, the solid volume is higher, and the amount of PCM volume is less. Due to this, the completion of melting is found quicker at 0.8 porosity and slower at 0.95 porosity and vice versa for solidification.

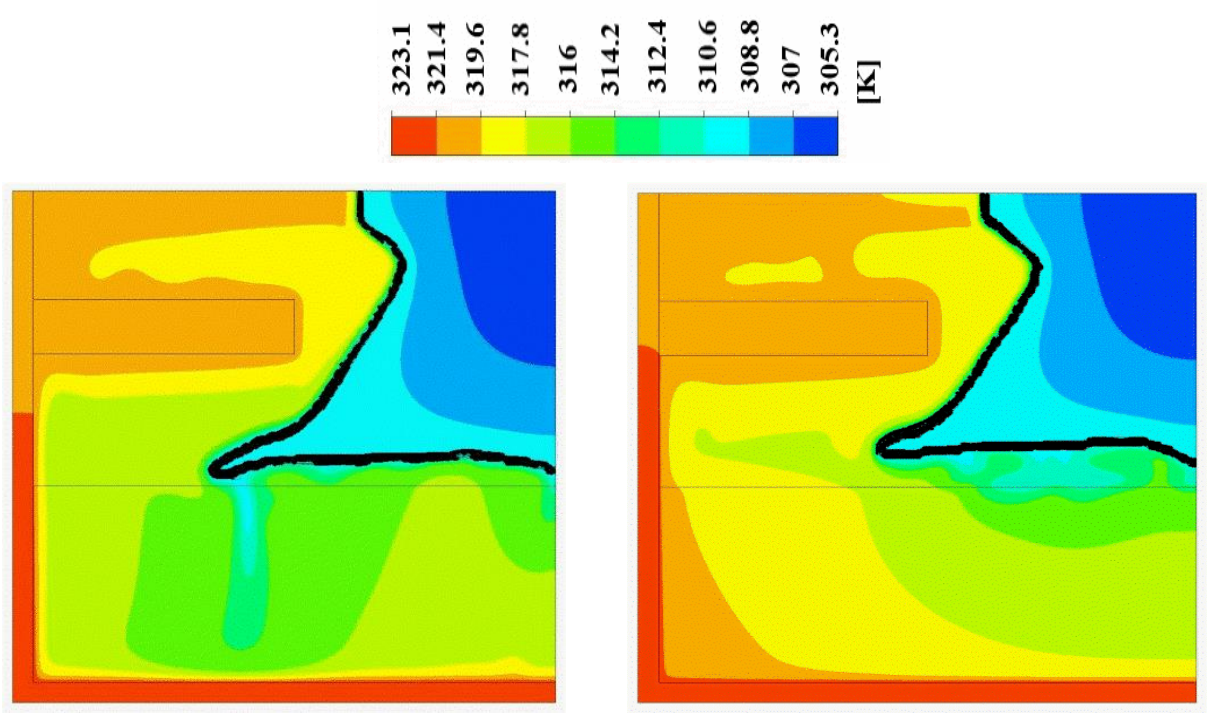

(a) (b)

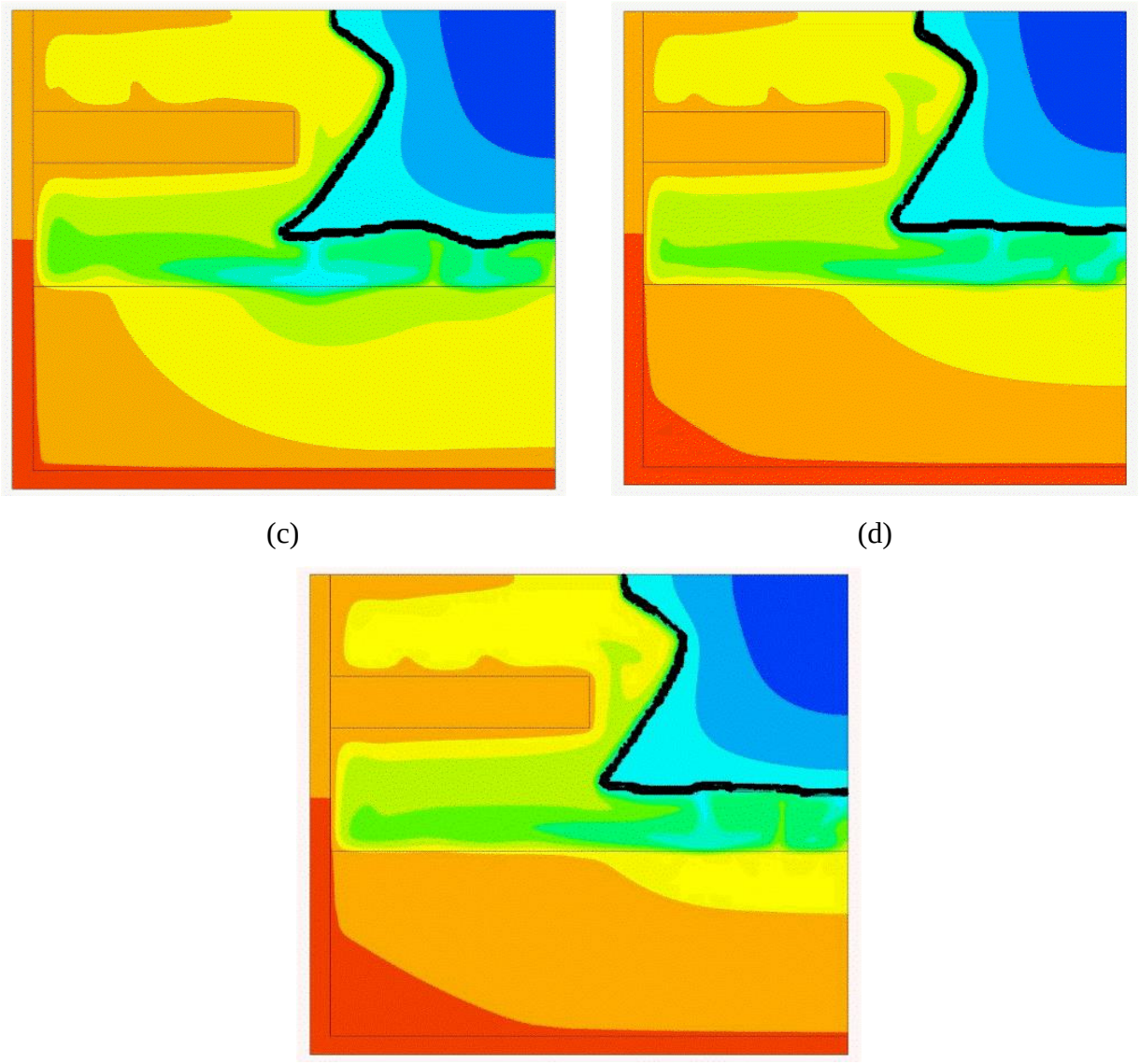

(c) (d)

(e)

Fig. 4.12 Contours of the heat sink with filling height 20 mm at 0.95 porosity for different pore densities (a) 5 PPI (b) 10 PPI (c) 15 PPI (d) 20 PPI (e) 25 PPI.

Next, in Figure 4.12, at 0.95 porosity, different pore densities are varied, and contours are plotted. A significant difference in temperature distribution and melt fraction curve is observed in Figure 4.12. As mentioned above, the solid volume influences the melting and solidification processes. With higher PPI in both cycles, the heat transfer performance is

enhanced and completes the process at a faster rate. Also, the ideal positive/negative solutions value for all five criteria is given in Table 4.4.

4.8 SUMMARY

A 2D numerical model for 60 cases was developed in ANSYS Fluent 19. The geometry with varying filling heights and different pore structures was established in this study. The filling height was varied from 10 mm to 30 mm for a feasible heat sink strategy. The porosity ranging from 0.8-0.95 with increasing pore density from 5-25 PPI is altered for the study. A reliable algorithm of TOPSIS was used for multi-objective optimization. The two objective functions of the investigation were minimizing solidification time and maximizing melting time. Five criteria were selected based on the input weightage towards the objective function. On the basis of each criterion, performance scores were plotted for the required filling height, and the following observations were made.

- The evaluation of fin shape, fin placement, and height is done initially. The rectangular fin shape with uniform thickness enhances the heat transfer with uniform temperature distribution within the enclosure. Considering the effective outcome, the fins can be placed 11 mm from the top surface with a height of 25 mm and a thickness of 5.6 mm.
- For criteria-1, the weightage is solely set towards the minimization of solidification, and no weightage is set for maximizing melting time. Hence, the higher filling heights yield accelerated solidification. Considering the porous structure, the porosity of 0.8 with 25 PPI delivers the best performance for all cases of filling heights.
- In criteria-2, there is a one-quarter weightage towards maximizing the charging cycle and remaining towards minimizing discharging cycle. Similar to 1st criteria, filling height with a higher value also performs better. When it comes to porosity and PPI, for 10 mm and 30 mm filling height cases, 0.95 and 25 PPI provide higher scores. But for the 20 mm case, 0.8 porosity at 25 PPI has a preferable outcome.

- The weightage is shared equally between both the objective functions in criteria-3. Higher filling height dominates when the weightage is equal and more for minimizing solidification time with respect to maximizing melting time. Hence for the first three criteria, the filling height of 30 mm has a superior response compared to other filling heights. 25 PPI with 0.95 porosity has higher performance scores for all cases of filling heights.
- At criteria-4, the weightage is in favor of a prolonged melting period. When the weightage is altered, lesser filling height influences the system. Here for all filling heights, 0.95 porosity shows better results. Whereas accounting PPI, 25, 5, and 10 give high scores for filling heights of 10 mm, 20 mm, and 30 mm, respectively.
- In the last criteria, opposite to criteria-1, the weightage is specified only for melting time maximization. As mentioned, when the weightage is applied to maximize the charging cycle, 10 mm filling height dominates other cases. Assessing the porous structure, 5 PPI with 0.95 porosity metal foam generates prolonged melting.

4.9 CLOSURE

This chapter concludes that the porous matrix impacts the finned PCM-based systems at varying filling heights. Depending upon the weightage required, the filling height and porous physical characteristics can be selected. This description provides a deeper analysis of a wide range of porous sizes and densities. Thus, these guidelines can be beneficial when partial filling can be employed with a fin on a PCM-based heat sink. In the next chapter, multiple PCM is employed in the heat sinks, and their effect on heat transfer performances are discussed.

CHAPTER 5

ANALYSIS OF PCM-BASED HEAT SINK WITH MULTIPLE PCM DURING CHARGING CYCLES

5.1 INTRODUCTION

This chapter aims to present a numerical study for a prolonged charging cycle with a multiple PCM storage heat sink. A combination of two types of enhancers comprises a hybrid heat sink to provide the required outcome. In this work, fins, as thermal spreaders, are introduced to the multiple PCM storage units. Generally, the chosen material does not have similar thermal properties for different melting temperatures. Here, nonetheless, three different PCMs, RT-28HC, RT-35HC, and RT-44HC, with almost identical thermophysical properties, are taken into consideration. The objective is to characterize the effect of fin orientation for prolonged melting and also to assess the significance of a triple PCMs system during melting compared to single and double PCM designs. The initial conditions of the sink and PCM are varied, and their significance is also analyzed. The melt fraction, temperature distribution, and enhancement percentage are explored for various heat fluxes.

5.2 COMPUTATIONAL DOMAIN

By utilizing a two-dimensional model, the numerical solution of PCM-based heat sinks can be simplified, as depicted in Figure 5.1. A rectangular cavity made of aluminum contains the PCM cavity and acts as a thermal spreader. The dimensions of the rectangular cavity are l_s (100 mm), h_s (25 mm), and w_{st} (5 mm). Heat input is specified by uniform heat flux (q) and is defined at the bottom of the heat sink. Three different PCM are placed inside the aluminum sink, with equal b_p (29 mm) and h_p (20 mm) dimensions. RT-28HC, RT-35HC, and RT-44HC are the materials employed, and these are arranged in the increasing order of their melting temperature, respectively.

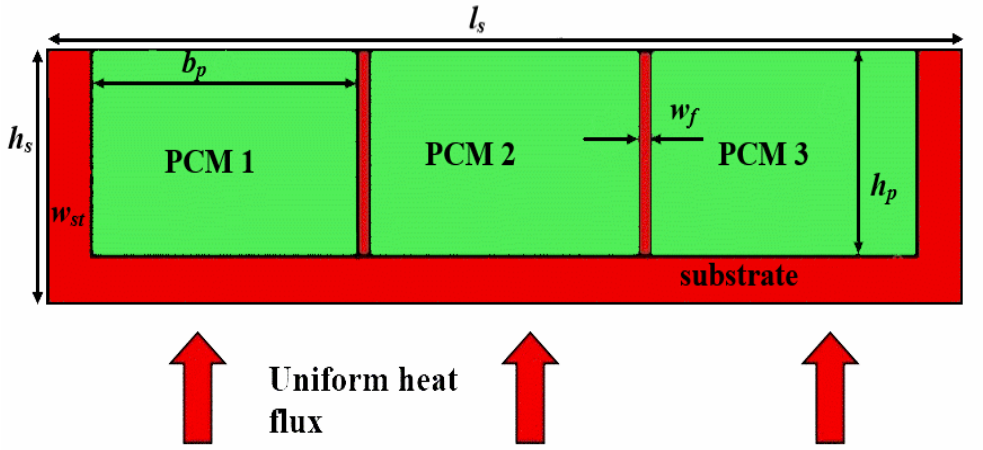

Figure 5.1 2-D Geometry of multiple PCM-based heat sinks.

Among the PCMs, two fins with a thickness (w_f) of 1.5 mm each are placed between them to provide uniform cooling. These fins can act as a thermal spreader and a splitter to contain different materials. Fins with equal thickness are oriented at different angles for a favorable thermal outcome. By placing the vertical fin as a reference, the inclination angle (θ) ranges from positive orientation, 60^o (left side of vertical fin), to negative orientation, -60^o (right side of vertical fin). Aluminum is selected as a material for both the substrate and fins. Figure 5.2 projects the geometry of 9 different cases included in this study. The properties of the materials incorporated are listed in Table 5.1.

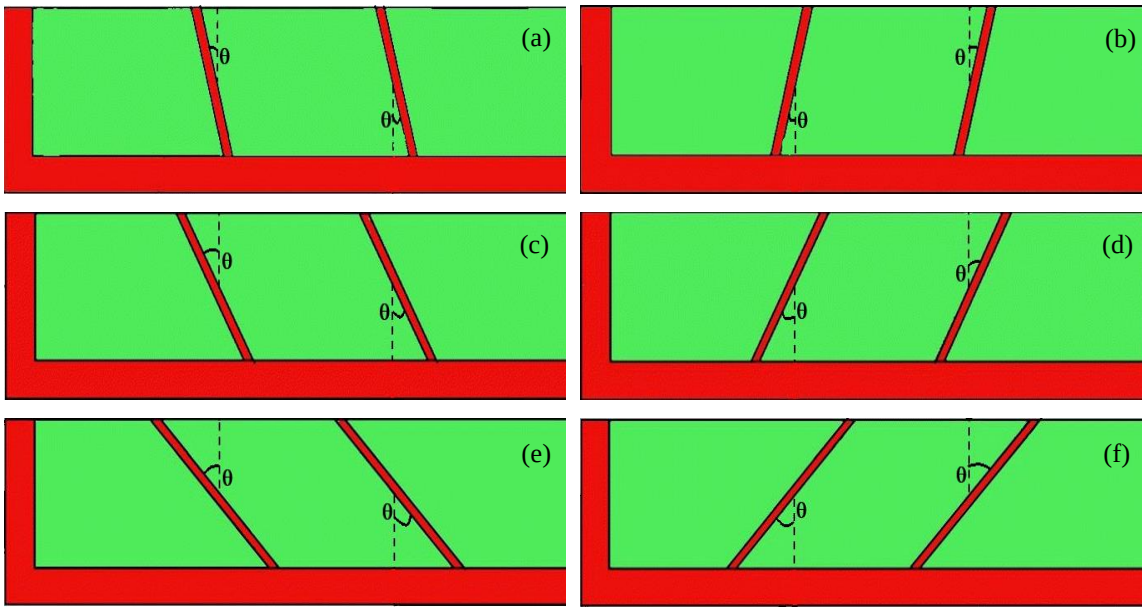

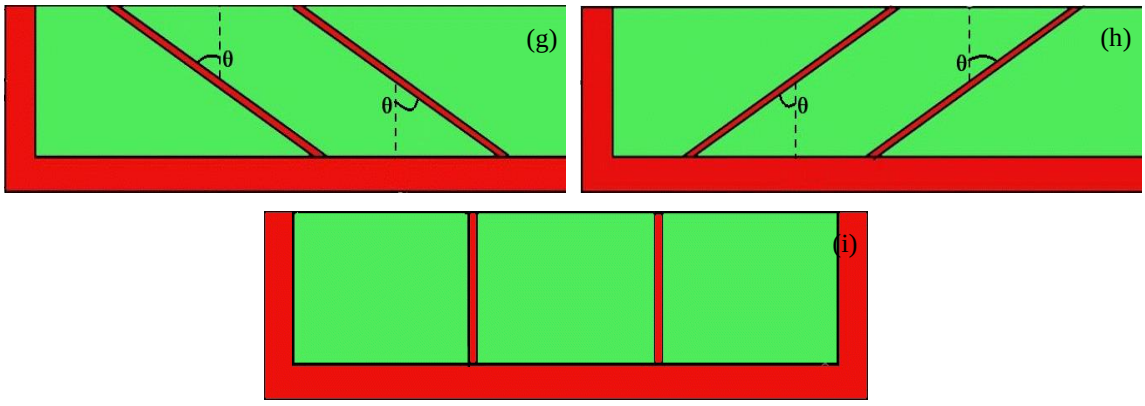

Figure 5.2 Design of tilted fins with various angles: (a) +15º (b) -15º (c) +30º (d) -30º (e) +45º

(f) -45º (g) +60º (h) -60º (i) 0º.

Table 5.1 Properties of the materials

Thermal Properties		Unit	RT-28HC	RT-35HC	RT-44HC	Aluminium
ρ		kg/m^3	770	778.2	700	2719
c_p		kJ/kg.K	2	2	2.1	0.871
L		kJ/kg	245	220	218	-
k		W/m.K	0.2	0.116	0.2	202.4
μ		kg/m.s	0.002387	0.0044	0.008	-
β_0		K^{-1}	0.0005	0.000865	0.00259	-
Phase change temperature	T_s	K	300.15	307.65	315.5	-
	T_l		302.15	309.15	317.15	-

5.3 NUMERICAL MODELS

Melting and solidification of PCM are done using ANSYS Fluent based on the enthalpy porosity technique. In this technique, the solid/liquid interface in the phase change process is not tracked explicitly. Alternatively, in the PCM domain at each cell volume, an amount of liquid phase is computed. This is called a liquid fraction and is derived from enthalpy balance.

Porosity one indicates material is in liquid form, and the value of the liquid fraction is 1. Porosity is zero means it is in solid form, and a liquid fraction is 0, where the velocity also drops to zero. The region between 0 and 1 where liquid fractions occur is called the mushy zone. The governing equations are discussed earlier in Chapter 3.4.1

5.3.1 Numerical details

An FVM technique-based commercial software ANSYS Fluent 19 is applied to solve the governing equations. The SIMPLE algorithm and PRESTO scheme are employed for the pressure-velocity coupling and pressure correction equation. The second-order upwind scheme has opted for the discretization of momentum and energy equations. The convergence criterion considered for continuity, momentum, and energy equation is 10^{-5}, 10^{-5}, and 10^{-8}, respectively.

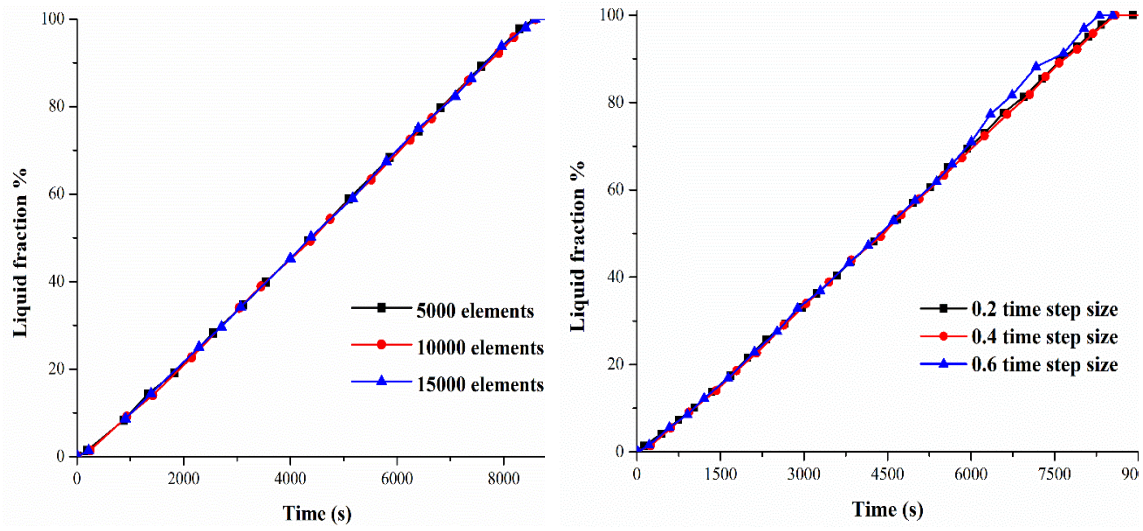

(a) (b)

Figure 5.3 Grid independence study.

A transient formulation with a constant thermophysical property for PCM (except for density) and laminar flow is considered. The fluid is assumed to be Newtonian and incompressible. During the charging cycle, the expansion of PCM is neglected. Natural convection can be exploited by applying the Boussinesq approximation within the PCM.

An enthalpy-based formulation is adopted in this work, where the liquid fraction is not tracked explicitly.

Different grid sizes, such as 5000, 10000, and 20000 elements with a constant time step size of 0.4 s, are simulated, and liquid fraction vs. time is plotted in Figure 5.3. For heat flux of 400 W/m^2, the time step sizes of 0.2, 0.4, and 0.6 were tested by fixing 10000 elements, and the liquid fraction results were plotted. After the comparison, the grid size and time step size selected for the simulation are 10000 elements and 0.4 s step size, respectively.

5.4 VALIDATION

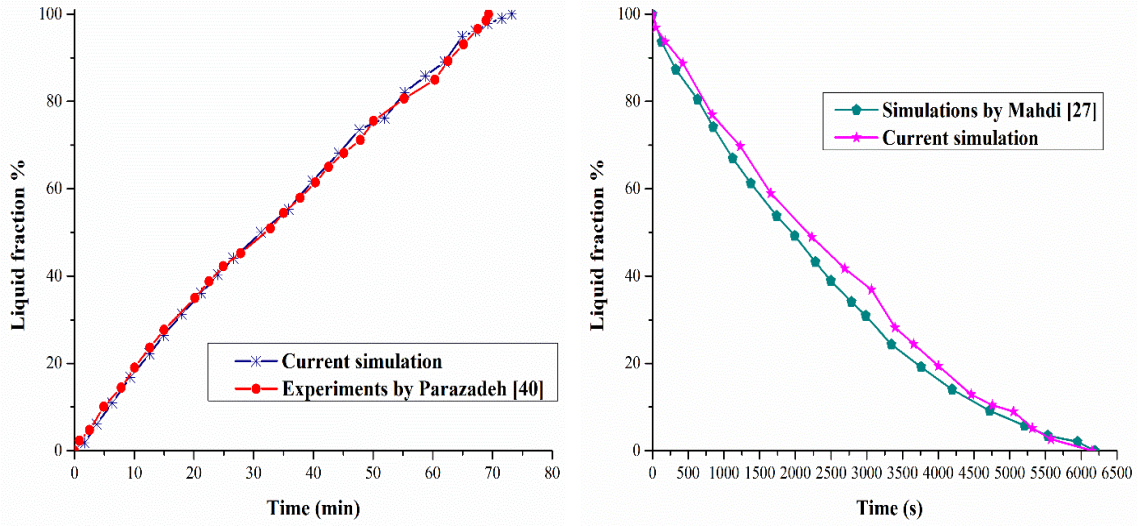

(a) (b)

Figure 5.4 Validation for (a) single PCM and (b) multiple PCM**.**

Our numerical results are validated against the experimental work carried out by Parsazadeh and Zuan (2020). A PCM (coconut oil) melting behavior in a 60 x 60 mm square enclosure is investigated. The enclosure is heated isothermally at the bottom, and the rest of the walls are insulated. The initial temperature of the square enclosure is at 15^{o}C, and a constant heated wall temperature of 55^{o}C is specified. The liquid fraction percentage is plotted against time in Figure 5.4 (a), and fine accordance between numerical and experimental results is observed. An average deviation of 4.56% is spotted between experimental and numerical simulations.

When using multiple PCMs, our results were compared with those obtained by (Mahdi et al. 2020), which used three different PCMs, RT-55, RT-60, and RT-65. At the initial temperature of 353 K, a shell and tube heat exchanger was simulated, with an adiabatic boundary condition at the shell side. In Figure 5.4 (b), a 3.2 % of average deviation is observed when the liquid fraction is plotted against time.

5.5 INFLUENCE OF DIFFERENT ARRANGEMENTS

As shown in Table 5.2, six different cases are considered with straight fins in order to determine the best PCM arrangement.

Table 5.2 Different arrangements of multiple PCM.

Cases	PCM-1	PCM-2	PCM-3
A	RT-44HC	RT-28HC	RT-35HC
B	RT-44HC	RT-35HC	RT-28HC
C	RT-35HC	RT-44HC	RT-28HC
D	RT-35HC	RT-28HC	RT-44HC
E	RT-28HC	RT-35HC	RT-44HC
F	RT-28HC	RT-44HC	RT-35HC

An investigation was conducted to evaluate the effects of different arrangements on a multi-PCM heat sink operating at 500 W/m^2. The average heater temperature of a heat sink is taken and plotted against time in Figure 5.5 (a). As seen, the cases studied here lead to indistinguishable wall temperatures. Moreover, the time taken for the heater to reach a set point temperature (SPT) of 45^{o}C and 50^{o}C is plotted in Figure 5.5 (b). The total time required to attain those temperatures is almost the same for all the cases. The time difference between all the cases is found to be 15-20 s. Hence, as demonstrated by Figure 5.5 (a), (b), the PCMs can be arranged in any order, in parallel compartments for this basal heating problem.

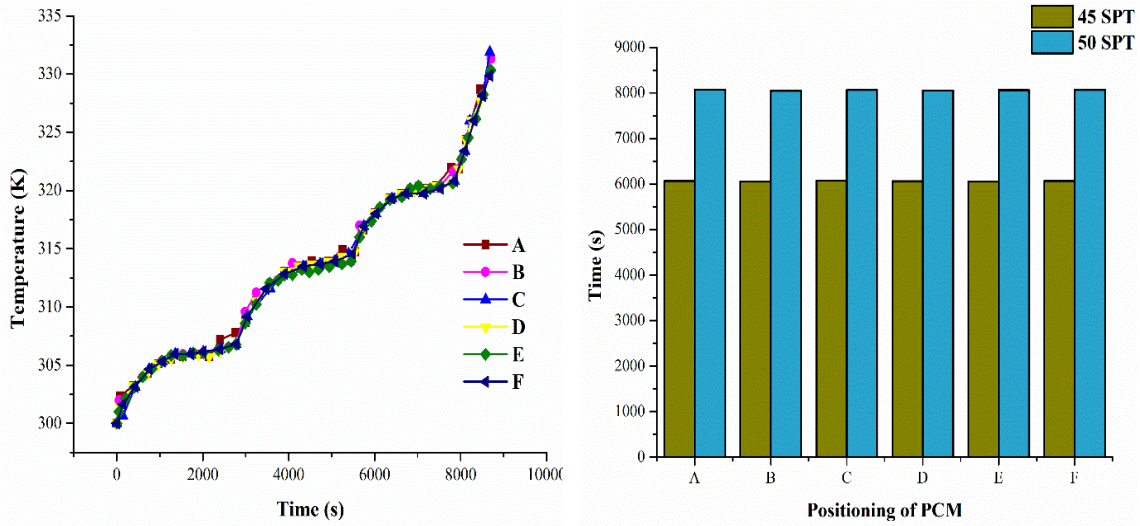

(a) (b)

Figure 5.5 (a) Heater temperature v/s time. (b) Time to attain setpoint temperature for different positioning of PCM.

5.6 SIGNIFICANCE OF MULTIPLE PCM

The better performance of the multiple PCM is indicated in Figure 5.6. A heat sink with a straight fin is selected for this comparison. Four different sinks are investigated: three of them with single-PCM, RT-28HC, RT-35HC, or RT-44HC, and a triple PCM that all three fill the enclosure. A uniform heat flux of 500 W/m^2 is specified at the bottom of the sink. A charging cycle should have an extended duration of melting, and the discharging cycle must have a reduced duration of solidification for an effective heat sink Sridharan et al. (2018). Hence, numerical simulation has been performed to compare RT-28 HC PCM heat sink and multiple PCM during solidification. The boundary condition of the heater is specified as ambient temperature, and the PCM is at a liquid state with 323 K as an initial condition. In Figure 5.6 (c), the solidification time taken for the multiple PCM is 7000 s faster than the heat sink filled with RT-28HC. The latent heat is higher for RT-28HC; hence during the charging cycle, it helps in prolonged melting, but during the discharging cycle, it increases the time to solidify.

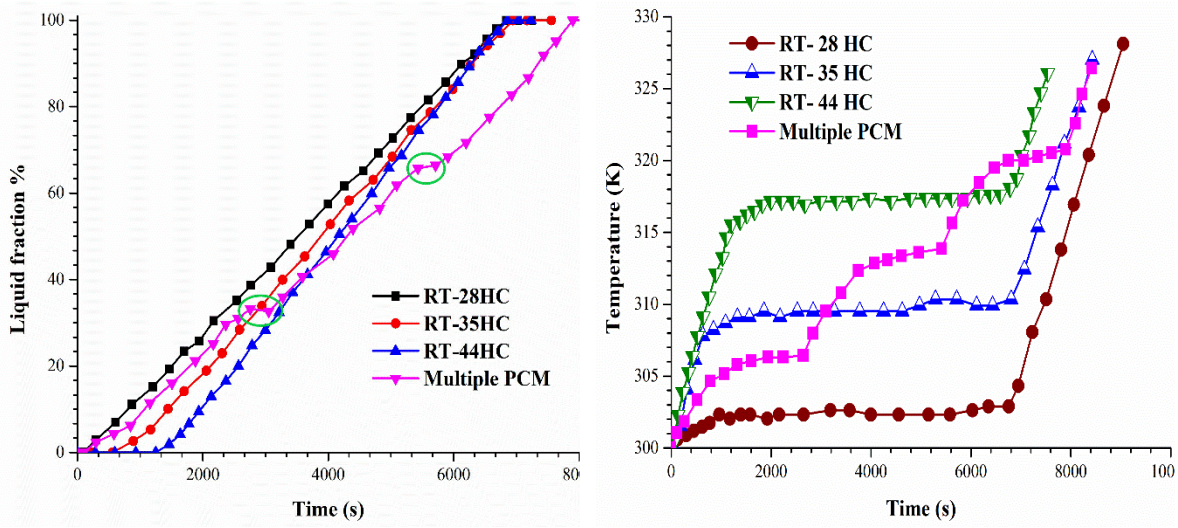

(a) (b)

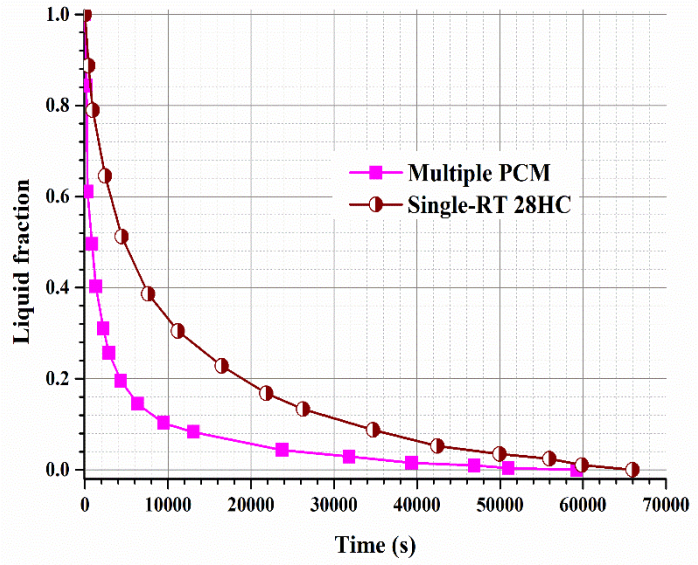

(c)

Figure 5.6 Comparison of single PCM v/s multiple PCM (a) liquid fraction v/s time, (b) heater temperature v/s time, and (c) liquid fraction v/s time.

Hence, for the charging cycle a different PCM and for the discharging cycle a different PCM cannot be selected. Therefore, for both cycles, a similar PCM unit must be selected. The incorporation of PCM in a heat sink should account for a longer charging cycle and shortened discharging cycle. To account for longer melting, shorter solidification, and transient heat loads, multiple PCM can be suitable for better performance than other cases.

Therefore, in this study for melting cases, multiple PCM is selected. Next, an investigation of a double-PCM design for the different cases is listed below in Table 5.3.

Table 5.3 Different cases of double PCM-filled heat sink.

Cases	PCM-1	PCM-2	PCM-3
A’	RT-35HC	RT-28HC	RT-35HC
B’	RT-44HC	RT-28HC	RT-44HC
C’	RT-28HC	RT-35HC	RT-28HC
D’	RT-44HC	RT-35HC	RT-44HC
E’	RT-28HC	RT-44HC	RT-28HC
F’	RT-35HC	RT-44HC	RT-35HC

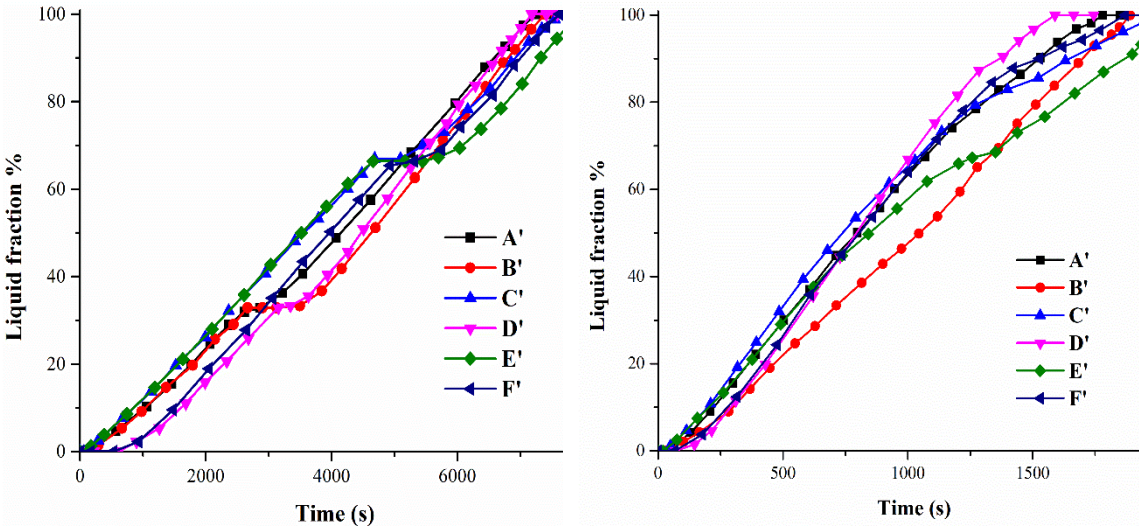

(a) (b)

Figure 5.7 Liquid fraction %of double PCM heat sink (a) For 500 W/m^2 and (b) 3000 W/m^2.

The evolution of liquid fraction for different cases with double PCM for 500 W/m^2 and 3000 W/m^2 heat flux is shown in Figure 5.7. Case E' provides a more extended melting period for both the heat fluxes than other cases. It is due to the combined effect of the properties of RT-28HC and RT-44HC. RT-28 possesses longer latent heat, and it is

incorporated on both sides, which increases the latent heat period. Then, RT-44HC contains a higher melting temperature where the heat sink takes a long time to attain this temperature. So, the combined effect of these properties provides a longer duration of the charging cycle.

For a better understanding, all the cases are compared to multiple PCM-based enclosures. For all the double cases, the time duration to complete the charging cycle of double PCM is compared with multiple PCM. In Figure 5.8, the "time difference" between the double PCM cases and the triple PCM case is shown. As seen, the time difference is the shortest with case E' because of the favorable thermophysical properties. Next, case C' indicates a lesser time difference; the outer area is filled with RT-28HC. Due to its higher latent heat, the time taken also increases. Whereas case D' displays a longer time difference than the other cases. Here, the reason seems to be the combined effect of RT-35HC and RT-44HC. This combined case of PCM provides a faster melting rate because the difference in melting temperature of both the PCM is lesser and low latent heat compared with others.

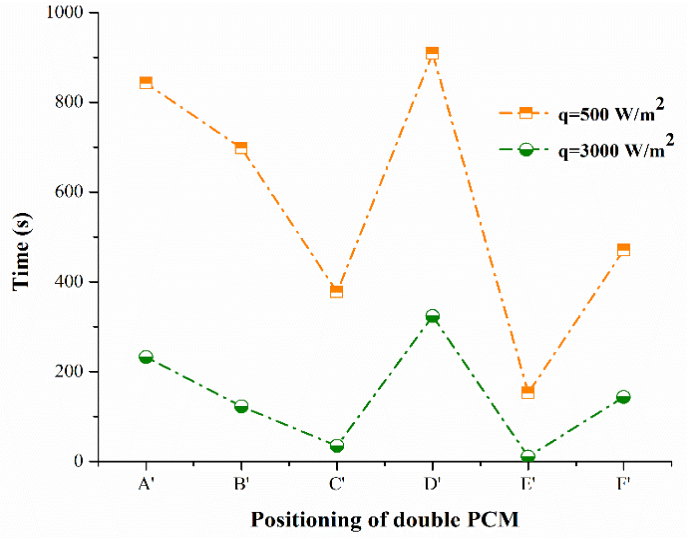

Figure 5.8 Time difference between double PCM and multiple PCM for completion of melting.

5.7 RESULTS AND DISCUSSIONS

5.7.1 Cases with low heat flux

At the bottom of the sink, the average heater temperature against varying heat fluxes of 100-500 W/m^2 is presented for different tilted angles. The PCM mass remains the same throughout all cases for all these comparisons. It is observed that because of the insertion of three different PCMs, there are three latent heat zones and four sensible heat zones. This latent heat zone depends upon the latent heat of the material, and here latent heat of the three PCM are almost similar. So, it is noticed that for all heat fluxes, this zone remains identical. As the heat fluxes increase, the latent heat zone decreases proportionally. All the cases show similar trends. Hence, the period for each heat sink case to reach 45°C and 50°C is plotted to distinguish the difference between them.

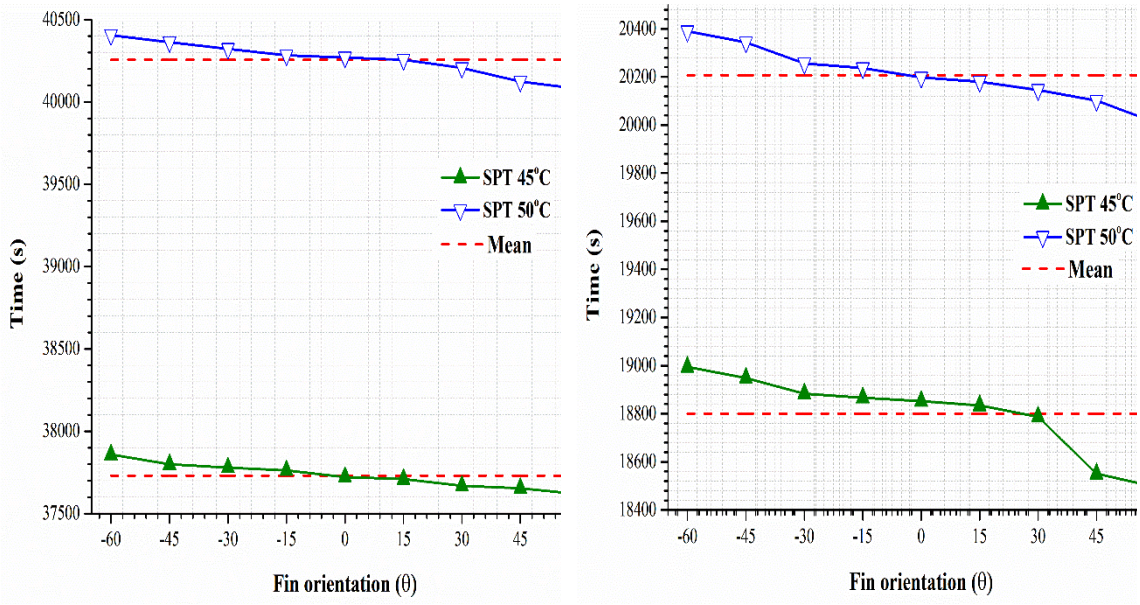

(a) (b)

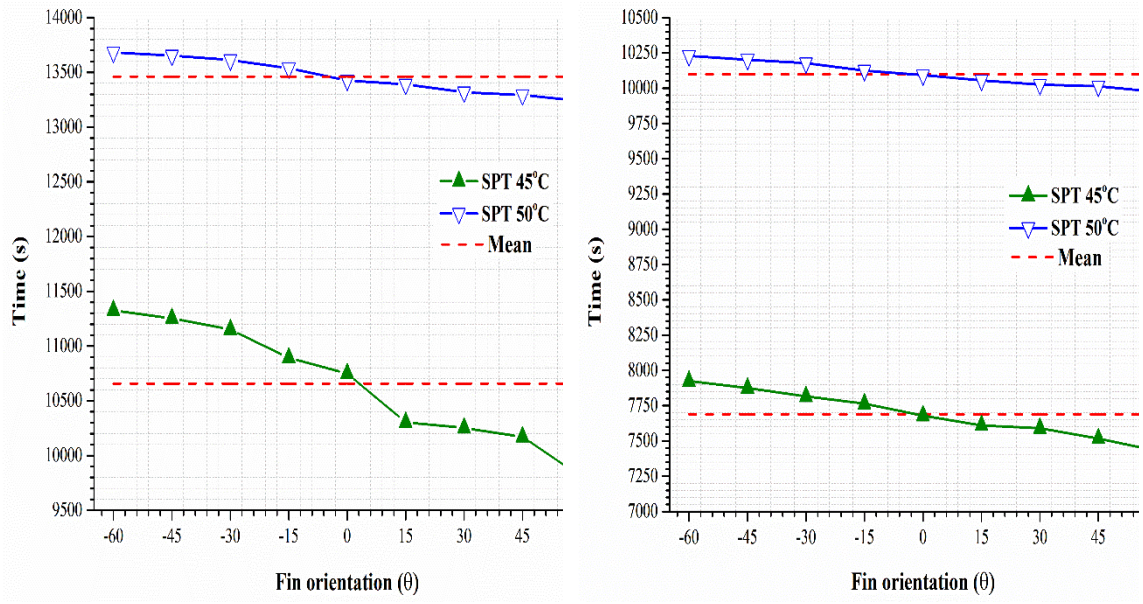

(c) (d)

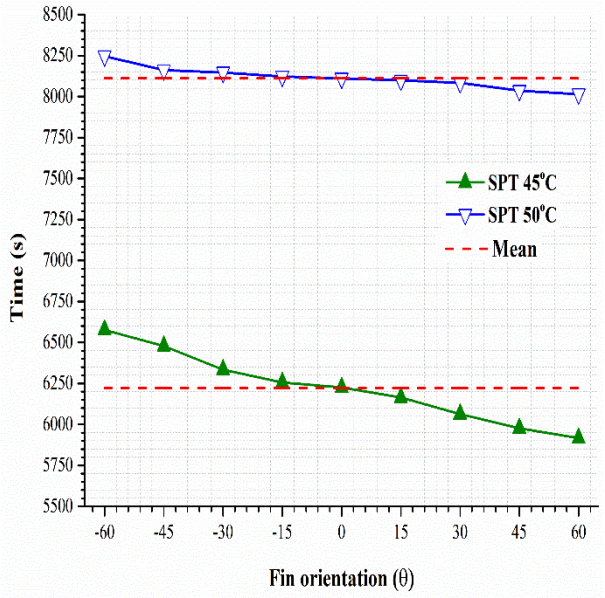

(e)

Figure 5.9 For varying heat flux, time to reach SPT of 45°C and 50°C. (a) 100 W/m^2, (b) 200 W/m^2, (c) 300 W/m^2, (d) 400 W/m^2, and (e) 500 W/m^2.

The mean value is plotted in the figure to observe the difference between the fin orientations. The difference from the mean value gives a clear visualization that there are some significant changes in the time intervals. Figure 5.9 displays the time required for the

heat sinks to reach 45°C and 50°C for 100–500 W/m^2. It is noted from the figure that +60° is quicker to reach 45°C and 50°C than other cases, and -60° is slower to attain this temperature. The reason behind this is, in the positive orientation of fins, the amount of PCM in the RT-28HC zone exposes more to the heater surface and melts quicker than the negative cases. Hence, it is faster to reach the SPT. Likewise, reaching SPT is longer for negative orientation, but melting is faster for negative cases. It is because, at a later period, RT-44HC exposed to the bottom of the heater is more and hence higher heat transfer because of natural convection. Though the positive orientation reaches quicker to SPT, the completion of melting takes longer because the RT-44HC zone exposed to the heater is small. Since a lesser amount is exposed to the heater, the PCM present at the top side takes longer to melt. The contours of temperature distribution within the enclosure and mass fraction of multiple PCMs are displayed in Figure 5.10 to have a clear visualization. For increasing angle, the unmelted zone expands with positive fin orientation, and with negative fin orientation, the unmelted area shrinks at the RT-44HC spot. The reason is the natural convection dominance at higher angles at negative orientation and a more high melting temperature zone exposed to the heater. The melting rate is expedited at a high melting temperature PCM/RT-44HC zone for negative orientation.

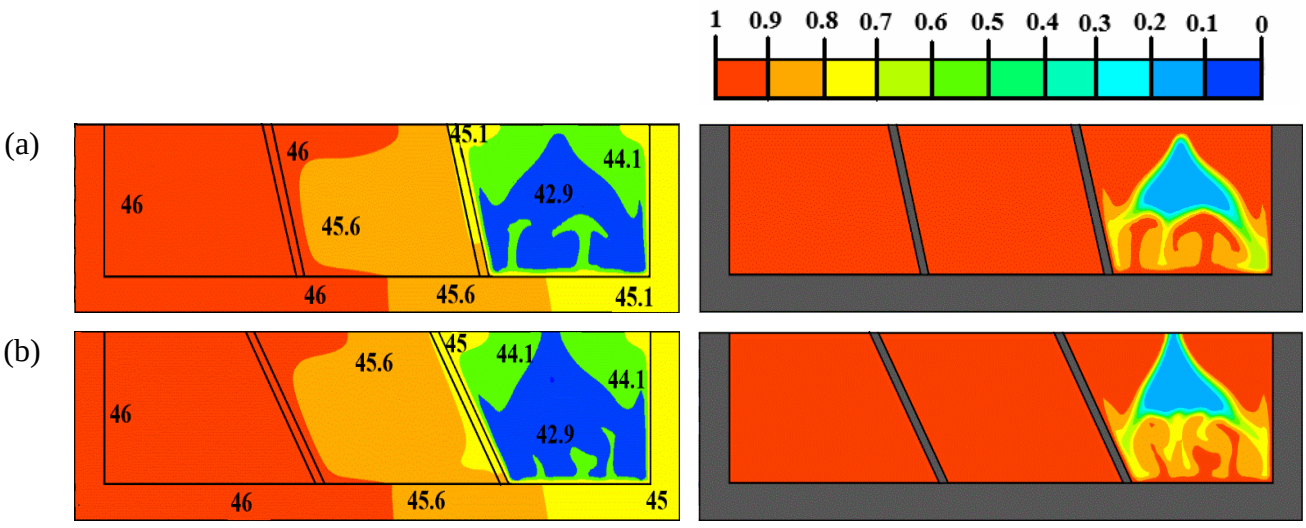

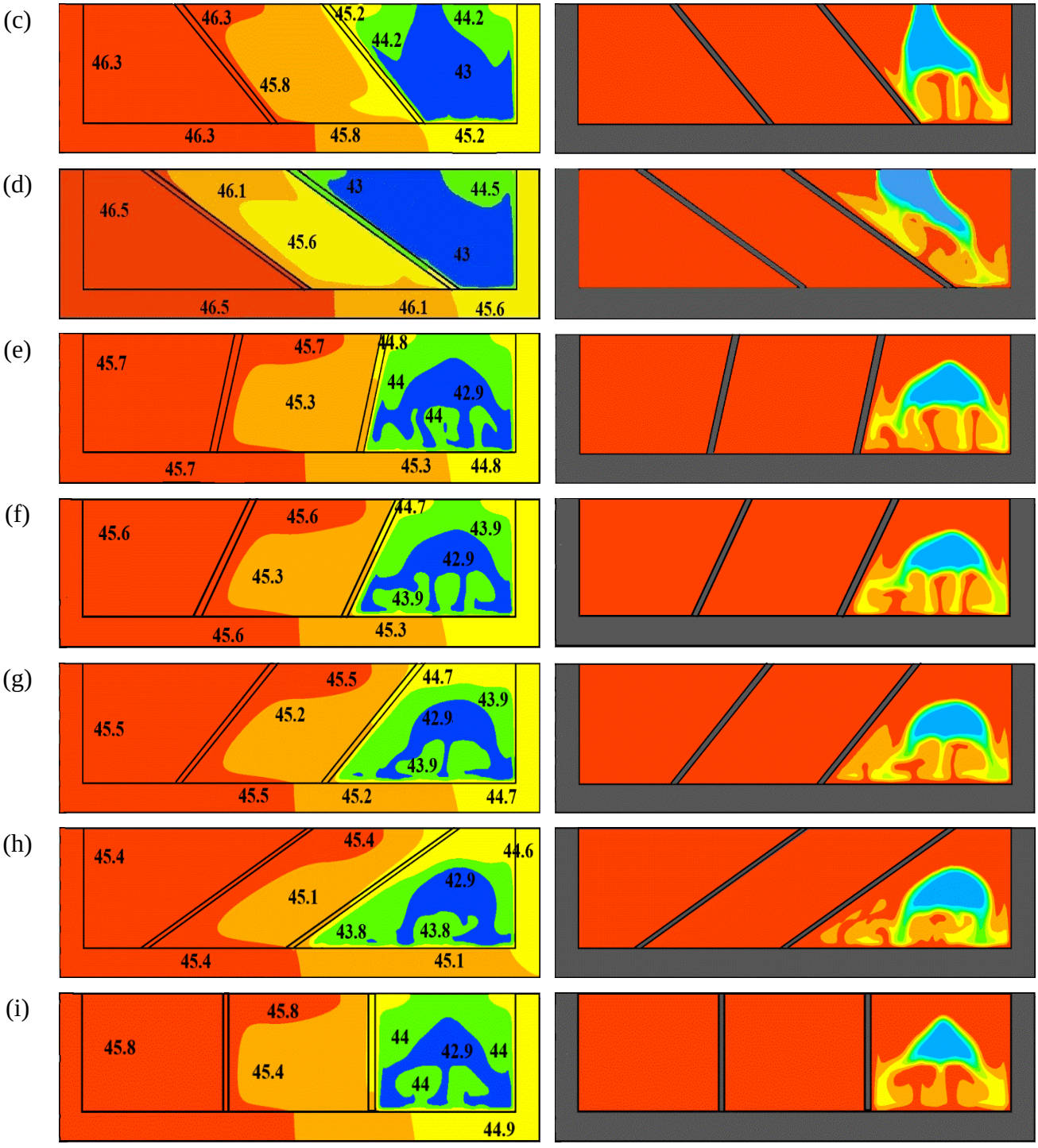

Figure 5.10 Contours of temperature distribution and mass fraction at 12000s (a) +15° (b) +30° (c) +45° (d) +60° (e) -15° (f) -30° (g) -45° (h) -60° (i) 0°.

5.7.2 Cases with high heat flux

The heat fluxes are further increased from 1000-5000 W/m^2 to monitor the effect of the orientation of fins at higher inputs. The time required for complete melting diminishes with increasing heat flux. As the heat flux increases, the latent heat zone reduces further. As mentioned before, the latent heat zone, which is seen at lower heat fluxes, is absent at higher flux. The time taken for the completion of charging cycles for higher heat flux is presented in Figure 5.11. Compared with straight fins (0^o), the positive angle tilted fins show an extended melting time. It is easily understood that melting is delayed when the fins are oriented towards the left side of the enclosure (+ve). This is because of the amount of higher melting temperature PCM remaining at the end, and when angles are increased, the completion of melting is retarded. Considering the negative orientation of fins, contrariwise, positive orientation occurs. For all varying heat flux, -60^o orientation yields a shortened melting rate since the heater is at the bottom of the enclosure; the high melting temperature PCM (RT-44HC) is mainly exposed to the heater and sidewalls of the enclosure. Thus, less part at the top of the heater melts earlier in this case due to gravity. These phenomena are observed for both low and high heat flux.

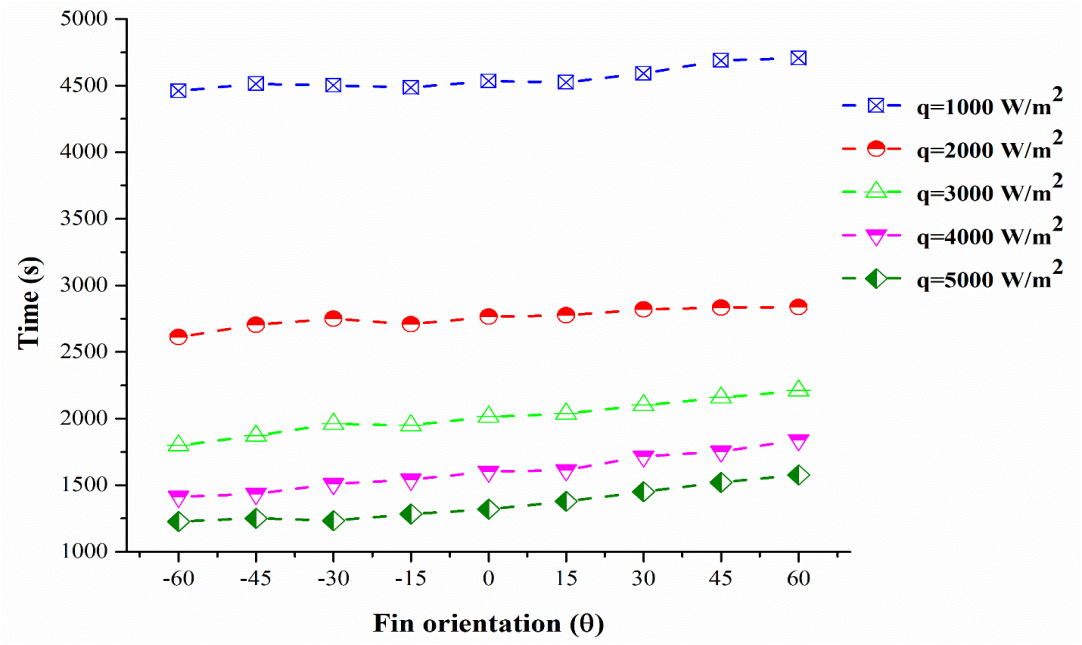

Figure 5.11 Completion of charging cycle duration for various fin orientations.

5.7.3 Cases with different initial conditions

As the initial temperature is varied, the PCM state inside the enclosure also varies. Here the initial temperatures included for the study are 300 K, 303 K, and 310 K. For 300 K, all three PCMs are solid-state. With 303 K as the initial condition, RT-28HC is in the liquid state, and RT-35HC and RT-44HC are solid. Simultaneously, for 310 K, RT-28 and RT-35HC are liquid, and RT-44HC is solid-state. For low (100 and 500 W/m^2) and high (3000 W/m^2) heat flux, the melting completion duration is given in Figure 5.12.

For any heat flux, at 300 K and 310 K initial conditions, the time taken for the charging cycle to complete is longer for positive orientation and shorter for negative orientation. At 300 K, all three PCMs are in solid state. As discussed earlier, for the 300 K initial conditions, the melting rate is higher for positive orientation at the initial period. Still, at the later melting period, negative orientation accelerates the melting. Hence, the positive orientation of fins shows prolonged melting. At initial condition 310 K, only RT-44HC is in the solid state; at this state, the RT-44 HC near the bottom is more for negative orientation and less for positive orientation. With natural convection, the lesser amount on the top side of the enclosure melts faster for negative orientation. Inversely, for positive orientation, the top side of the enclosure contains more PCM. Though the convection influences the melting, it provides a longer charging cycle.

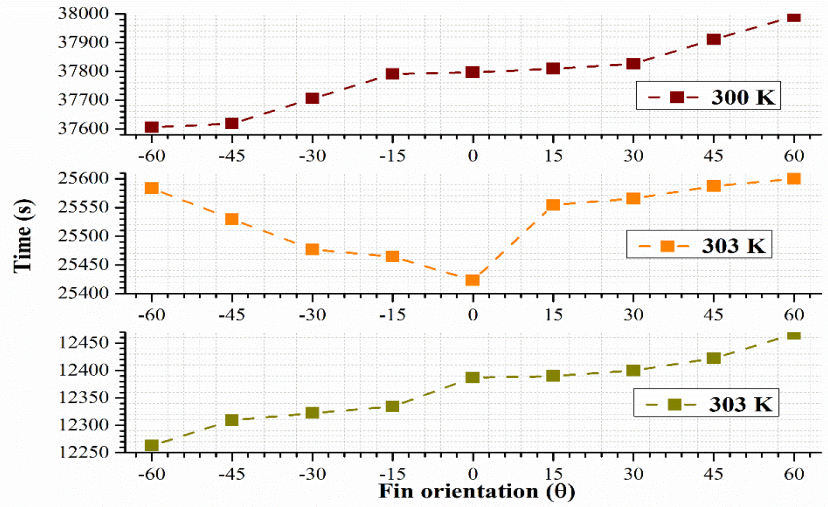

(a)

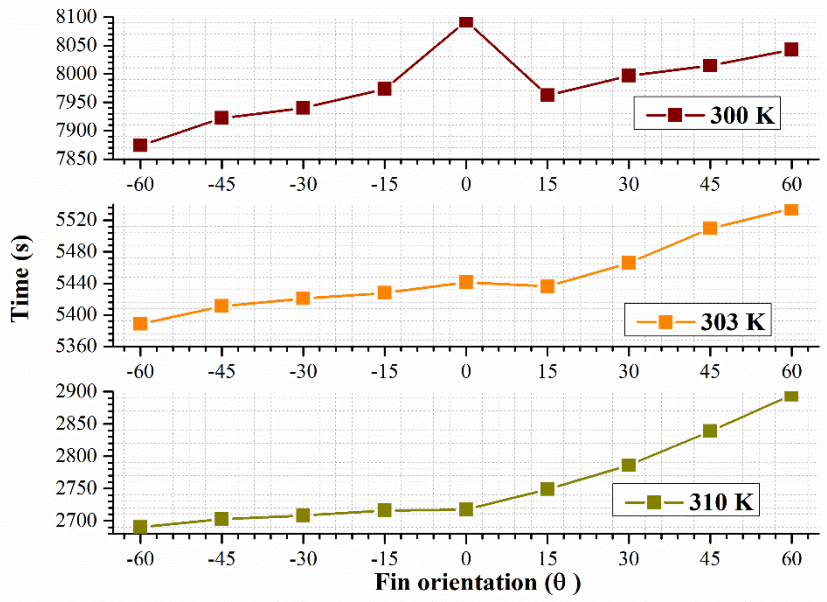

(b)

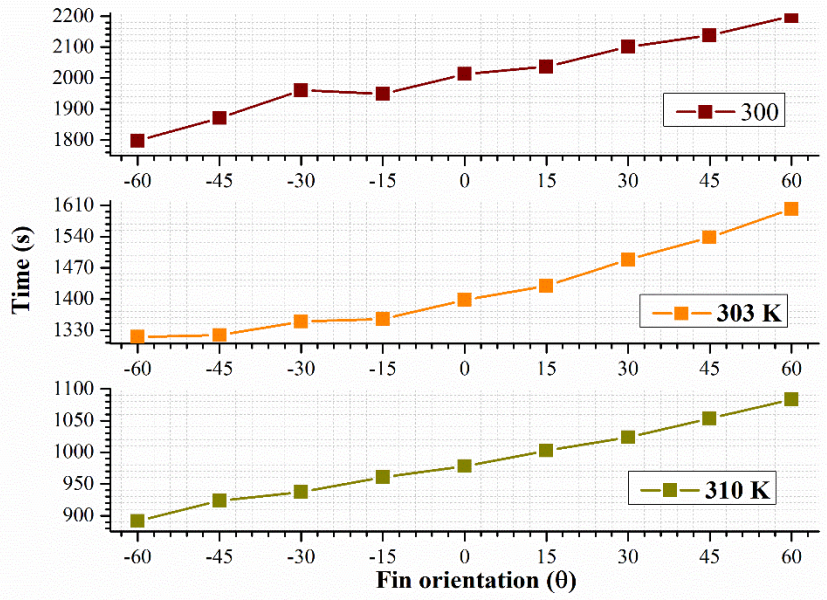

(c)

Figure 5.12 Time duration for completion of melting at different initial conditions at (a) 100 W/m^2, (b) 500 W/m^2, and (c) 3000 W/m^2.

Similarly, for 303 K, RT-35 HC and RT-44 HC are in the solid state. For 500 W/m^2 and 3000 W/m^2 positive orientation provides longer melting, and negative orientation shows a shorter melting period. However, at 100 W/m^2, it is found that the negative orientation also

displays a slower melting rate compared to straight fins. Possibly, at this point, the natural convection domination for tilted fins is less pronounced. The heat required to melt the PCM for angled fins is insufficient at this heat flux compared with straight fins. The enhancement percentage for all orientations compared with straight fins is deduced from Eq. (5.1). For any initial conditions, $t_{\theta i}$ is the total melting time of PCM for respective angled fins, and t_{sti} is the total PCM melting time of straight fin case. The orientation of fins and how it influences melting at different initial conditions is governed by this factor.

$$\text{Enhancement \%} = \frac{t_{st_i} - t_{\theta_i}}{t_{st_i}} \text{ x } 100 \qquad (5.1)$$

Figure 5.13 displays the enhancement percentage for a different initial condition with varying heat flux. The negative enhancement % states that the corresponding case's total melting time lags with the straight fin (0^o) total melting time. At 303 K initial condition, when the heat flux is $100W/m^2$ almost for both positive and negative cases, enhancement % is lagging.

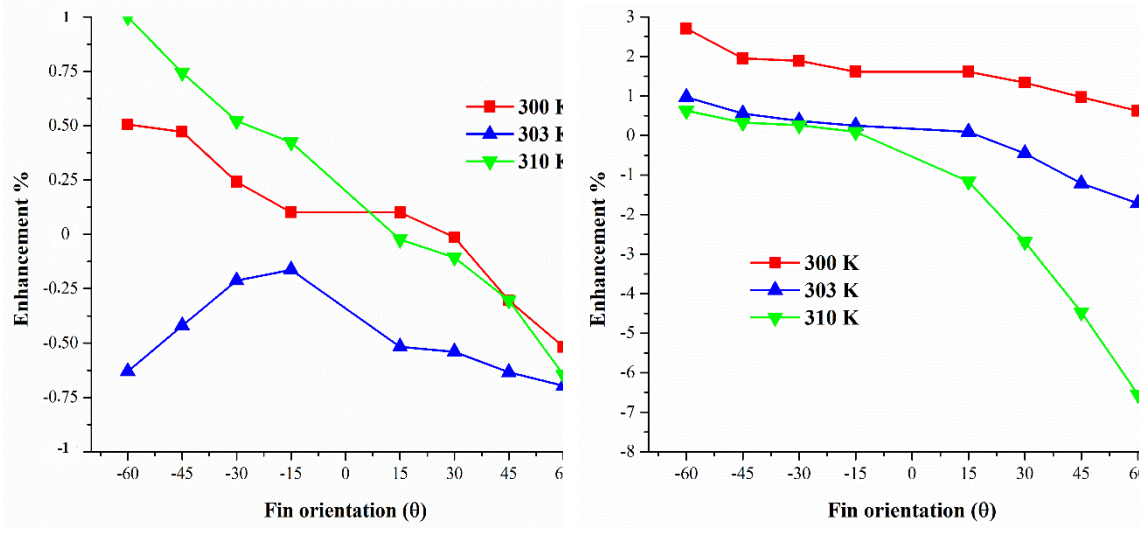

(a) (b)

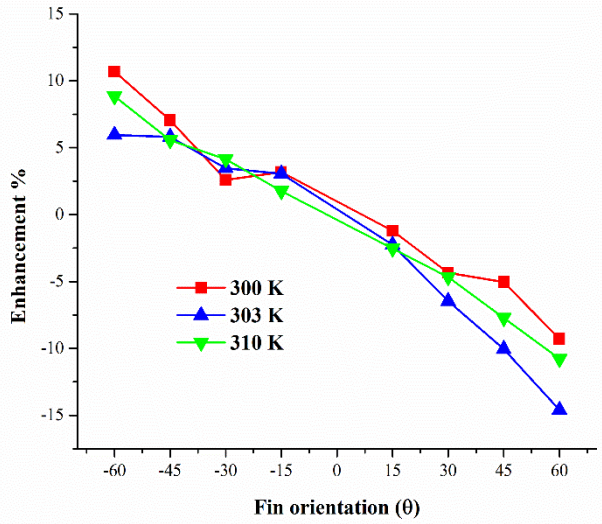

(c)

Figure 5.13 Enhancement percentage of tilted fins at different initial conditions for (a) 100 W/m^2, (b) 500 W/m^2, and (c) 3000 W/m^2.

As mentioned above, at this low heat flux, a straight fin provides superior melting. For all heat inputs and at many conditions, -60^o tilted fins have a higher enhancement percentage than the remaining cases. Inversely, the least enhancement percentage is found at 60^o. It is also perceived that at a higher heat flux of 3000 W/m^2, the enhancement percentage for both orientations escalates for all initial conditions. Other than 303 K at 100 W/m^2, the negative orientation fins exhibit positive enhancement showing a better melting rate than straight fins. Similarly, for positive orientation, other than the 300 K initial condition at 500 W/m^2, the enhancement percentage is negative for all cases. It reveals that the duration of the charging cycle is lengthened than the straight fins. In these scenarios, the calculated enhancement ratio values exhibit negative values. These negative values indicate a reduction in thermal performance compared to the baseline case, which is straight fin case. The occurrence of negative enhancement ratios can be attributed to slow melting rate.

After these discussions, when employing a triple PCM heat sink with longitudinal fins, the fins can be oriented either way, depending on the scenarios. When a prolonged charging cycle is required, positively oriented fins are suitable. The observation states that fins oriented towards the low melting temperature PCM zone for a longer charging cycle are

preferred. For rapid melting, -60^{o} angled fins, i.e., oriented towards the high melting temperature zone, can be selected. The enhancement percentage is larger with 3000 W/m^2 heat flux at initial conditions. Compared with single and double PCM-based heat sinks, multiple PCM exhibits prolonged melting. For the double PCM heat sink cases, the enclosure contains RT-28HC on both sides, providing extended melting than other double PCM cases.

5.8 SUMMARY

A 2-D rectangular enclosure with multiple PCM is considered for the numerical study. Three different PCM RT-28HC, RT-35HC, and RT-44HC with similar properties are selected and incorporated. Two fins with the same thickness are employed and act as a thermal spreader. In this study, the effects of fin orientation from +60^{o} to -60^{o} are analyzed for charging cycles. The positive and negative orientations are defined by keeping a straight fin as a reference. Fins tilted to the left side of straight fins are positive, and those tilted towards the right are negative fin orientation. The initial conditions, like initial temperature and the initial state of PCM, are varied and investigated. A transient model based on the enthalpy-porosity technique was solved using ANSYS fluent 19. The results obtained conclude that,

- The arrangement of PCM in the enclosure does not significantly affect the melting period. For 500 W/m^2, the average heater temperature plotted against time intervals displays a similar trend. The time required to attain the SPT of 45^{o}C and 50^{o}C also has an inconsiderable deviation between all cases.
- This study compared a single PCM heat sink to multiple PCM heat sinks. Only one PCM is filled in a single PCM enclosure in the entire area. The liquid fraction plotted shows; the multiple PCM enclosures manifest prolonged melting.
- Using a double PCM heat sink, we further explored the significance of multiple PCMs. Two PCMs were filled inside each sink to analyze six different cases. RT-28 HC filled on both sides of the enclosure possesses extended melting than any other cases. The reason is RT-28 HC possesses higher latent heat than other PCM.

- In the case of varying heat fluxes, the negative fin orientation enhances the melting rate compared to the positive orientation of fins. Though the positive orientation fins initially attain SPT of 45^{o}C and 50^{o}C quicker, melting completion is delayed. The reason is due to high melting temperature PCM exposure towards the bottom wall, and the enclosure heater is very less for positive orientation of fins. Conclusively, -60^{o} and +60^{o} have shortened melting and extended melting, respectively, for low and high heat fluxes.
- The initial temperature of the enclosure is varied by 300 K, 303 K, and 310 K. Simultaneously, the state of the PCM is altered. The enhancement % is found for different heat fluxes, and the effect of this factor is stated. For an initial temperature of 303 K at 100 W/m^{2}, enhancement % is negative for any cases. At remaining conditions and at different heat fluxes, -60^{o} has a higher enhancement, and +60^{o} possesses a lower enhancement.

5.9 CLOSURE

In most cases, with the addition of different enhancers, the weight and cost of the enclosures increase. In this study, the enclosure size is compact, and when the enclosure size increases, the PCM volume also increases. Then the enhancement in melting for all angled fin cases also varies. So, in a PCM-based heat sink, the enhancer orientations also play a major role. This small deviation of angles in the enclosure can lead to a preferable effect. In the next chapter, experimental investigations are done by comparing the performance of the proposed and conventional fins heat sinks.

CHAPTER 6

PCM ENCLOSURE WITH MODIFIED FIN ARRANGEMENT

6.1 INTRODUCTION

This chapter compares the impact of modified fin arrangements (i.e., variable height fin heat sinks) over existing fin arrangements (i.e., constant height fin heat sinks) at constant and power surge loads. The power loads are applied along with constant heat load and no-load conditions. Further, power loads are applied at pulsating ON and OFF conditions. The effect of these conditions on a PCM enclosure is discussed using temperature-time history. The thermal performance of both heat sinks is evaluated and compared based on the results.

6.2 EXPERIMENTAL SETUP

In Figure 6.1, the schematic diagram of the experimental setup is presented. The setup constitutes a computer, DC power supply, data logger, and the finned heat sink.

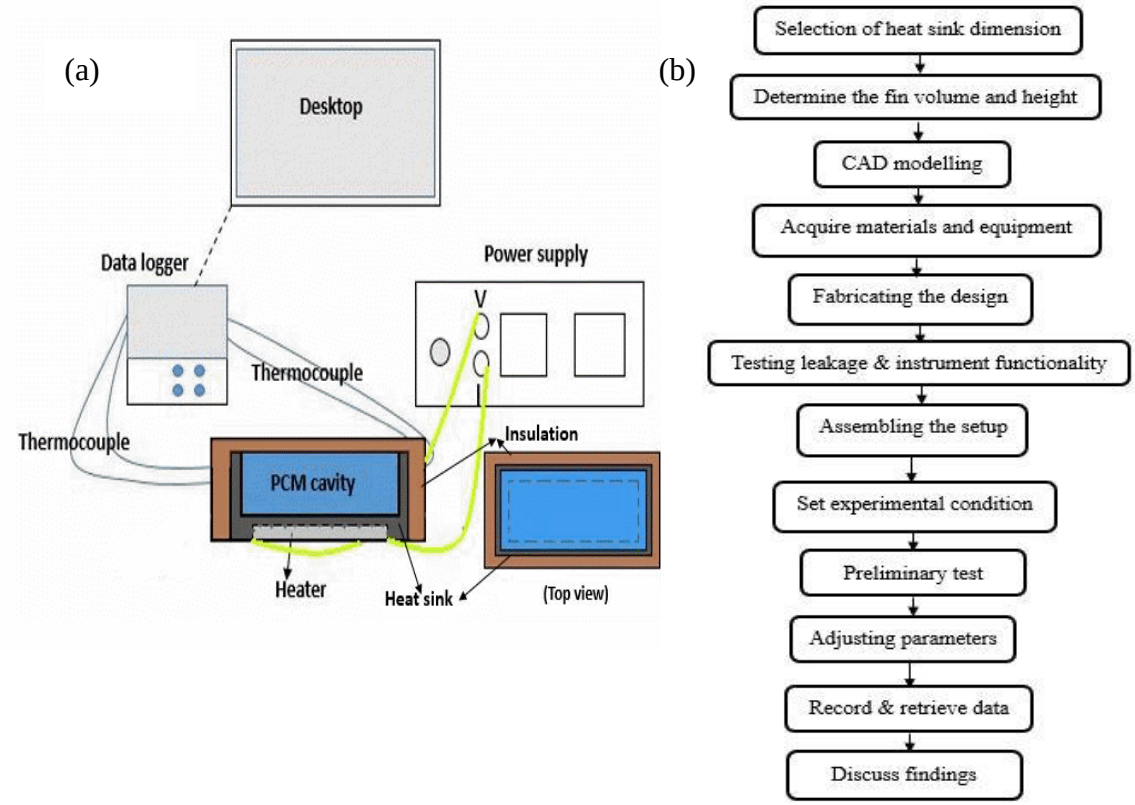

Figure 6.1 (a) Schematic of the experimental setup and (b) Experimental flowchart.

The heat sink is made of aluminum, and the dimensions are 100 mm x 50 mm with a depth of 25 mm. In the heat sink, the PCM cavity is 90 mm x 40 mm with a depth of 20 mm. The heater slot is grooved for 2 mm at the bottom of the heat sink with dimensions of 86 mm x 36 mm. The experimental setup serves the purpose of comparing the thermal performance between variable and constant fin heat sinks. The computer operates as the control center, overseeing the entire process. The DC Power Supply provides a controlled heat source for the heat sinks, while the Data Logger records temperature data from the strategically placed thermocouples on the heat sink's surface. The Data Logger captures real-time temperature variations, enabling a detailed analysis of the thermal behavior and performance of the heat sinks. The thermocouple provisions are over checked by leakage tests.

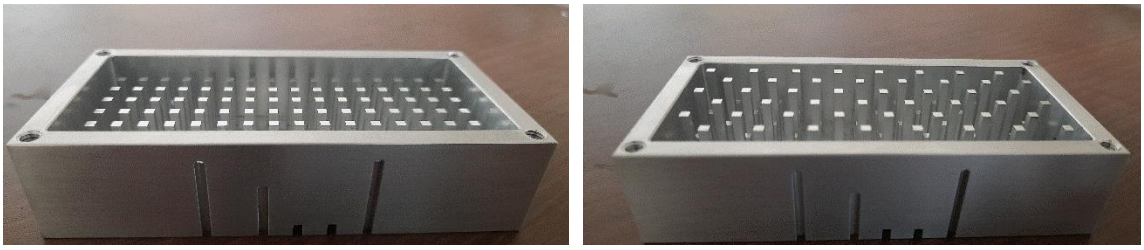

(a) (b)

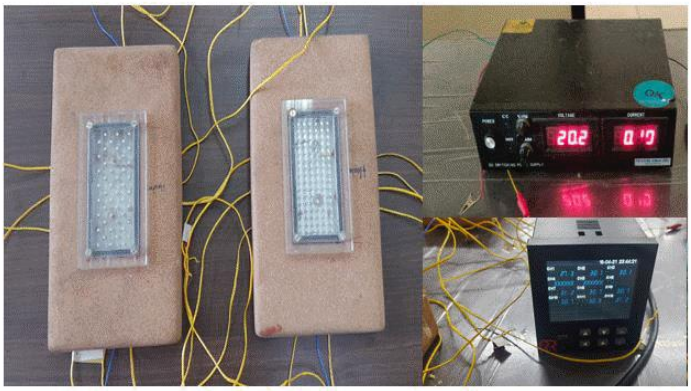

(c)

Figure 6.2 Photographic display of (a) Constant finned heat sink, (b) Variable finned heat sink, and (c) Heat sink assembly with setup.

Based on the previous research by Saha et al. (2008), an optimal volume fraction of TCE 8 % is chosen. The TCE volume fraction is determined by the ratio of the fin volume to the

PCM volume. Two heat sinks consisting of 96 pin fins with constant fin height and variable fin height are shown in Figure 6.2. The fins are employed in the heat sink by the milling process. In a constant fin height arrangement, all fins are at the same height of 15 mm. Whereas, for variable fin height assembly, one fin is 20 mm, and the other is 10 mm, and the fins are scattered successively. Both the heat sink comprises fin area dimensions of 2 mm x 2mm.

The heat sink assembly is covered by cork on all sides except the top side for insulation purposes. On the top surface, an acrylic sheet is placed and fixed over the heat sink assembly by tightening the screw. A rubber gasket is placed between the acrylic and aluminum surfaces to prevent leaks. Thermocouples are placed in the heat sink to measure the heater, wall, and PCM temperatures. A nichrome wire heater wounded over mica sheets generates the power supply to the enclosure. The dimension of the plate heater is 86 mm x 36 mm with a 2 mm thickness, and it is fit into the grove slot at the bottom of the enclosure.

Table 6.1 Properties of the material.

materials	n-eicosane	Aluminum	Cork
c_p (kJ/kgK)	2200	870	2.05
k (W/mK)	0.16	200.4	0.05
T_m (^oC)	36.5	660	-
density (kg/m^3)	780	-	-
viscosity (kg/ms)	0.00355	-	-
coefficient of thermal expansion (1/K)	0.001	-	-
L (J/kg)	247,000	-	-

A thermal conducting paste with a conductivity of 1.42 W/mK is applied at the slot to increase the conduction pathway. The PCM incorporated in this study is n-eicosane. The DSC analysis was carried out to determine the latent heat capacity of the material. The sample was alternatively heated and cooled in the range of 0-100^{o}C by a fixed

heating/cooling rate of 10 K/min. Prior to the main experimentation, preliminary tests have been conducted to ensure the integrity and functionality of the setup. The procedure is repeated thrice, and latent heat is determined. The properties of all the materials are listed in Table 6.1.

All the thermocouples are inserted into the heat sink using Araldite epoxy. Two thermocouples, T_1 and T_2, are located at the base where the heater is attached to the slot. Within the PCM, six thermocouples (T_5, T_6, T_7, T_8, T_9, and T_{10}) are inserted from all sides. Among these six, two thermocouples, T_5 and T_6, are 20 mm from the base, and another two thermocouples, T7 and T8, are 10 mm in height on the long side of the wall. The remaining two thermocouples, T_9 and T_{10}, are placed from the short sides with a height of 15 mm. All the thermocouples within the PCM are at a distance of 10 mm from each side. Two thermocouples, T_3 and T_4, are located on the long side of the walls to measure the wall temperature. Finally, the last thermocouple is kept outside to measure ambient temperature. The thermocouples are then connected to the data logger, and the positioning of the thermocouples is shown in Figure 6.3.

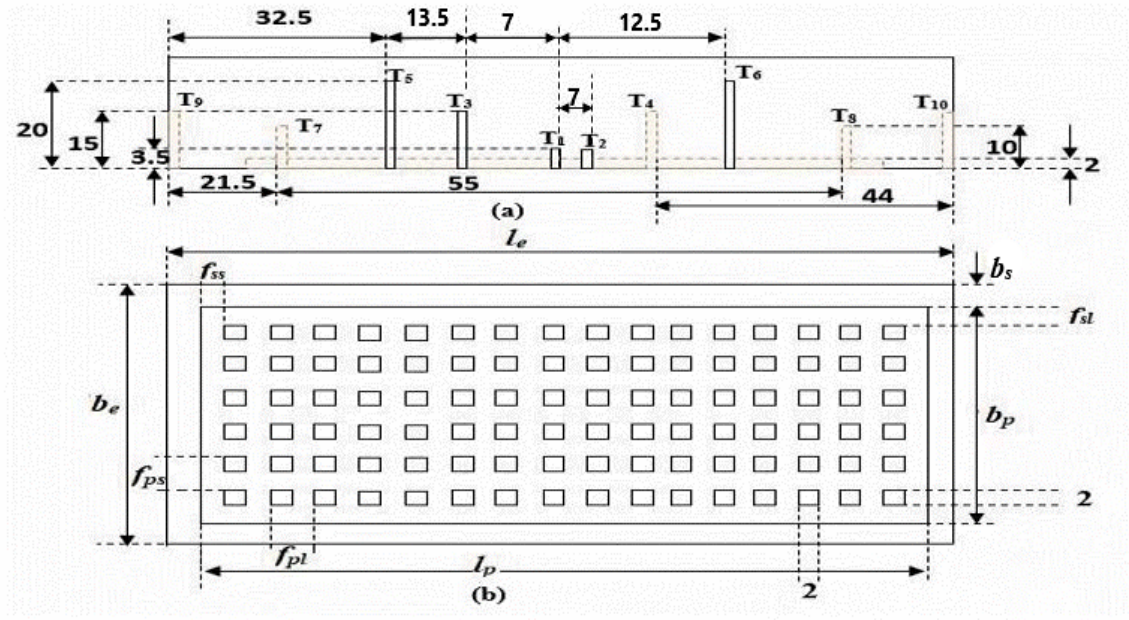

Figure 6.3 Thermocouple positioning for both the heat sinks with dimensions in mm (a) front view and (b) top view.

The surge test was conducted manually, and a five-second clearance was provided before and after the power surge load was applied. Next, to calibrate thermocouples, a standard thermometer with a resolution of 0.1^{o}C is used to measure the accuracy of the thermocouples. In a calibration bath with temperatures ranging from 30-70^{o}C, the error in temperature is within the range of ±0.25^{o}C. The uncertainty analysis of voltage and current from power input is based on the propagation method of error as mentioned in Eq. 1. The uncertainty in the input heat is measured based on the least count of current ±0.01 A and voltage ±0.1V. For a 10 W power supply, the uncertainty calculated is ± 0.667.

$$\omega_{P_{it}} = \pm\sqrt{\left(\frac{\partial P_{it}}{\partial V_{it}}\omega_{V_{it}}\right)^2 + \left(\frac{\partial P_{it}}{\partial I_{it}}\omega_{I_{it}}\right)^2} \tag{6.1}$$

6.3. RESULTS AND DISCUSSION

6.3.1 Constant heat load

The heat flux is varied from 4 W to 50 W, where 4 W-10 W is considered a light load and 20 W- 50 W is considered a power load. The ambient temperature for all the experiments is close to 26^{o}C. The heat sink base temperature of both enclosures is compared in Figure 6.4. The heat sink base temperatures are calculated based on the average of two thermocouples placed at the bottom of the sink surface near the heater. For all heat fluxes, the completion of melting is faster in the variable height fin heat sink. This faster melting is due to the significant effect of fin height non-uniformity in the enclosure, which accelerates the charging cycle. In variable height fin heat sink, since half of the fin heights are near the top surface, it increases the heat transfer within the PCM at the top side. The fins are the same size in a constant height fin heat sink, and the top side PCM in the enclosure takes longer to melt. In the absence of fin exposure at the top side, PCM melts based on its own thermal conductivity, which is generally less. Hence, the heat transfer from the heater to the PCM is reduced; thus, a longer melting time is observed.

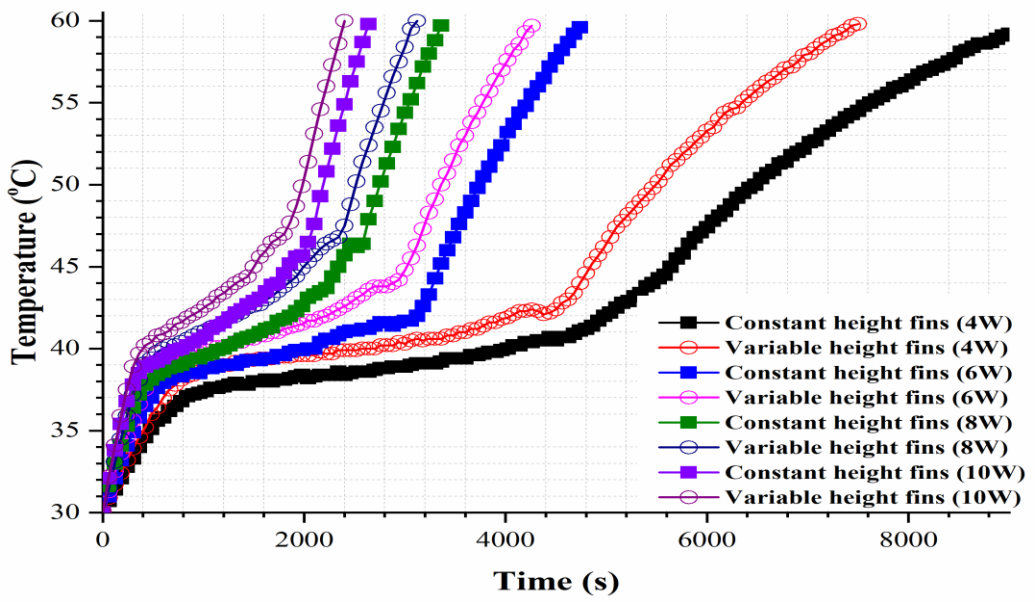

(a)

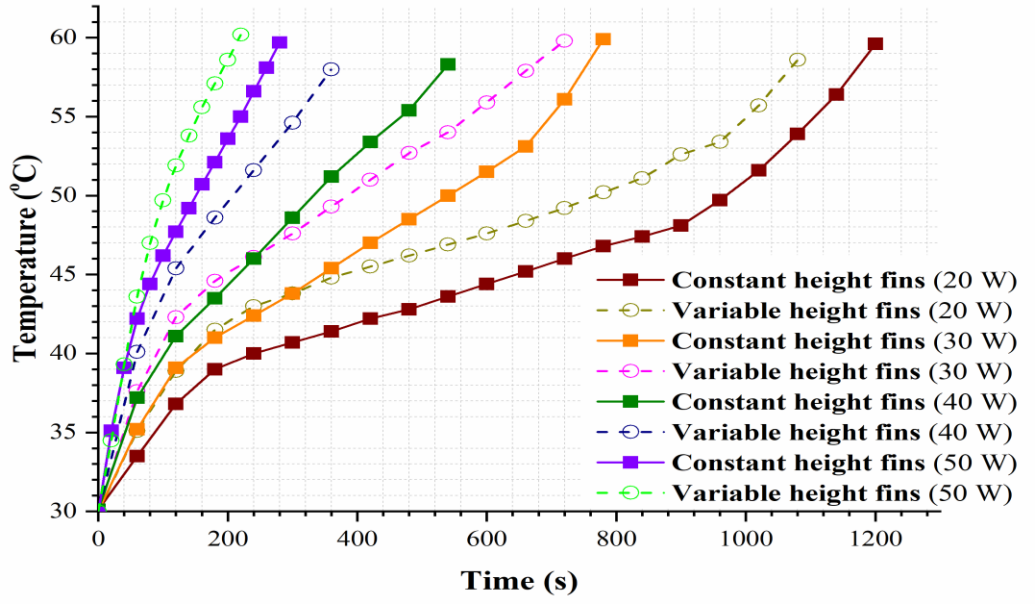

(b)

Figure 6.4 Heat sink base temperature against time intervals for various heat inputs.

When the heat load increases, the initiation time of the phase transition reduces. This is due to the high heat generation to the enclosure, which melts the PCM at a faster rate by overcoming its poor thermal conductivity. This result is seen for both the heat sinks, but for variable height fin heat sinks, it is higher compared with constant height fin heat sinks.

The reason is in the variable height fin heat sink, the thermal conductance offered by the fins to the PCM is more and initiates the phase transition at an earlier stage. At the same time, the temperature plots at power loads show a faster melting rate. In the loads (30 W-50 W), it is observed that the latent heat period of PCM vanishes in both heat sinks. Because the heat supplied to the PCM is high enough to overcome the latent heat of fusion, only sensible heating is observed. Hence, the phase transition happens rapidly at high power loads compared with low power loads. For any loads in Fig. 4, the trend follows the same for both the heat sinks.

A figure is plotted to understand the heat transfer within the PCM and the heat transfer through the side walls. In Figure 6.5, the temperature difference between the PCM and sidewall temperature of the heat sink until the heat sink base reaches 60°C is reported. The average temperature of six thermocouples (T_5, T_6, T_7, T_8, T_9, and T_{10}) kept in PCM and the average of two thermocouples (T_9, T_{10}) placed on the walls are considered here.

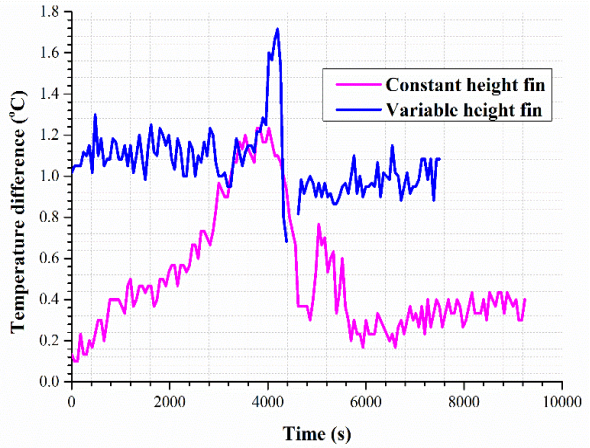

(a) 4 W

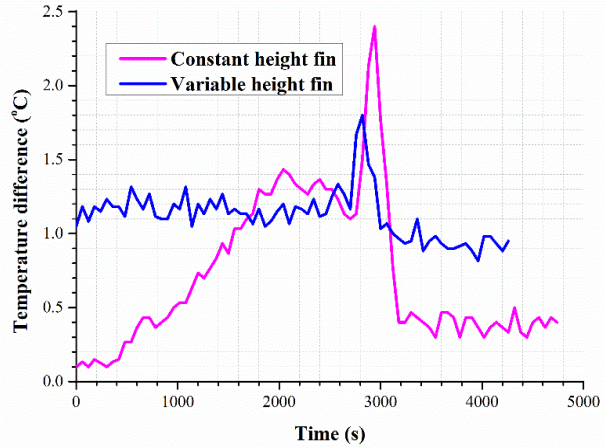

(b) 6 W

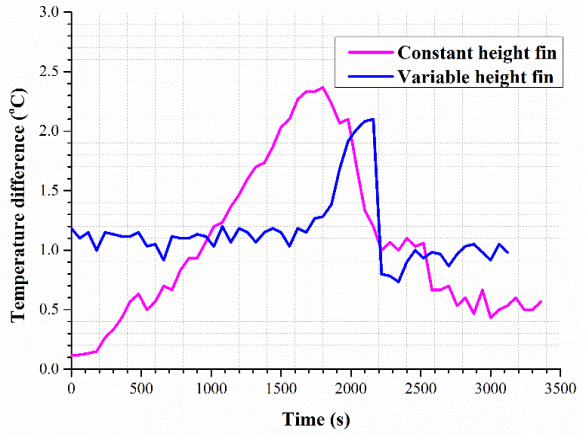

(c) 8 W

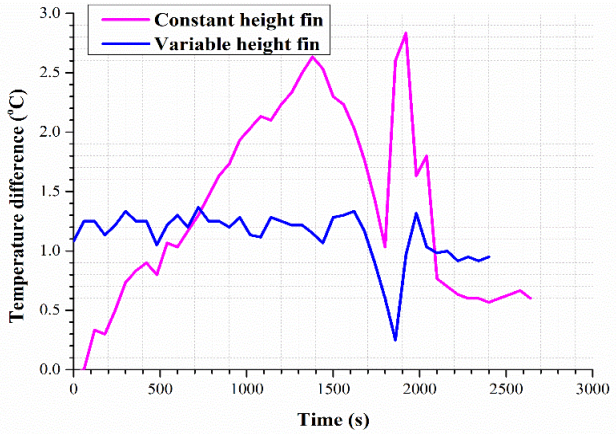

(d) 10 W

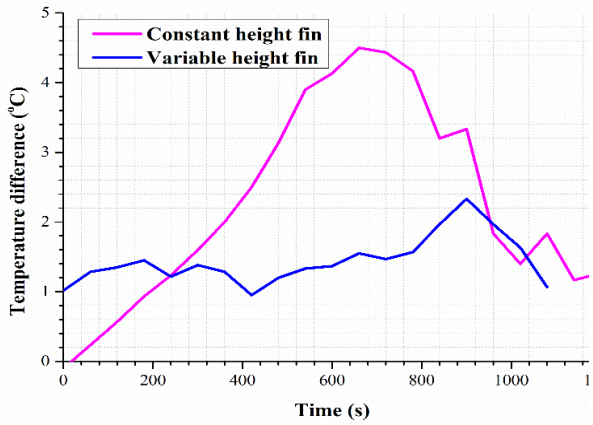

(e) 20 W

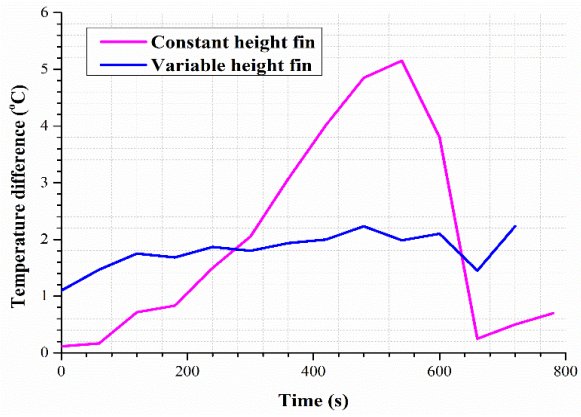

(f) 30 W

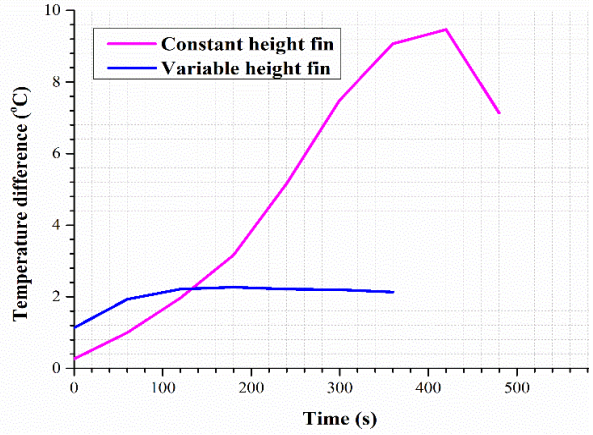

(g) 40 W

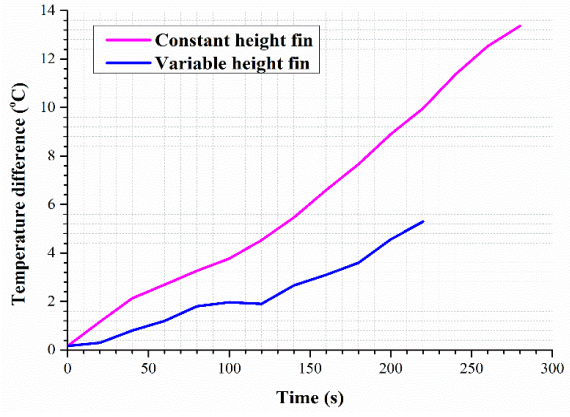

(h) 50 W

Figure 6.5 The temperature difference between the PCM and side wall temperature at various heat inputs.

In these cases, the variable fin height has a higher temperature difference at the initial stage. But, the deviation after the initiation of melting is found to be less. This shows the uniformity of heat distribution within the enclosure. This is due to the fin exposed area within the enclosure being high; at all heights, there is a uniformity of heat transfer. Whereas in the constant height fin heat sinks, the initial difference is less, but once the melting starts, the temperature rises with time. The heat sink has no uniform temperature distribution between the side walls and the PCM compared to variable height fin heat sinks. The peak temperature difference is obtained for both cases, which implies the latent heat zone, and once the post-sensible heat zone starts, the temperature falls and attains a lesser difference.

Then both the heat sinks are evaluated during the discharging cycle at various heat fluxes. In Figure 6.6, the time taken for the heat sink base to reach 30^{o}C for both the heat sinks is plotted. Unlike melting, the solidification of PCM takes a longer time because of its poor thermal conductivity and no natural convection to enhance the solidification. Variable height fins show a faster discharging rate than constant height fins. The reason is similar to melting; the heat transfer region of PCM with fins was found to be high for a variable height heat sink. As the heat flux increases, the time taken for the PCM to get solidified is reduced. This is because, at higher heat flux, the heat sink base temperature expands suddenly and achieves 60^{o}C sooner. When the heater is then switched off, the heat is transferred to the PCM and side walls, and it attains 30^{o}C faster than other walls and PCM. But at low heat flux, the heat sink base temperature, side wall, and PCM temperature reach 30^{o}C simultaneously with smaller gaps.

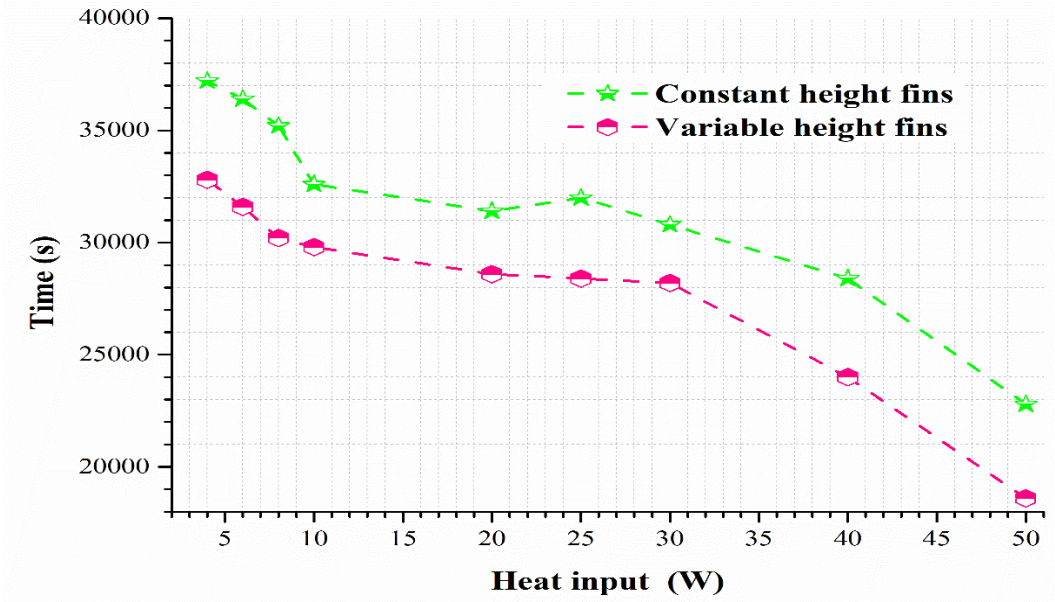

Figure 6.6 Solidification time to reach 30°C for different heat inputs.

6.3.2 Power surge with constant load

A constant load of 4 W for 1800 s, then continued by power load for 100 s, is applied. Next, a constant load of 4 W for 1800 s, continued by a power load for 100 s, and the solidification time of 1800 s are recorded, unlike the previous one. Both the durations considered for this study are taken from the previous literature by Shaikh and Lafdi (2010); Yoo and Joshi (2002) as a reference to obtain the performance of two heat sinks. The 25 W and 50 W power surges are considered, and three cycles were run under similar conditions. In Figure 6.7 (a) and (b), the base temperature of constant height fin and variable height fin heat sinks are compared without solidification time. The variable height fin heat sink attained the peak temperature in the first cycle. The reason is due to the faster melting occurring in a variable height heat sink with the help of non-uniform fin heights. Once the power surge is removed and constant load is applied, the PCM comes to the latent heat period, where it is not completely in to the liquid state. Hence, the PCM is at a lower temperature when the second cycle power load starts for both the heat sinks. But comparatively, the PCM temperature for the variable height heat sink is lower at the end of the second cycle (constant load of 4W) due to its higher absorption rate. This helps the variable height fins at the second pulsed load to obtain a lower peak temperature than

constant fins. This high heat transfer within the variable height fin heat sink is continued with increasing cycles. Also, the differences in the peak temperature of the two heat sinks are increased further. This is observed in the third cycle, where the peak temperature of the constant height fin is 68^{o}C, and the variable height fin is 61^{o}C at 25 W. At 50 W, the peak temperatures are 87^{o}C and 80^{o}C for constant and variable height fins, respectively.

In the next cycle, the constant load and the power load are added along with the solidification time of the 1800s. The heat sink base temperature of both the heat sinks is plotted in Figure 6.7 (c) and (d). The first cycle is similar to the previous one, where the variable height fin with a higher melting rate melts quicker and attains a higher peak temperature at constant and power loads. But, during the resting time, the PCM solidifies and almost reaches the temperature of 36^{o}C. Hence, the PCM is in a solid state at the beginning of the second cycle, but the temperature is higher than the initial temperature. Due to the higher solidification rate of the variable height fin heat sink, the initial temperature is lower than the constant fin heat sink when the second cycle starts. Consequently, the peak temperature value is also shifted towards a constant fin heat sink. Then the cycle is continued and is noted with a higher temperature difference between the variable and constant height fins. The peak temperature differences observed between constant and variable height fins at 25 W and 50 W at the end of cycles are 9^{o}C and 6^{o}C, respectively. At these varying loads of constant and power loads, variable height heat sinks perform better than the constant height fin heat sinks. The explanation behind this better performance is that the fins placed at different heights within the enclosure reduce the resistance offered by the PCM at all heights and enhance the melting/solidification process.

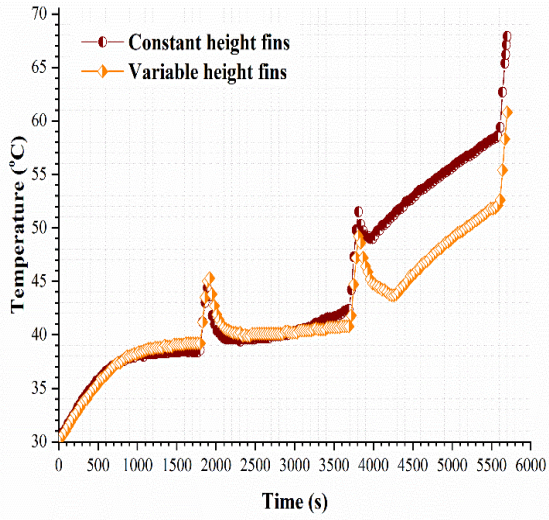

(a) 4 W-25 W

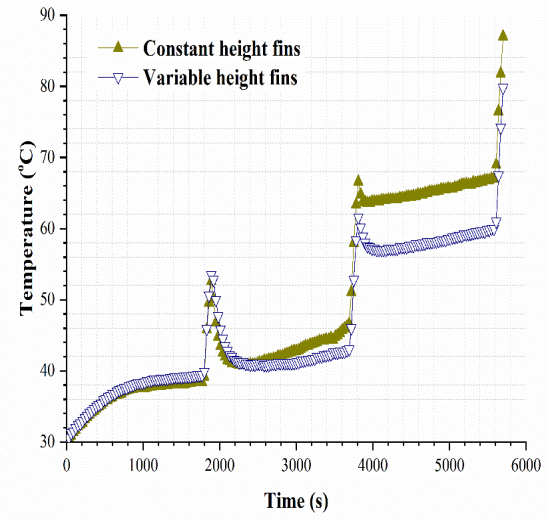

(b) 4 W-50 W

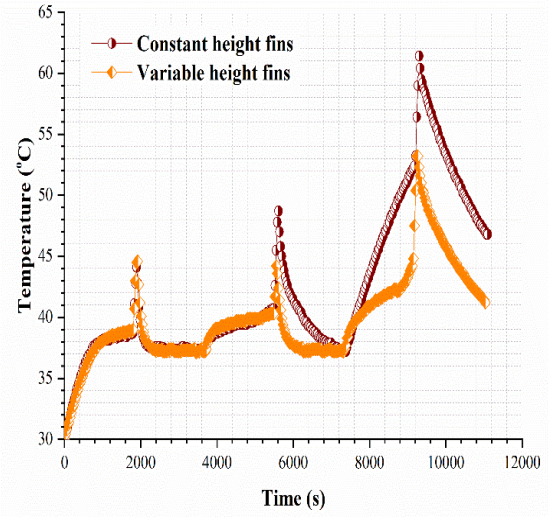

(c) 4 W-25 W- OFF

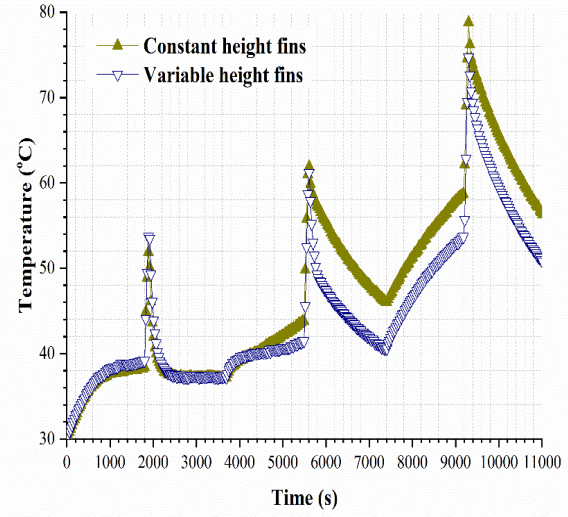

(d) 4 W-50 W- OFF

Figure 6.7 Heat sink base temperature v/s time for a combination of 4 W- power load (a) 25 W (b) 50 W and combination of 4 W- power load - 1800 s OFF condition for (c) 25 W (d) 50 W.

6.3.3 Power surge- ON and OFF condition

Next, only power loads with varying durations and resting times are applied, neglecting the constant load. The power load is employed for a duration of 50 s, 100 s, and 150 s, and the OFF condition is 1800 s for all time durations. In Figure 6.8, the heat sink base

temperature of both heat sinks at 25 W and 50 W power loads are represented. During the 50 s power surge, the peak and the least temperature are observed for almost all cycles for variable height fins. The variable height fin heat sink melts the PCM during load time and solidifies the PCM during a resting time faster than constant height fins by increasing its thermal conductance within the PCM and heat transfer between the walls and the PCM. At a power load of 50 W, with a 50 s duration, the peak temperature is observed for variable height fins except for the 6^{th} cycle, and the least temperature is found for variable height heat sink at all cycles. At the beginning of the cycles, the peak temperature difference between the heat sinks is high, and after the 5^{th} cycle, it becomes lesser. This is because the constant height fins show slower melting, reducing its time to attain peak temperature for a certain cycle. Also, it tries to compensate for the slower solidification rate up to certain cycles. This compensation can be seen for 100 s and 150 s at the 5^{th} cycle and 4^{th} cycle in Figure 6.8 (d) and (f), respectively. Once it crosses that cycle, the peak temperature is shifted towards the constant height fins. But, this shift is not observed for 50 s durations because of less duration, but the temperature difference between them is reduced a lot.

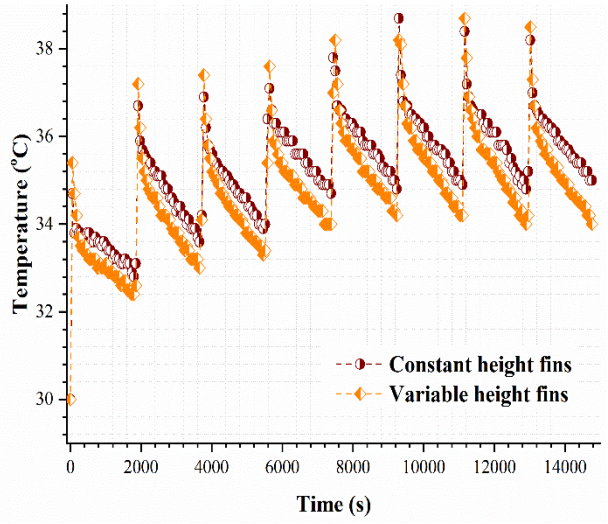

(a) 25 W with 50 s power surge

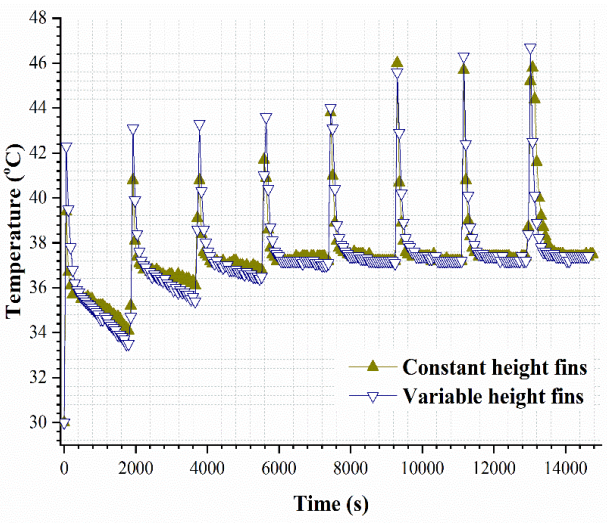

(b) 50 W with 50 s power surge

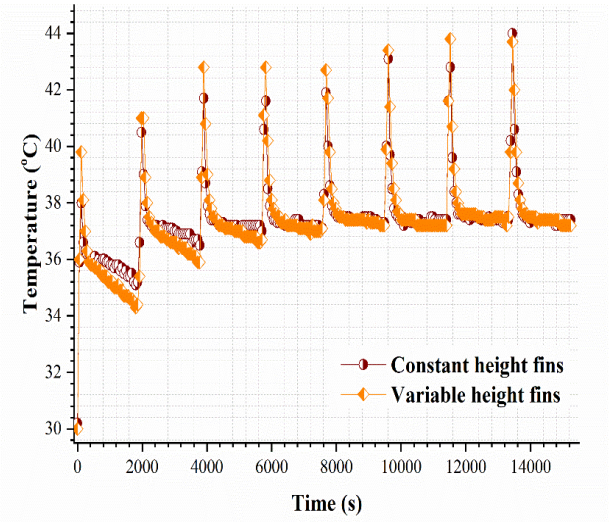

(c) 25 W with 100 s power surge

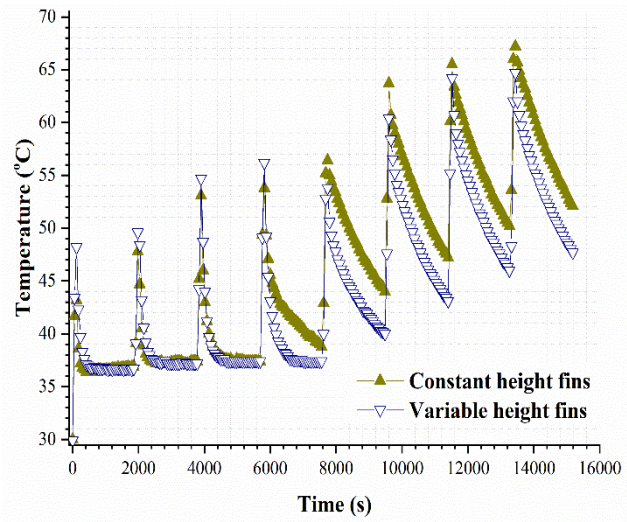

(d) 50 W with 100 s power surge

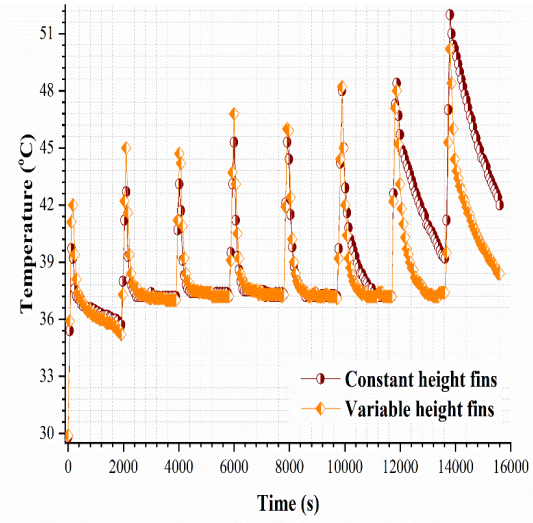

(e) 25 W with 150 s power surge

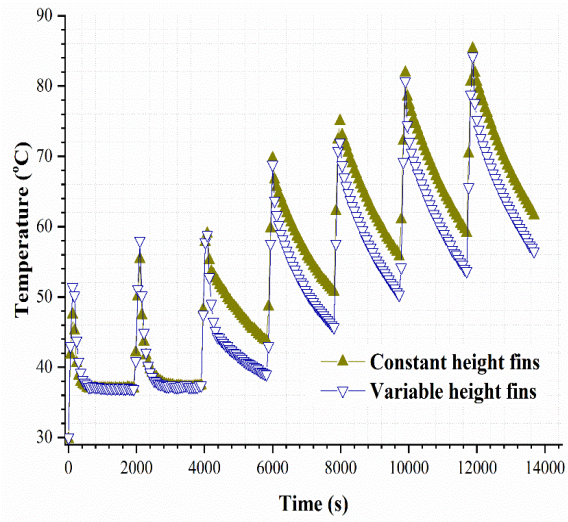

(f) 50 W with 150 s power surge

Figure 6.8 Power surge with different durations of 50 s, 100 s, and 150 s at 25 W and 50 W inputs for Heat sink base temperature against time.

Similarly, for 25 W power loads, the peak temperature shift occurrence can be seen at 150 s at the 7th cycle. During the 100 s duration at the 8th cycle, the constant height fin reaches peak temperature than variable height fins with a slighter margin. But at 50 s, the peak temperature shifts to constant height fins appear at the 6th cycle, and then again, the peak temperature is shifted to variable height fins. The reason is the same as the 50 W power load, where the time duration is not enough for variable height fins to overcome the slow

solidification rate of constant fins. So, from this explanation, with the increasing power surge and time duration of these surges, constant cycles show a higher peak temperature after a few cycles than variable height fins.

The experimentation was conducted on the existing constant height fin heat sinks and proposed variable height fin heat sinks. The volume of PCM and the volume of the fin remains constant, and only the fin height is varied in the enclosure. First, the results are obtained based on the temperature-time graphs at constant heat load with different heat fluxes. Next, power surge load is applied under different scenarios, and the results are discussed using plots. From the analysis, it is understood that considering all types of heat load at different conditions, variable height fin heat sink performs better than the conventional constant height fin heat sinks

6.4 SUMMARY

A pin-fin heat sinks with constant height fin height and variable height fin height arrangements was experimentally and numerically investigated. The fins employed in both heat sinks have a constant volume fraction of 8 %. The PCM incorporated in this analysis is n-eicosane. First, experimental analysis was done to obtain a better heat sink configuration among conventional constant height fin heat sinks and modified variable fin height heat sinks. Under constant heat load and power surge heat load, temperature-time histories were evaluated. Based on the outcomes, a comparative interpretation was made in various scenarios.

- The variable height fin heat sink accelerates any load's melting rate. The time difference between the wall and the PCM is also less for the variable height fin heat sink. The reason is that the distribution of fins throughout the enclosure reduces the resistance the PCM offers. This results in a uniform melting and high heat transfer rate within the enclosure.
- Similar to the melting, a faster discharging rate is noticed during solidification in the variable height fin heat sink. But for both heat sinks, there is a disparity between

solidification and melting time. When the heat input is increased, the time taken for the heat sink base to reach 30^{o}C is shortened.

6.5 CLOSURE

The significance of varying the fin configuration was investigated experimentally in this chapter. The heat inputs are varied by constant heat load and power surge loads for constant height fin heat sinks and variable height fin heat sinks. Additionally, the power surge loads are exerted for different scenarios, along with the constant load, resting time, and ON/OFF condition. From the insights, it is understood under diverse settings, and the variable height fin heat sinks acquire a better thermal response. The final Chapter highlights the overall conclusions of the current research.

CHAPTER 7

CONCLUSIONS AND FUTURE SCOPE

Overall, this research has addressed the critical issue of poor thermal conductivity in Phase Change Materials (PCM) within heat sinks by incorporating various thermal enhancers. Through a systematic exploration of machined fins, metal foams, nanoparticles, encapsulation, and heat pipes, the researchers aimed to overcome the limitations of PCM, enhance its storage capacity, and optimize heat sink performance. These thermal enhancers have high thermal conductivity, which reduces the resistance offered by the PCM and also enhances the storage capacity of the PCM. The thermal enhancers can be machined fins, metal foams, adding nanoparticles, encapsulation, and heat pipes. All these external additions to the PCM in a heat sink have a better advantage than the drawbacks. Hence in this work, the different thermal enhancers are integrated with one another for a superior thermal outcome. The effects of merging enhancers and modifying the existing enhancer under different conditions and with different materials are investigated briefly. Besides these investigations, obtaining an effective heat sink is also necessary. This effective heat sink with PCM should possess a longer period of energy storage and a faster energy retrieval capacity. These studies are carried out by both numerical and experimental analysis. The simulations are performed using ANSYS Fluent on a 2D computational heat sink model with the PCM and different thermal enhancers.

The present thesis leads off with an introduction that covers the necessity of electronic cooling and an approach to resolve it by overcoming the existing cooling techniques. The offered passive technique is implemented by comprising the PCM in a heat sink. The PCM advantages, applications, and limitations are elaborated on in **Chapter 1**. Additionally, the methods to overcome the flaw of the PCM are also briefed in this chapter. The overview of the research executed and the organization of the thesis was also presented at the end of the chapter. **Chapter 2** illustrates the critical review of the literature, which includes the numerical and experimental techniques involved with PCM-based heat sinks and ways of fusing enhancers into the PCM-filled heat sink. The distinct optimization strategies that

can be beneficial to the current work are also highlighted. Finally, the scope and objectives of the present research are presented.

Chapter 3 presents the outcome of incorporating fins on the horizontal walls along with vertical fins and vertically placed partial metal foams. Initially, only fins were considered during melting, and the significance of fins and fin shapes were examined at a constant heat flux of 2000 W/m^2. The materials used are aluminum (heat sink, fins, and foams) and n-eicosane (PCM). The contour plots are obtained for the melt fraction of PCM and temperature distribution. The tapered fins display a steady temperature distribution within the PCM compared with the rectangular fins. It is due to the increase in the surface area of tapered fins near the base, the tapered fins absorb the thermal stress and increase the heat flow path. Then, the vertical fins replaced the partial metal foams fillings by fixing the horizontal wall fins. The foams have a porosity of 90 % and 10 PPI. The heights of foam are varied by 10 mm, 15 mm, and 20 mm, and it found that there is a negligible difference in the completion of melting. The maximum velocity during melting for all cases indicates the effect of natural convection within the heat sink design. The conduction effect dominates at the early stages when fins are introduced. This restricts the natural convection at early stages for fin cases. During the solidification process, all the cases without fins, with only fins, and with fins and foams were evaluated. The no-fin case completes the solidification by 85,000 s which is 15 times longer than the melting time. The reason is no convection found within the heat sink and no movement of PCM, unlike melting. The solidification occurs entirely by the effect of conduction. From the results, it is determined that the increase in filling height has a desirable outcome, and the fin shape has an insignificant effect. This is due to the strong conduction effect which takes place within the foams. The increase in filling heights increases the volume of foams, thus reducing the amount of PCM.

Following this investigation, **Chapter 4** explores the optimization study for PCM-based heat sinks with the combination of fins and metal foams. The optimization technique employed to solve the objective function is TOPSIS. The multi-objective functions considered are maximizing the melting time and minimizing the solidification time to

achieve an effective heat sink. Initially, the fin height and the fin location were established. For an effective outcome of fin placement, it is recommended to position the fins 11 mm from the top surface, with a height of 25 mm and a thickness of 5.6 mm. The heightened fins contribute to increased heat conduction within the PCM, thereby accelerating the process. Furthermore, proximity to the top wall significantly influences natural convection, further expediting the overall heat transfer. Later, 60 different cases were evaluated based on the variations of porosity and pore size. From the five weightages applied, the performance scores are acquired based on TOPSIS. In conclusion, for equal balance in weightage between melting and solidification, or a higher emphasis on melting, leads to superior outcomes characterized by increased filling heights and higher pore density. This is attributed to the distribution of a more solid structure within the phase change material (PCM), resulting in a dominant conduction effect. Conversely, prioritizing prolonged melting favours a design with a less solid structure, enhancing overall responsiveness. Depending on the weightages, the user can select the porosity and PPI for an optimized PCM-filled storage unit.

Chapter 5 dealt with the analysis of multiple PCM heat sink designs during the charging cycle. The PCM is arranged within the enclosure, and fins are attached longitudinally. The fins act as the separator of different PCM incorporated as well as the additional enhancer for the heat sink. Three different PCMs, RT-28HC, RT-35 HC, and RT-44HC, with different melting temperatures, are employed in this investigation. The arrangement of PCMs inside the enclosure does not influence the melting in a PCM-based heat sink. The significance of the triple PCM design was derived by comparing it with the single PCM and double PCM-filled heat sink with similar geometry. The combination of three different PCMs with distinct thermal properties allows for a more efficient utilization of temperature ranges, enabling the system to accommodate both charging and discharging cycles. The orientations of fins vary at different angles and heat flux ranges. At any heat flux condition, the negatively oriented fins possess faster melting, and positively oriented fins have slower melting. This can be seen with the help of temperature and liquid fraction contours. Negatively oriented fins exhibit faster melting due to increased natural convection

dominance at higher angles, facilitating a higher melting temperature zone exposure to the heater. The observed phenomena persist when altering initial conditions by 300 K, 303 K, and 310 K, and the state of the PCM. The temperatures are selected so that at different conditions, the PCM is either a liquid or solid state. From the above findings, the results indicate that the higher enhancement % is found for -60^{o} angled fins, and the lower enhancement % is found for +60^{o} angled fins.

The experimental investigations are explored in **Chapter** 6. Two heat sinks with a conventional fin design of uniform height and a proposed fin design with varying heights are considered. The two heat sinks are designed and fabricated with the same dimensions of 100 x 50 x 25 mm. The PCM cavity was also fixed for both the heat sinks, and the dimensions are 90 x 40 x 20 mm, and the PCM incorporated is n-eicosane. The fin volume fraction was kept constant, but only the fin heights were varied within the heat sink. This influence of fin height variations under the constant heat load and power surge loads is analyzed. The power surges are applied at different conditions. The improved performance of variable height fins, resulting in a faster charging and discharging rate compared to constant height fins, can be attributed to the larger heat transfer region within the phase change material (PCM). In variable height heat sinks, the varied fin heights enhance the heat transfer area, facilitating more efficient dissipation of heat from the PCM, thereby accelerating the processes. During power surge cycles, variable fin height is better suited due to its enhanced performance in the melting/solidification process. The non-uniform fin heights in variable height heat sinks facilitate faster melting. The higher absorption rate of the variable height fins leads to a lower peak temperature compared to constant height fins, especially in successive cycles. This is attributed to reduced resistance offered by the phase change material at all heights and improving overall performance under varying loads.

Overall, the research contributes to advancing PCM-based heat sink designs for electronic cooling, offering insights into the integration of thermal enhancers and optimization techniques to achieve superior thermal performance. The combination of numerical simulations and experimental analyses provides a comprehensive understanding of the proposed approaches.

7.1 SCOPE FOR FUTURE WORK

The aim of this investigation is to incorporate different thermal enhancers and combine them for a better solution while integrating with PCM, which owns poor thermal conductivity. The significance of the foams and fins combination, multiple PCM with fins, and modified fin configuration were discussed in the investigations. These results will be the guidelines for the upcoming study, and the following points are suggested for future works,

- The combination of fins and foams can be extended with the experimental investigations for different materials, and the implementation of gradient foams within the enclosure can be analyzed for better thermal performance.
- In the TOPSIS algorithm, the weightage was considered manually. But with different methods, such as objective weighing methods and subjective weighing, the optimization can be carried out based on the weightages calculated using these techniques.
- In a triple PCM design, the number of PCM and the fin density can be increased, and an optimization study can be further done for the proposed variations.
- The numerical investigation can examine the influence of fin spacing, fin numbers, and enclosure aspect ratio for the modified variable fin height heat sinks.

REFERENCES

Abdulateef, A. M., Abdulateef, J., Al-Abidi, A. A., Sopian, K., Mat, S., and Mahdi, M. S. (2019). "A combination of fins-nanoparticle for enhancing the discharging of phase-change material used for liquid desiccant air conditioning unite." *J. Energy Storage*, 24(February), 100784.

Akhilesh, R., Narasimhan, A., and Balaji, C. (2005). "Method to improve geometry for heat transfer enhancement in PCM composite heat sinks." *Int. J. Heat Mass Transf.*, 48(13), 2759–2770.

Ali, H. M., Arshad, A., Janjua, M. M., Baig, W., and Sajjad, U. (2018a). "Thermal performance of LHSU for electronics under steady and transient operations modes." *Int. J. Heat Mass Transf.*, 127, 1223–1232.

Ali, H. M., Ashraf, M. J., Giovannelli, A., Irfan, M., Irshad, T. Bin, Hamid, H. M., Hassan, F., and Arshad, A. (2018b). "Thermal management of electronics: An experimental analysis of triangular, rectangular and circular pin-fin heat sinks for various PCMs." *Int. J. Heat Mass Transf.*, 123, 272–284.

Alshaer, W. G., Nada, S. A., Rady, M. A., Barrio, E. P. Del, and Sommier, A. (2015). "Thermal management of electronic devices using carbon foam and PCM/nano-composite." *Int. J. Therm. Sci.*, 89, 79–86.

ANSYS FLUENT. (2009). "ANSYS Fluent 12.0 user's guide." *Ansys Inc*, <http://scholar.google.com/scholar?hl=en&btnG=Search&q=intitle:ANSYS+FLUENT+User+'+s+Guide#1>.

Arshad, A., Ibrahim Alabdullatif, M., Jabbal, M., and Yan, Y. (2021). "Towards the thermal management of electronic devices: A parametric investigation of finned heat sink filled with PCM." *Int. Commun. Heat Mass Transf.*, 129(October), 105643.

Ashraf, M. J., Ali, H. M., Usman, H., and Arshad, A. (2017). "Experimental passive electronics cooling: Parametric investigation of pin-fin geometries and efficient phase change materials." *Int. J. Heat Mass Transf.*, 115, 251–263.

Augspurger, M., Choi, K. K., and Udaykumar, H. S. (2018). “Optimizing fin design for a PCM-based thermal storage device using dynamic Kriging.” *Int. J. Heat Mass Transf.*, 121, 290–308.

Avci, M., and Yazici, M. Y. (2018). “An experimental study on effect of inclination angle on the performance of a PCM-based flat-type heat sink.” *Appl. Therm. Eng.*, 131, 806–814.

Baby, R., and Balaji, C. (2012). “Experimental investigations on phase change material based finned heat sinks for electronic equipment cooling.” *Int. J. Heat Mass Transf.*, 55(5–6), 1642–1649.

Baby, R., and Balaji, C. (2013a). “Experimental investigations on thermal performance enhancement and effect of orientation on porous matrix filled PCM based heat sink.” *Int. Commun. Heat Mass Transf.*, 46, 27–30.

Baby, R., and Balaji, C. (2013b). “Thermal optimization of PCM based pin fin heat sinks: An experimental study.” *Appl. Therm. Eng.*, 54(1), 65–77.

Boomsma, K., and Poulikakos, D. (2011). “Erratum: On the effective thermal conductivity of a three-dimensionally structured fluid-saturated metal foam (International Journal of Heat and Mass Transfer (2001) 44 (827-836)).” *Int. J. Heat Mass Transf.*, 54(1–3), 746–748.

Boudali Errebai, F., Chikh, S., and Derradji, L. (2018). “Experimental and numerical investigation for improving the thermal performance of a microencapsulated phase change material plasterboard.” *Energy Convers. Manag.*, 174(August), 309–321.

Calmidi, V. V. (1998). “Transport phenomena in high porosity fibrous metal foams.” *Mater. Sci.*

Calmidi, V. V., and Mahajan, R. L. (2000). “Forced convection in high porosity metal foams.” *J. Heat Transfer*, 122(3), 557–565.

Chen, Z., Gao, D., and Shi, J. (2014). “Experimental and numerical study on melting of phase change materials in metal foams at pore scale.” *Int. J. Heat Mass Transf.*, 72, 646–

655.

Cheng, X., and Zhai, X. (2018). “Thermal performance analysis of a cascaded cold storage unit using multiple PCMs.” *Energy*, 143, 448–457.

Desai, A. N., Shah, H., and Singh, V. K. (2021). “Novel inverted fin configurations for enhancing the thermal performance of PCM based thermal control unit: A numerical study.” *Appl. Therm. Eng.*, 195(June), 117155.

Dinesh, B. V. S., and Bhattacharya, A. (2020). “Comparison of energy absorption characteristics of PCM-metal foam systems with different pore size distributions.” *J. Energy Storage*, 28(January), 101190.

Du, R., Li, W., Xiong, T., Yang, X., Wang, Y., and Shah, K. W. (2019). “Numerical investigation on the melting of nanoparticle-enhanced PCM in latent heat energy storage unit with spiral coil heat exchanger.” *Build. Simul.*, 12(5), 869–879.

Elsanusi, O. S., and Nsofor, E. C. (2021). “Melting of multiple PCMs with different arrangements inside a heat exchanger for energy storage.” *Appl. Therm. Eng.*, 185(August 2020), 116046.

Ezra, M., Kozak, Y., Dubovsky, V., and Ziskind, G. (2016). “Analysis and optimization of melting temperature span for a multiple-PCM latent heat thermal energy storage unit.” *Appl. Therm. Eng.*, 93, 315–329.

Faraji, H., Faraji, M., and Alami, M. El. (2021). “Numerical Study of the Transient Melting Of Nano-Enhanced Phase Change Material.” *Heat Transf. Eng.*, 42(2), 120–139.

G, T., and N, G. (2021). “Numerical study on maximizing heat transfer and minimizing flow resistance behavior of metal foams owing to their structural properties.” *Int. J. Therm. Sci.*, 159(September 2020), 106617.

Ghanbarpour, A., Hosseini, M. J., Ranjbar, A. A., Rahimi, M., Bahrampoury, R., and Ghanbarpour, M. (2021). “Evaluation of heat sink performance using PCM and vapor chamber/heat pipe.” *Renew. Energy*, 163, 698–719.

Ghosh, D., and Guha, C. (2019). “Numerical and experimental investigation of paraffin wax melting in spherical cavity.” *Heat Mass Transf.*, 55(1427–1437).

Hasan, M. I., and Tbena, H. L. (2018). “Using of phase change materials to enhance the thermal performance of micro channel heat sink.” *Eng. Sci. Technol. an Int. J.*, 21(3), 517–526.

Ho, C. J., Hsu, S. T., Rashidi, S., and Yan, W. M. (2020). “Water-based nano-PCM emulsion flow and heat transfer in divergent mini-channel heat sink—An experimental investigation.” *Int. J. Heat Mass Transf.*, 148.

Hu, Z., Li, A., Gao, R., and Yin, H. (2015). “Enhanced heat transfer for PCM melting in the frustum-shaped unit with multiple PCMs.” *J. Therm. Anal. Calorim.*, 120(2), 1407–1416.

Huang, P., Wei, G., Cui, L., Xu, C., and Du, X. (2022). “Experimental and numerical optimization of cascaded PCM heat sink by using low melting point alloys.” *Energy Convers. Manag.*, 269(August), 116149.

Jadhav, P. H., G, T., Gnanasekaran, N., and Mobedi, M. (2022). “Performance score based multi-objective optimization for thermal design of partially filled high porosity metal foam pipes under forced convection.” *Int. J. Heat Mass Transf.*, 182.

Jalil, J. M., Mahdi, H. S., and Allawy, A. S. (2022). “Cooling performance investigation of PCM integrated into heat sink with nano particles addition.” *J. Energy Storage*, 55(PA), 105466.

Ji, C., Qin, Z., Dubey, S., Choo, F. H., and Duan, F. (2018a). “Simulation on PCM melting enhancement with double-fin length arrangements in a rectangular enclosure induced by natural convection.” *Int. J. Heat Mass Transf.*, 127, 255–265.

Ji, C., Qin, Z., Low, Z., Dubey, S., Choo, F. H., and Duan, F. (2018b). “Simulation on PCM melting enhancement with double-fin length arrangements in a rectangular enclosure induced by natural convection.” *Int. J. Heat Mass Transf.*, 129, 269–279.

Ji, C., Qin, Z., Low, Z., Dubey, S., Choo, F. H., and Duan, F. (2018c). “Non-uniform heat transfer suppression to enhance PCM melting by angled fins.” *Appl. Therm. Eng.*, 129, 269–279.

Joseph, M., and Sajith, V. (2019). “Graphene enhanced paraffin nanocomposite based hybrid cooling system for thermal management of electronics.” *Appl. Therm. Eng.*, 163(April), 114342.

Kandasamy, R., Wang, X. Q., and Mujumdar, A. S. (2007). “Application of phase change materials in thermal management of electronics.” *Appl. Therm. Eng.*, 27(17–18), 2822–2832.

Kandasamy, R., Wang, X. Q., and Mujumdar, A. S. (2008). “Transient cooling of electronics using phase change material (PCM)-based heat sinks.” *Appl. Therm. Eng.*, 28(8–9), 1047–1057.

Kasper, L., Pernsteiner, D., Koller, M., Schirrer, A., Jakubek, S., and Hofmann, R. (2021). “Numerical studies on the influence of natural convection under inclination on optimal aluminium proportions and fin spacings in a rectangular aluminium finned latent-heat thermal energy storage.” *Appl. Therm. Eng.*, 190(November 2020).

Kurhade, A., Talele, V., Venkateswara Rao, T., Chandak, A., and Mathew, V. K. (2021). “Computational study of PCM cooling for electronic circuit of smart-phone.” *Mater. Today Proc.*, 47, 3171–3176.

Levin, P. P., Shitzer, A., and Hetsroni, G. (2013). “Numerical optimization of a PCM-based heat sink with internal fins.” *Int. J. Heat Mass Transf.*, 61(1), 638–645.

Li, Z. W., Lv, L. C., and Li, J. (2016). “Combination of heat storage and thermal spreading for high power portable electronics cooling.” *Int. J. Heat Mass Transf.*, 98, 550–557.

Ling, Y. Z., Zhang, X. S., Wang, F., and She, X. H. (2020). “Performance study of phase change materials coupled with three-dimensional oscillating heat pipes with different structures for electronic cooling.” *Renew. Energy*, 154, 636–649.

Lohrasbi, S., Gorji-Bandpy, M., and Ganji, D. D. (2017). "Thermal penetration depth enhancement in latent heat thermal energy storage system in the presence of heat pipe based on both charging and discharging processes." *Energy Convers. Manag.*, 148, 646–667.

Luo, X., Gu, J., Ma, H., Xie, Y., Li, A., Wang, J., and Ding, R. (2022). "Numerical study on enhanced melting heat transfer of PCM by the combined fractal fins." *J. Energy Storage*, 45(November 2021), 103780.

Luo, Z., Cho, H., Luo, X., and Cho, K. il. (2008). "System thermal analysis for mobile phone." *Appl. Therm. Eng.*, 28(14–15), 1889–1895.

Mahdi, J. M., Mohammed, H. I., Hashim, E. T., Talebizadehsardari, P., and Nsofor, E. C. (2020). "Solidification enhancement with multiple PCMs, cascaded metal foam and nanoparticles in the shell-and-tube energy storage system." *Appl. Energy*, 257(October 2019), 113993.

Mahdi, J. M., and Nsofor, E. C. (2018). "Multiple-segment metal foam application in the shell-and-tube PCM thermal energy storage system." *J. Energy Storage*, 20(November), 529–541.

Mahmoud, S., Tang, A., Toh, C., AL-Dadah, R., and Soo, S. L. (2013). "Experimental investigation of inserts configurations and PCM type on the thermal performance of PCM based heat sinks." *Appl. Energy*, 112, 1349–1356.

Mancin, S., Diani, A., Doretti, L., Hooman, K., and Rossetto, L. (2015). "Experimental analysis of phase change phenomenon of paraffin waxes embedded in copper foams." *Int. J. Therm. Sci.*, 90, 79–89.

Mozafari, M., and Lee, A. (2022). "Thermal performance enhancement of a new dual-PCM heat sink using two-objective optimization." *Therm. Sci. Eng. Prog.*, 33(December 2021), 101383.

N., L. N. (2019). "Assessment of latent heat thermal storage systems operating with multiple phase change materials." *J. Energy Storage*, 23(April), 442–455.

Nagose, A., Somani, A., Shrot, A., and Narasimhan, A. (2008). “Genetic algorithm based optimization of PCM based heat sinks and effect of heat sink parameters on operational time.” *J. Heat Transfer*, 130(1), 1–8.

Nayak, K. C., Saha, S. K., Srinivasan, K., and Dutta, P. (2006). “A numerical model for heat sinks with phase change materials and thermal conductivity enhancers.” *Int. J. Heat Mass Transf.*, 49(11–12), 1833–1844.

Nazir, H., Batool, M., Bolivar Osorio, F. J., Isaza-Ruiz, M., Xu, X., Vignarooban, K., Phelan, P., Inamuddin, and Kannan, A. M. (2019). “Recent developments in phase change materials for energy storage applications: A review.” *Int. J. Heat Mass Transf.*, 129, 491–523.

Nedumaran, M. S., and Gnanasekaran, N. (2022). “Comprehensive analysis of hybrid heat sinks with phase change materials for both charging and discharging cycles.” *Heat Transf. Eng.*, 0(0), 1–19.

Parsazadeh, M., and Duan, X. (2020). “Numerical and Experimental Investigation of Phase Change Heat Transfer in the Presence of Rayleigh–Benard Convection.” *J. Heat Transfer*, 142(6), 1–13.

Pizzolato, A., Sharma, A., Maute, K., Sciacovelli, A., and Verda, V. (2017). “Design of effective fins for fast PCM melting and solidification in shell-and-tube latent heat thermal energy storage through topology optimization.” *Appl. Energy*, 208(September), 210–227.

Rehman, T. ur, and Ali, H. M. (2018). “Experimental investigation on paraffin wax integrated with copper foam based heat sinks for electronic components thermal cooling.” *Int. Commun. Heat Mass Transf.*, 98(September), 155–162.

Rehman, T. ur, Ali, H. M., Saieed, A., Pao, W., and Ali, M. (2018). “Copper foam/PCMs based heat sinks: An experimental study for electronic cooling systems.” *Int. J. Heat Mass Transf.*, 127, 381–393.

Ren, Q., Guo, P., and Zhu, J. (2020). “Thermal management of electronic devices using

pin-fin based cascade microencapsulated PCM/expanded graphite composite." *Int. J. Heat Mass Transf.*, 149, 1–16.

Sadrameli, S. M., Motaharinejad, F., Mohammadpour, M., and Dorkoosh, F. (2019). "An experimental investigation to the thermal conductivity enhancement of paraffin wax as a phase change material using diamond nanoparticles as a promoting factor." *Heat Mass Transf. und Stoffuebertragung*, 55(6), 1801–1808.

Saha, S. K., and Dutta, P. (2010). "Heat transfer correlations for PCM-based heat sinks with plate fins." *Appl. Therm. Eng.*, 30(16), 2485–2491.

Saha, S. K., and Dutta, P. (2015). "Performance Analysis of Heat Sinks With Phase-Change Materials Subjected to Transient and Cyclic Heating." *Heat Transf. Eng.*, 36(16), 1349–1359.

Saha, S. K., Srinivasan, K., and Dutta, P. (2008). "Studies on optimum distribution of fins in heat sinks filled with phase change materials." *J. Heat Transfer*, 130(3), 1–4.

Shaikh, S., and Lafdi, K. (2010). "C/C composite, carbon nanotube and paraffin wax hybrid systems for the thermal control of pulsed power in electronics." *Carbon N. Y.*, 48(3), 813–824.

Sheikh, Y., Fatih Orhan, M., and Kanoglu, M. (2022). "Heat transfer enhancement of a bio-based PCM/metal foam composite heat sink." *Therm. Sci. Eng. Prog.*, 36(October), 101536.

Sheikholeslami, M., Lohrasbi, S., and Ganji, D. D. (2016). "Numerical analysis of discharging process acceleration in LHTESS by immersing innovative fin configuration using finite element method." *Appl. Therm. Eng.*, 107, 154–166.

Singh, A., Rangarajan, S., Choobineh, L., and Sammakia, B. (2022). "Figure of Merit-Based Optimization Approach of Phase Change Material-Based Composites for Portable Electronics Using Simplified Model." *J. Electron. Packag. Trans. ASME*, 144(2), 021104(1–7).

Siyabi, I. Al, Khanna, S., Mallick, T., and Sundaram, S. (2018). “Multiple Phase Change Material (PCM) Configuration for PCM-Based Heat Sinks-An Experimental Study.” *Energies*, 11(7).

Srikanth, R., Nemani, P., and Balaji, C. (2015). “Multi-objective geometric optimization of a PCM based matrix type composite heat sink.” *Appl. Energy*, 156, 703–714.

Srinivasan, S., Diallo, M. S., Saha, S. K., Abass, O. A., Sharma, A., and Balasubramanian, G. (2017). “Effect of temperature and graphite particle fillers on thermal conductivity and viscosity of phase change material n-eicosane.” *Int. J. Heat Mass Transf.*, 114, 318–323.

Srivatsa, P., Baby, R., and Balaji, C. (2016). “Geometric Optimization of a PCM-Based Heat Sink-A Coupled ANN and GA Approach.” *Heat Transf. Eng.*, 37(10), 875–888.

Tharwan, M. Y., and Hadidi, H. M. (2022). “Experimental investigation on the thermal performance of a heat sink filled with PCM.” *Alexandria Eng. J.*, 61(9), 7045–7054.

Tian, Y., and Zhao, C. Y. (2011). “A numerical investigation of heat transfer in phase change materials (PCMs) embedded in porous metals.” *Energy*, 36(9), 5539–5546.

Vigneswaran, V. S., Kumaresan, G., Dinakar, B. V., Kamal, K. K., and Velraj, R. (2019). “Augmenting the productivity of solar still using multiple PCMs as heat energy storage.” *J. Energy Storage*, 26(October), 101019.

Wang, Y. H., and Yang, Y. T. (2011). “Three-dimensional transient cooling simulations of a portable electronic device using PCM (phase change materials) in multi-fin heat sink.” *Energy*, 36(8), 5214–5224.

Xie, J., Lee, H. M., and Xiang, J. (2019). “Numerical study of thermally optimized metal structures in a Phase Change Material (PCM) enclosure.” *Appl. Therm. Eng.*, 148(August 2018), 825–837.

Yoo, D., and Joshi, Y. (2002). “Energy efficient thermal management of electronic components using solid liquid phase change materials.” *Intersoc. Conf. Therm. Thermomechanical Phenom. Electron. Syst. ITHERM*, 2002-Janua(4), 800–807.

Zhao, C., Opolot, M., Liu, M., Bruno, F., Mancin, S., and Hooman, K. (2021). “Phase change behaviour study of PCM tanks partially filled with graphite foam.” *Appl. Therm. Eng.*, 196(March), 117313.

Zheng, H., Wang, C., Liu, Q., Tian, Z., and Fan, X. (2018). “Thermal performance of copper foam/paraffin composite phase change material.” *Energy Convers. Manag.*, 157(December 2017), 372–381.

Zhu, Z. Q., Huang, Y. K., Hu, N., Zeng, Y., and Fan, L. W. (2018). “Transient performance of a PCM-based heat sink with a partially filled metal foam: Effects of the filling height ratio.” *Appl. Therm. Eng.*, 128, 966–972.

Zukauskas, A. (1987). "*Convective heat transfer in cross flow"*. In: Hartnett, JP.,Irvine, TF. (Eds.), *Advances in Heat Transfer*. Elsevier, pp. 87–159.

LIST OF PUBLICATIONS

JOURNALS

1. Muthamil Selvan, N. and Gnanasekaran, N., (2021). "Comprehensive analysis of hybrid heat sinks with phase change materials for both charging and discharging cycles," ***Heat Transfer Engineering*., (IF: 2.43),** 44 (4) April.

DOI: https://doi.org/10.1080/01457632.2022.2059216

2. Muthamil Selvan, N., Gnanasekaran, N. and Kamel Hooman., (2022), "Numerical analysis of multiple phase change materials based heat sink with angled thermal conductivity enhancer." ***Journal of Energy Storage*, (IF: 8.907)**, 55 105316 (1-14).

DOI : //doi.org/10.1016/j.est.2022.105316

3. Muthamil Selvan, N., Gnanasekaran, N. and Kamel Hooman., (2022), "Multi-objective optimization of hybrid heat sinks with phase change materials," ***Heat Transfer Engineering*., (IF: 2.43).**

DOI : https://doi.org/10.1080/01457632.2023.2234770

4. Muthamil Selvan, N., Gnanasekaran, N. and Kamel Hooman., (2023), "Extensive analysis of PCM-based heat sink with different fin arrangements under varying load conditions and variable aspect ratio." ***Journal of Energy Storage*, (IF: 8.907)**, 73 108870 (1-17).

DOI : https://doi.org/10.1016/j.est.2023.108870

CONFERENCE

1. Muthamil Selvan, N., Trilok, G., and N. Gnanasekaran. "Multi-objective optimization of various type finned heat sink with phase change material. "*IOP Conference Series: Earth and Environmental Science, International Conference on Green Energy and Technology,"* Vol 1100, 2022.

DOI: 10.1088/1755-1315/1100/1/012006

BIODATA

NAME: MUTHAMIL SELVAN N

DATE OF BIRTH: 29/10/1992

Mobile No.: +91 9677719778

Email: tamil29oct1992@gmail.com

ADDRESS:

3/183, Shri Hare Krishna Nivas, Vaigai Vadakarai, Thiruppuvanam, Sivaganga (Dt), Tamilnadu-630611

QUALIFICATION:

Examination	Board/Institute	Year	Percentage/ CGPA
Ph.D. (Thermal systems)	NITK, Surathkal	2023	7.75
M.E. (Energy Engg.)	PSG College of Technology, Coimbatore	2018	7.82
B.E. (Mechanical Engg.)	CSI College of Engineering, Ketti	2016	6.9
HSLC	Tamilnadu state board	2010	86.75%
SSLC	Tamilnadu state board	2008	93.8%

ACTIVITIES:

1. Industrial training in TVS motors, Madurai
2. QIP Short Term Course on Thermal Energy Storage for Effective Energy Management - IIT Kanpur, Feb. 2020
3. International Conference on Green Energy and Technology - SSN College of Engineering, Chennai, Nov. 2021
4. Qualified GATE Exam in 2016.

FIELD OF INTEREST:

Thermal systems, Computational fluid dynamics (CFD), Energy storage, Heat transfer, and Porous media.